

AD-A045 242

ADVISORY GROUP FOR AEROSPACE RESEARCH AND DEVELOPMENT--ETC F/6 1/1
STRUCTURAL ASPECTS OF ACTIVE CONTROLS. (U)

AUG 77

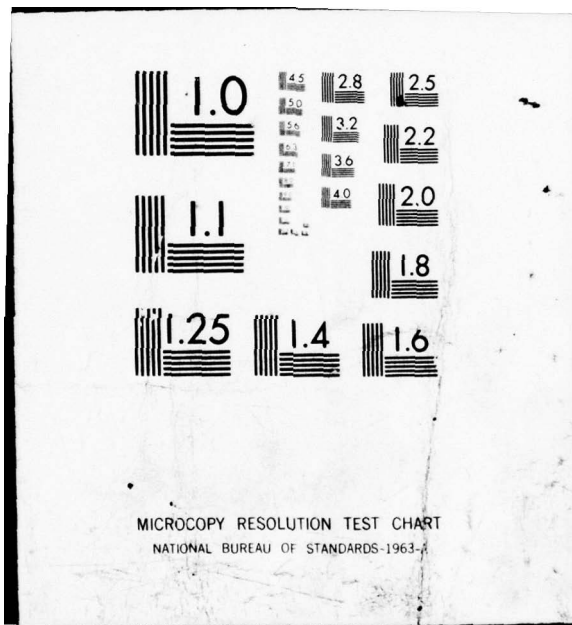
UNCLASSIFIED

1 OF 2
AD
A045 242

AGARD-CP-228

NL





ADA 045242

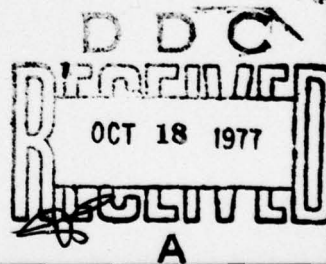
AGARD

ADVISORY GROUP FOR AEROSPACE RESEARCH & DEVELOPMENT

7 RUE ANCELLE 92200 NEUILLY SUR SEINE FRANCE

AGARD CONFERENCE PROCEEDINGS No. 228

Structural Aspects of Active Controls



NORTH ATLANTIC TREATY ORGANIZATION



DISTRIBUTION AND AVAILABILITY
ON BACK COVER

DISTRIBUTION STATEMENT A
Approved for public release
Distribution Unlimited

AD 045242
DDC FILE COPY

14

AGARD-CP-228

NORTH ATLANTIC TREATY ORGANIZATION

ADVISORY GROUP FOR AEROSPACE RESEARCH AND DEVELOPMENT

(ORGANISATION DU TRAITE DE L'ATLANTIQUE NORD)

9
AGARD Conference Proceedings No. 228

6

STRUCTURAL ASPECTS OF ACTIVE CONTROLS

11

Aug 77

12

103P.

B D C
RECORDED
OCT 18 1977
RECORDED
A

DISTRIBUTION STATEMENT A

Approved for public release
Distribution Unlimited

Papers presented at the 44th Meeting of the AGARD Structures and Material Panel
held in Lisbon, Portugal on 21 April 1977

100 043

mt

THE MISSION OF AGARD

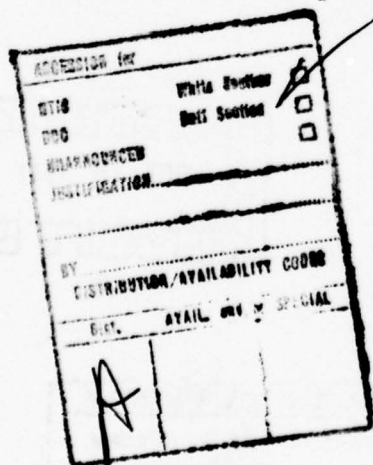
The mission of AGARD is to bring together the leading personalities of the NATO nations in the fields of science and technology relating to aerospace for the following purposes:

- Exchanging of scientific and technical information;
- Continuously stimulating advances in the aerospace sciences relevant to strengthening the common defence posture;
- Improving the co-operation among member nations in aerospace research and development;
- Providing scientific and technical advice and assistance to the North Atlantic Military Committee in the field of aerospace research and development;
- Rendering scientific and technical assistance, as requested, to other NATO bodies and to member nations in connection with research and development problems in the aerospace field;
- Providing assistance to member nations for the purpose of increasing their scientific and technical potential;
- Recommending effective ways for the member nations to use their research and development capabilities for the common benefit of the NATO community.

The highest authority within AGARD is the National Delegates Board consisting of officially appointed senior representatives from each member nation. The mission of AGARD is carried out through the Panels which are composed of experts appointed by the National Delegates, the Consultant and Exchange Program and the Aerospace Applications Studies Program. The results of AGARD work are reported to the member nations and the NATO Authorities through the AGARD series of publications of which this is one.

Participation in AGARD activities is by invitation only and is normally limited to citizens of the NATO nations.

The content of this publication has been reproduced directly from material supplied by AGARD or the authors.



Published August 1977

Copyright © AGARD 1977
All Rights Reserved

ISBN 92-835-0200-0



Printed by Technical Editing and Reproduction Ltd
Harford House, 7-9 Charlotte St, London, W1P 1HD

PREFACE

Active control technology has steadily emerged and offers a means for improving performance and operational flexibility and of changing air vehicle design concepts, procedures and methods. The use of active control devices on aircraft appears beneficial in at least six different areas: (1) quasi-steady load reductions, (2) flutter suppression, (3) reduced fatigue loading, (4) improved stability and control, (5) improved ride qualities, and (6) reduced margins. The Flight Dynamics Laboratory of Wright Patterson Air Force Base played a leading role in initiating the study effort on active controls, and since then groups in Europe as well as the United States have made marked advances in developing the concepts, in building hardware, and in testing, both in windtunnels and in full-scale flight.

The problem area is appropriate for joint consideration by the NATO nations, and work appears to follow logically under the cognizance of the SMP, FMP and GCP. In the October 1973 meeting (the Hague), the SMP held a plenary session on Active Control Devices, in which five papers were presented. At their April 1975 meeting in Brussels; the SMP held a specialist meeting on Flutter Suppression and Structural Load Alleviation, at which eight papers were presented. In October 1974, the FMP and GCP held a four-day symposium on the subject entitled "Impact of Active Control Technology on Airplane Design".

At the April 1977 meeting (Lisbon) the SMP held a specialist meeting on Structural Aspects of Active Controls, at which seven papers were presented. These Proceedings are a compilation of the papers presented. The specialist meeting covered here was organized and conducted by the Ad hoc Group on Structural Aspects of Active Controls.

It is hoped that effort within the SMP has helped in the dissemination of knowledge on the subject and that these Proceedings will help promote useful thoughts and contribute to the development of means for increasing the safety, performance, and utility of aircraft.

John C.HOUBOLT
Chairman, Ad hoc Group
on Structural Aspects of
Active Controls

CONTENTS

	Page
PREFACE	iii
Reference	
A PRACTICAL OPTIMUM SELECTION PROCEDURE FOR A MOTIVATOR IN ACTIVE FLUTTER SUPPRESSION SYSTEM DESIGN ON AN AIRCRAFT WITH UNDERWING STORES by M.R.Turner and C.G.Lodge	1
IMPACT OF A COMMAND AND STABILITY AUGMENTATION SYSTEM ON GUST RESPONSE OF A COMBAT AIRCRAFT by K.D.Collmann and O.Sensburg	2
ACTIVE FLUTTER SUPPRESSION ON AN AIRPLANE WITH WING MOUNTED EXTERNAL STORES by H.Hönlinder	3
AIRPLANE MATH MODELING METHODS FOR ACTIVE CONTROL DESIGN by K.L.Roger	4
CONSISTENCY IN AIRCRAFT STRUCTURAL AND FLIGHT CONTROL ANALYSIS by R.W.Schwanz	5
YC-14 CONTROL SYSTEM REDUNDANCY by W.T.Hamilton	6
ETUDE EN SOUFFLERIE D'UN SUPPRESSEUR DE FLOTTEMENT par R.Destuynder	7

A PRACTICAL OPTIMUM SELECTION PROCEDURE FOR A
MOTIVATOR IN ACTIVE FLUTTER SUPPRESSION SYSTEM DESIGN
ON AN AIRCRAFT WITH UNDERWING STORES

M. R. Turner

British Aircraft Corporation,
Commercial Aircraft Division,
Filton, Bristol, England.

C. G. Lodge

British Aircraft Corporation,
Military Aircraft Division,
Warton, Lancs, England

Abstract

Theoretical active flutter control of a variable sweep wing with external stores with four combinations of store configuration/wing sweep/Mach Number was studied. Electrically modified outputs of a structure mounted transducer were used to drive an auxiliary control surface on the wing or store. The best transducer/force positions on the wing and stores were found using Nyquist Plots and representing the control surface loads by point forces.

The object was to see if a common active flutter control system using a control surface on the wing could be found for a range of stores, Mach Numbers and wing sweep angles. Difficulties were due to two instabilities with close frequencies in two of the configurations and very low dampings in some of the stable modes.

1. INTRODUCTION

The use of active flutter control could have significant advantages over the established methods of structural modification and adding concentrated masses. However, if no suitable control surface is already available to act as a motivator for an active flutter control system, an auxiliary control surface must be introduced.

This paper describes a practical optimum selection procedure for the position of the auxiliary control surface and the feedback transducer. The procedure is illustrated by application to the control of flutter of a variable sweep aircraft with underwing stores.

2. OBJECTIVE

A theoretical study was made of the use of active controls to suppress the flutter of a variable sweep wing (Figure 1) with the four cases of store configuration, Mach Number and wing sweep angle shown in Figure 2. The wing had no suitable control surface already available which could be used for active flutter control. Therefore the addition of an auxiliary control surface on the wing or store was necessary.

The object was to find the most effective control surface position, transducer position and feedback law to suppress flutter for each of the four cases. It was also intended to find the best common system using a control surface on the wing. This is logically more appealing than to use control surfaces on each store.

3. MATHEMATICAL MODEL

3.1 Basic Wing-plus-Store Characteristics

Sixteen branch modes for each wing and store combination were used. These were normalised and the first eight were used for the active flutter control study. The fuselage was assumed fixed inboard of the wing pivot. Two dimensional aerodynamic derivatives were used in a strip theory sense for the wing flutter aerodynamics. These aerodynamic derivatives were chosen to give the same flutter speeds and similar subcritical characteristics to those given by three dimensional lifting surface theories.

Because (i) some stable roots had extremely low aerodynamic damping

(ii) the introduction of 1% structural damping into the first three modes excluded most of the basic store flutters

the study was done with no structural damping in the first three normal modes and 1% structural damping in modes 4 to 8.

Figure 3 shows the basic flutter characteristics for the four cases. Because the instabilities occur in the first three roots, which are close in frequency, only these roots are shown in the flutter plots. Notice that for cases 1 and 3 there are two unstable roots close in frequency.

3.2 Auxiliary Control System

To choose the best position for the auxiliary control surface, the control surface forces were represented by a point force P

$$\text{where } P = \frac{1}{2} \rho V^2 K_o f(s) W$$

$$\frac{1}{2} \rho V^2 = \text{free stream dynamic pressure}$$

$$K_o = \text{overall feedback gain}$$

$$f(s) = \text{feedback filter}$$

$$W = \text{transducer output}$$

This assumes:

- (i) the actuator transfer function is unity
- (ii) the control surface rotational stiffness is infinite
- (iii) the frequency dependant part of the control surface aerodynamics can be ignored and
- (iv) the inertia forces due to control surface acceleration are negligible.

Therefore, the generalised excitation forces due to the control surface force acting on the modal system can be simply represented by:

$$\{\Delta\} P$$

Where $\{\Delta\}$ is the vector of modal deflections at the point force position.

The justification for using a single point force to represent the aerodynamic loading due to control surface rotation is as follows. We consider strip theory representation of the control surface aerodynamics to be adequate for preliminary design calculations on a high aspect ratio wing. If strip theory was used, the aerodynamic stiffness forces would be represented by a point force on each chordwise strip. Therefore, if the strips were the width of the control surface we would have the single point force representation used in this study.

Assumptions (iii) and (iv) are justified in the interest of providing an economic preliminary design procedure, while assumption (i) can be compensated for by a simple filter if necessary.

Generally, the error due to the point force assumption will only be significant at relatively high frequencies where it is difficult to accurately model the aeroelastic data and actuator anyway.

Obviously the most favourable positions given by the point force study should be checked with a full representation of the control surface forces. The actuator transfer function and impedance will emerge as requirements from the design study.

4. FLUTTER CONTROL SYSTEM DESIGN

4.1 Design Requirements

- (i) A design speed is chosen below which the aircraft must not be unstable. This is typically 15% above the maximum flight speed of the aircraft.
- (ii) Stability must be maintained in a 25 ft./sec. tuned (1-cosine) gust at the design speed.
- (iii) Overall aircraft stability and control characteristics must not be affected by the flutter control system.

4.2 Design Aims

To achieve these design requirements with a simple flutter control system with maximum reliability, low sensitivity and minimum weight penalty, the following are aimed for:

- (i) Only one transducer and one control surface will be used.
- (ii) Adequate closed loop gain and phase stability margins are to be available at all frequencies and speeds. This is to cover manufacturing and wear induced tolerances in the feedback hardware - particularly in the actuator. It may also be necessary to cover variations in the basic aircraft transfer function either from the predicted value or from variations in flight conditions such as fuel distribution or altitude.

In this study the requirements will be ± 6 db (i.e. $\times 2$ and $\div 2$) and $\pm 60^\circ$ because these are the margins in common use in control systems engineering.

- (iii) Only first order filters are to be used in the feedback law to obtain the necessary phase changes and attenuations. Notch filters will not be used to remove the response of an undesirable structural mode as this creates a sensitivity problem due to either inaccurate prediction of the modal frequency or its variation with flight conditions or fuel state.
- (iv) To avoid sensitivity to uncertainties in the control surface aerodynamics and the actuator transfer function, response of the higher frequency modes in the feedback signal will be filtered out.
- (v) No feedback gain and phase scheduling with speed will be considered.
- (vi) A common feedback system which can be used for all four cases will be searched for.

4.3 Design Procedure

For each case:

- (i) Produce Nyquist Plots at the design speed for a range of combinations of point load and transducer positions.
- (ii) Choose, for each Nyquist Plot from (i), a feedback gain and a filter which make the unstable modes stable, and the stable modes remain stable, with the best possible gain and phase margins.
- (iii) Choose the best force/transducer position combinations taking into account the Design Aims.
- (iv) For each of these chosen combinations produce Nyquist Plots for speeds below the design speed to see if a simple constant control law would satisfy the Design Aims at all speeds.
- (v) Find the maximum force required (from which the size and rotation of the control surface, and the actuator characteristics such as rate limit, are obtainable) by calculating the response of the controlled structure to a tuned 25 ft./sec. (1-cosine) gust at the design speed.

4.4 Point Force and Transducer Positions Investigated

The point force positions considered on the wing (Figure 4) were five spanwise stations at 55% chord (representing forces due to 25% chord trailing edge control surfaces) together with twenty chordwise positions near the wing tip. The wing transducer positions (Figure 4) were fifteen vertically and five measuring streamwise incidence.

The force and transducer positions on the stores (Figure 5) were vertical and lateral at each end of the store with two rotation transducers measuring store pitch and yaw. System designs using store excitation have been produced purely for comparison purposes, since it is well known that design of store excitation systems is relatively straightforward.

From operational considerations it is best to have both the control force and the transducer on the wing. Next best is the force on the wing and the transducer on the store. However, this combination is probably unacceptable because of the possible unreliability of any transfer function across the store/wing junction. Therefore the study has been with the force and transducer on the wing or both of them on the store.

5. RESULTS OF FLUTTER CONTROL SYSTEM DESIGN CALCULATIONS

5.1 Basic Aircraft Characteristics

Figures 6 and 7 show the basic aircraft flutter characteristics and the design speed frequencies and dampings.

At the design speed:

Case 1 has two instabilities, at 4.42 hz. (-1.56%) and 4.73 hz. (-1.08%). There is low damping in the stable roots at 10.47 hz. (1%) and 35.04 hz. (1.48%).

Case 2 has an instability at 6.27 hz. (-1.87%) with very low damping at 8.09 hz. (0.26%) and low damping at 11.8 hz. (0.98%) and 24.8 hz. (1.31%).

Case 3 has two instabilities, at 6.28 hz. (-1.93%) and 6.73 hz. (-6.12%) with low damping in the stable root at 9.57 hz. (0.88%).

Case 4 has an instability at 7.04 hz. with a small negative damping of -0.42%. However the second root at 6.21 hz. has an extremely small positive damping of 0.06%. There is also low damping at 9.69 hz. (1.09%), 15.16 hz. (1.33%), 36.04 hz. (1.49%) and 56.31 hz. (2.09%).

5.2 Chosen feedback systems

The Nyquist Plots for all combinations of force and transducer position, for all four cases at their design speeds were produced. Then the Nyquist Plots for the most promising force and transducer positions were produced for speeds below the design speeds. From these the chosen best nine combinations of force and transducer on the wing are shown in Figure 8.

5.3 Case 1 Force and Transducer on the wing (Figure 9)

From the point of view of double anticlockwise encirclement of the (-1,0) point to stabilise the two instabilities at 4.42 and 4.73 hz. the only forces at 55% chord to give reasonable results are P12 and P96.

For these force positions, the useful transducer positions are W1, W12, W21 and $\propto 110$ to $\propto 114$.

However, higher modes (in particular, 16.4 hz. and 30.4 hz.) cannot be filtered out using first order filters (either single or in cascade) so they can only be removed by double integration and changing the sign of the feedback gain.

The best remaining of these is P96/ $\propto 110$.

For $\propto 110$, loads were considered at a range of chordwise positions along the wing tip. From these the chosen feedbacks are P90 and P100. As the gain and phase margins are similar for these two load positions any force position between these two (including P96) can be expected to be as acceptable. This has the advantage of insensitivity of the feedback system to centre of pressure of the aerodynamics.

Whereas the gain margins are adequate, the phase margins at the design speed are as low as $\pm 30^\circ$. These phase margins improve as the speed decreases.

5.4 Case 2 Force and Transducer on the Wing (Figure 10)

P12 excites the unstable mode well relative to the other modes. For P12/W85, the velocity feedback will have to be integrated to avoid large response at high frequency and a high pass filter is then required to remove the low frequency response and balance the phase margins.

As the force moves outboard along the 55% chord line, the Nyquist Plots are spoilt by higher mode response, particularly the 8.09 hz. mode, which tend to distort the flutter mode circle. This is noticeable with P100/W43 where the 8.09 hz. response is the reason for the low ($\pm 25^\circ$) phase margins. Note that this 8.09 hz. mode has only 0.26% critical damping and its effect would be considerably reduced if it were given 1% structural damping!

Similarly, but more realistically, the other chosen feedback, P90/ $\propto 110$ loses phase margin because the large response in the 6.22 hz. stable mode distorts the flutter mode circle.

5.5 Case 3 Force and Transducer on the Wing (Figure 11)

Again, double encircling of the (-1,0) point is required. For transducers at 55% chord along the wing and wing tip forces between 25% and 75% chord : most plots are spoilt either by large responses in higher modes, particular in the lightly damped 9.6 hz. mode, or by poor phase margins due to distortion of the 6.73 hz. mode response.

Of the chosen, P90/W1 has small phase margins at the design speed ($\pm 32^\circ$) and would benefit from phase scheduling with speed because of the large phase lag of the unstable modes going from the design speed to the flutter speed.

For P100/W85 the phase margins are very small ($< \pm 15^\circ$)

5.6 Case 4 Force and Transducer on the Wing (Figure 12)

Whereas we would expect the 7.04 hz. mode to be easy to stabilise because it is only just unstable (-0.43% critical damping), the presence of the extremely lightly damped (+0.07%) mode nearby at 6.22 hz. creates problems.

Because of this, and the large response in the 36 hz. mode when the loading is aft on the wing tip, the best force position is forward on the wing tip.

Hence, P90/W1 and P90/ $\propto 114$ were selected. Both give good gain and phase margins.

5.7 Effect of Flutter Control System at Off-Design Conditions

Figure 13 shows a typical variation of Nyquist Plot with speed. The example given is for inboard slope ($\propto 110$) feedback to a wing tip trailing edge control surface (P100) for case 1 at speeds below the design speed. The second and third Nyquist Plots show the second root lobe expanding as the speed reduces and the root becomes less unstable (0.473 VR) until it has a 180° phase shift and rotates clockwise when it becomes stable (0.414 VR). The next two Nyquist Plots show the same happening to the first unstable root going from 0.355 VR to 0.296 VR.

As the speed reduces further, the lobes contract (0.237 VR) as damping increases, then expand (0.118 VR) as the aerodynamic dampings reduce. With the reduction of the aerodynamic forces, the lobes rotate towards the zero speed phasing.

At very low speed there is generally a danger of feedback instability due to very low open loop damping (structural alone) and a 180° phase shift because the inertia force now dominates the control surface force. This is particularly so when velocity feedback is used.

Figure 14 shows the corresponding closed loop frequencies and dampings against speed. Also shown are the gain and phase margins.

Figure 15 shows, for the same feedback law, the closed loop frequencies and dampings against feedback gain at the design speed. Notice there is a maximum possible closed loop damping of about 3% for the first unstable root and about 1% for the second unstable root.

5.8 Summary of Results for Force and Transducer on the Wing

Figure 8 shows the chosen nine feedback systems with force and transducer on the wing.

For six of these, the force or transducer is at the inboard end of the wing where the modal deflections are small. Because of this, it is necessary to include the aircraft rigid body and fuselage modes in the analysis.

Also, the rigid body modes need to be included because the chosen control systems use displacement, or integrated displacement, feedback and it is necessary to check that high pass filters can be used to prevent the flutter control system from affecting the overall aircraft stability and control characteristics.

No common system inside the Design Aims was found, nor did it appear likely that one would be found even if gain and phase scheduling, and notch filters, were allowed.

However the best common system used a force at the wing tip at 25% chord (P90) together with inboard slope ($\alpha 110$) feedback for inboard stores and inboard leading edge displacement (W1) feedback for outboard stores. For this common system, the phase margin requirement would need to be relaxed to about $\pm 30^\circ$ at 5 hz.

Therefore an all moving tip looks the most promising motivator but its aerodynamics forces are uncertain and need to be investigated.

5.9 Control Forces on the Store (Figure 16)

The feedback systems using a control force and transducer acting vertically on the store front are excellent because :

- (i) they provide $\pm 6\text{db}$ and $\pm 60^\circ$ margins at all speeds,
- (ii) a simple feedback law invariant with speed can be used,
- (iii) a common force/transducer position can be used for all four store/wing sweep/Mach Number combinations.

For each case, the behaviour of the velocity transfer function is like that of a system of uncoupled, lightly damped single degrees of freedom, where the unstable modes are separated from the stable modes by 180° giving perfect stability margins.

Also there is no response in higher frequency modes because each store on its pylon acts as a mechanical filter.

This mechanical filter and the velocity feedback remove the possibility of closed loop instability of high frequency modes. The velocity feedback reduces interference with the overall aircraft stability and control.

This is merely a manifestation of the importance of structural damping on store flutter which has provided, and continues to provide, effective passive flutter suppression.

6. GUST RESPONSE CALCULATIONS

The response to a 1-cosine gust of amplitude 25ft./sec. and tuned to give maximum response in the flutter modes was computed at the design speed at sea level with the feedback system operating.

This showed that the force that the control surface must be capable of producing to make this response stable depends upon its position.

Control Surface Position	Approximate Required Force
Wing Tip	3,000 lb
Wing Root	7,000 lb
Store Front	400 lb

These results show a surprisingly small difference between the required forces at the wing tip and wing root, and an even more surprisingly small force required on the store compared with the force required on the wing tip.

7. DISCUSSION OF RESULTS

This economical study has revealed that in order to proceed further we need a better representation of a wing tip control surface, including control aerodynamics, inertia and actuator.

Without this, no common feedback system could be found for a force and transducer on the wing which satisfied the Design Aims for all four cases. The difficulties were mainly due to

(i) two instabilities at very close frequencies

and (ii) very low dampings in some of the stable modes.

In addition, overall aircraft modelling is essential since problems with rigid body dynamics are likely.

It is possible that the search for a common system would be more successful if there was a better representation of the structural damping and the Design Aims were relaxed. In particular, it would be easier if the stability margin requirements were reduced. Also, using more than one transducer may help.

The excellent results for the force and transducer on the store are interesting but the difficulty in using such a system probably makes it impractical. However the small forces required on the store probably means that it is easy to suppress the flutter passively using a mechanical damper.

8. RECOMMENDATIONS FOR FURTHER WORK

- (1) Investigate the aerodynamics of an all moving wing tip
- (2) Confirm the flutter control efficiencies of the chosen systems when control surface aerodynamics and inertia, and total aircraft modes are included. Define the actuator requirements for active flutter control.
- (3) Investigate the effect of the active flutter control system on the clean wing stability. Define the actuator requirements to avoid introducing control surface flutter.
- (4) Investigate the effect on active flutter control requirements of:
 - (i) varying fuel distribution in the wing and store,
 - (ii) varying store attachment stiffness and inertia properties
 - (iii) using leading edge control surfaces.
- (5) Investigate the use of more than one transducer in a flutter control system.
- (6) Review the gain and phase margin requirements for a flutter control system.

9. CONCLUDING REMARKS

- (1) The procedure described here is based upon the use of Nyquist Plots. Using it with a point force to represent the loading due to a control surface on the wing facilitates an economic first assessment of the optimum position for an active flutter control system motivator.
- (2) For a variable sweep wing with underwing stores, no common active flutter control system using a control surface on the wing was found which gave good stability margins for four combinations of Mach Number, wing sweep and store configuration. The best common system found used an all moving wing tip.

The authors emphasise that the views expressed in this paper are their own.

This paper contains results which were achieved under contract for the British Ministry of Defence.

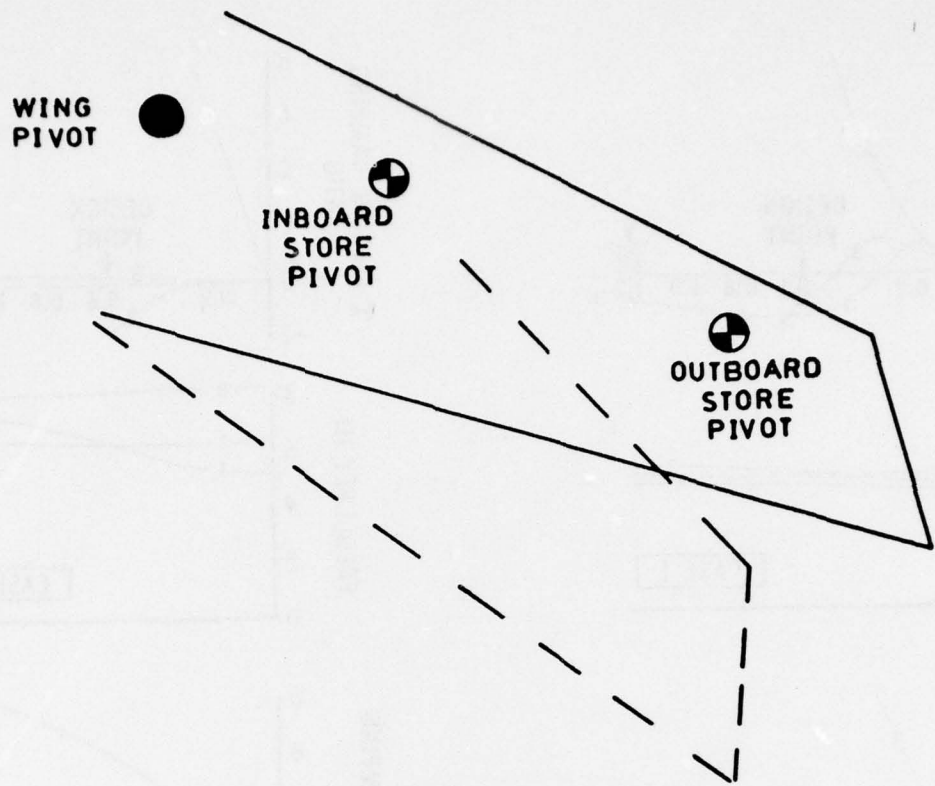


Fig.1 Swing wing

CASE	STORE AND POSITION	MACH NO.	WING SWEEP
1	STORE A INBOARD	0.8	25°
2	STORE B INBOARD	0.8	25°
3	STORE C OUTBOARD	0.9	45°
4	STORE C OUTBOARD	1.35	45°

Fig.2 Design cases

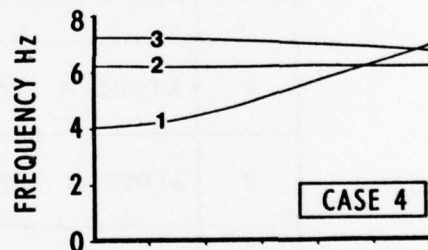
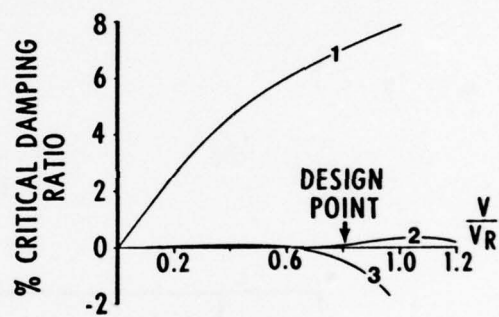
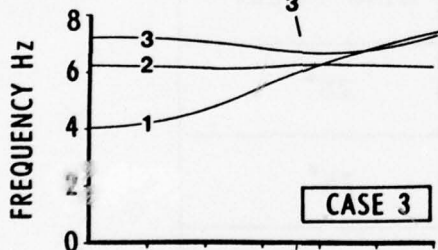
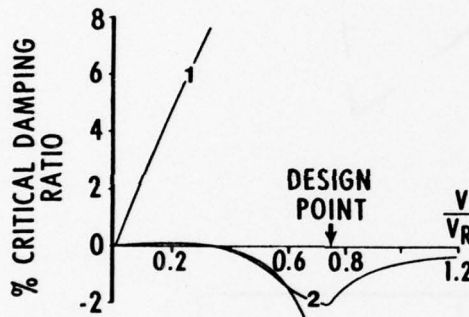
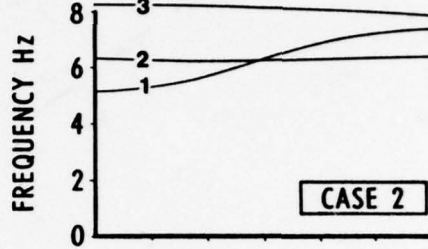
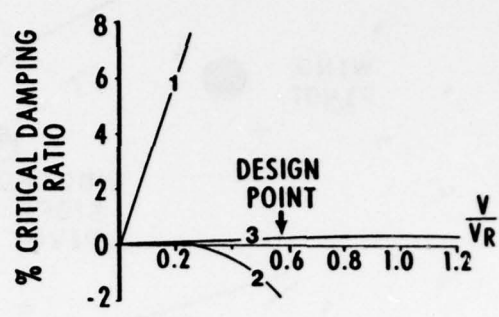
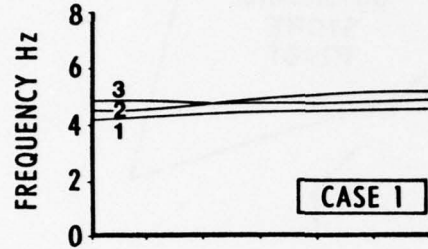
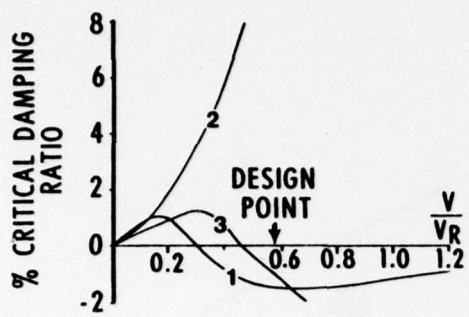
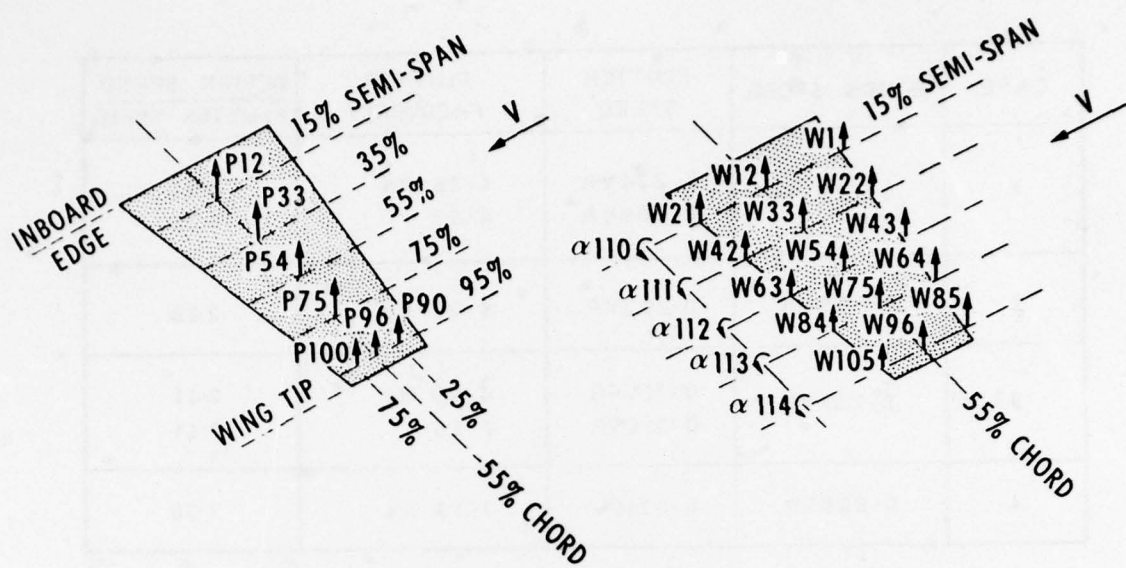


Fig.3 Basic aircraft flutter characteristics



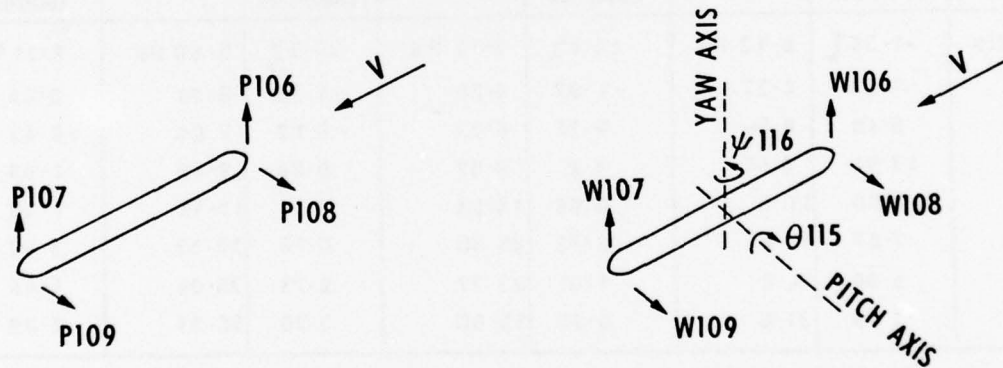
P85 to P105 are at 95% semi span at 5% chord
intervals from the leading edge to the trailing edge

α = WING INCIDENCE

FORCE POSITIONS ON THE WING
FIGURE 4a

TRANSDUCER POSITIONS ON THE WING
FIGURE 4b

Fig.4 Force and transducer positions on the wing



FORCE POSITIONS ON THE STORES
FIGURE 5a

TRANSDUCER POSITIONS ON THE STORE
FIGURE 5b

Fig.5 Force and transducer positions on the store

CASE	DESIGN SPEED	FLUTTER SPEED	FLUTTER FREQUENCY	DESIGN SPEED FLUTTER SPEED
1	0.575VR	0.296VR 0.459VR	4.36 Hz 4.73	1.94 1.25
2	0.575VR	0.252VR	6.30 Hz	2.28
3	0.757VR	0.314VR 0.314VR	6.20 Hz 7.15	2.41 2.41
4	0.805VR	0.621VR	7.13 Hz	1.30

VR = reference speed

Fig.6 Basic aircraft characteristics

CASE 1		CASE 2		CASE 3		CASE 4	
FREQUENCY	% CRITICAL DAMPING						
4.42 Hz	-1.56%	6.22 Hz	14.1%	6.11 Hz	20.9%	5.69 Hz	7.11%
4.73	-1.08	6.27	-1.87	6.28	-1.93	6.21	0.06
4.89	8.18	8.09	0.26	6.73	-6.12	7.04	-0.42
7.81	13.94	8.95	8.2	9.57	0.88	9.69	1.09
10.47	1.00	11.8	0.98	15.03	2.34	15.16	1.33
16.41	7.87	17.4	6.75	28.30	6.76	28.53	3.42
30.35	6.90	24.8	1.31	32.77	9.73	36.04	1.49
35.04	1.48	31.6	6.90	55.90	3.90	56.31	2.09

1% structural damping in normal modes 4 to 8

Fig.7 Design speed frequencies and damping

CASE	FORCE POSITION	TRANSDUCER POSITION	FILTER ON VELOCITY	GAIN K
1	P90	$\alpha 110$	$\frac{1}{S(S+79.4)}$	$-1.45 \times 10^8 \left(\frac{V}{0.575VR}\right)^2$
	P100	$\alpha 110$	$\frac{1}{S(S+62)}$	$-1.14 \times 10^8 \left(\frac{V}{0.575VR}\right)^2$
2	P12	W85	$\frac{1}{S}$	$3.8 \times 10^5 \left(\frac{V}{0.575VR}\right)^2$
	P90	$\alpha 110$	$\frac{1}{S+22.5}$	$-2.2 \times 10^6 \left(\frac{V}{0.575VR}\right)^2$
	P100	W43	$\frac{1}{S}$	$7.8 \times 10^5 \left(\frac{V}{0.575VR}\right)^2$
3	P90	W1	$\frac{1}{S}$	$1.64 \times 10^7 \left(\frac{V}{0.757VR}\right)^2$
	P100	W85	$\frac{1}{S}$	$9.37 \times 10^5 \left(\frac{V}{0.757VR}\right)^2$
4	P90	$\alpha 114$	$\frac{1}{(S+6)^2}$	$5.11 \times 10^6 \left(\frac{V}{0.805VR}\right)^2$
	P90	W1	$\frac{1}{(S+6)^2}$	$-1.06 \times 10^8 \left(\frac{V}{0.805VR}\right)^2$

FEEDBACK LAW: $P = K f(s) \dot{W}$

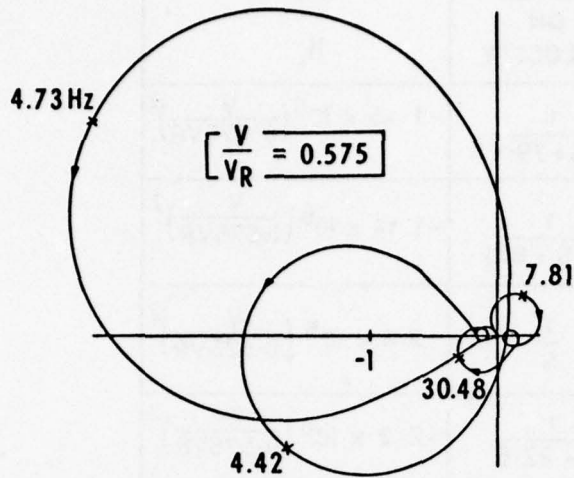
P = POINT FORCE

K = FEEDBACK GAIN

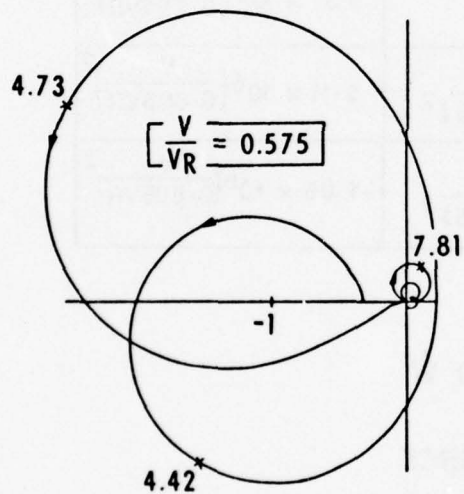
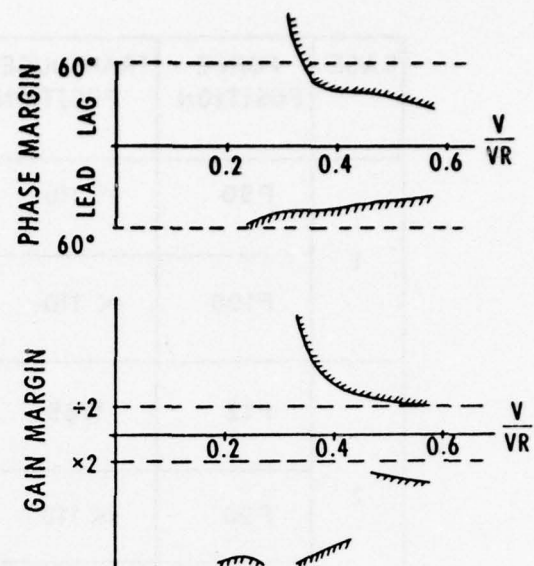
$f(s)$ = FEEDBACK FILTER

\dot{W} = STRUCTURAL VELOCITY

Fig.8 Chosen best flutter control systems with control surface on the wing



$$P_{90} = -1.45 \times 10^8 \frac{1}{S(S+79.4)} \left(\frac{V}{0.575 V_R} \right)^2 \alpha 110$$



$$P_{100} = -1.14 \times 10^8 \frac{1}{S(S+62)} \left(\frac{V}{0.575 V_R} \right)^2 \alpha 110$$

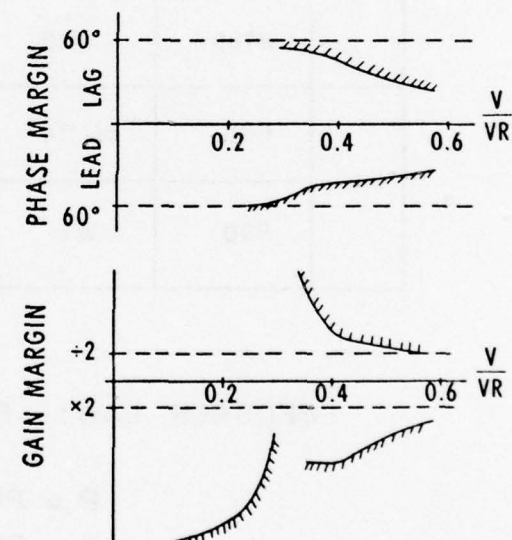
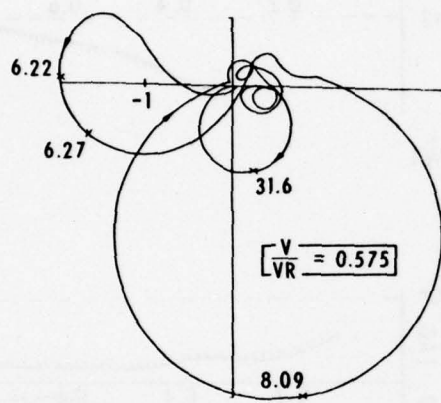
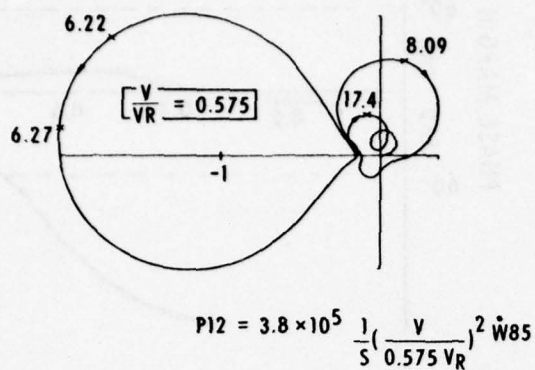
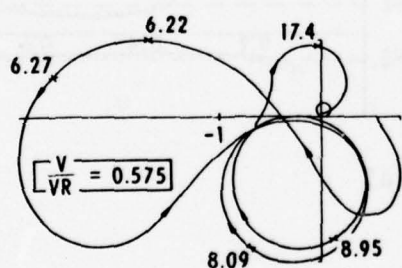


Fig. 9 Design speed Nyquist Plots and stability margins. Best wing feedback systems – Case 1



$$P_{90} = -2.2 \times 10^6 \frac{1}{(s+22.5)} \left(\frac{V}{0.575 V_R} \right)^2 \alpha 110$$



$$P_{100} = 7.8 \times 10^5 \frac{1}{s} \left(\frac{V}{0.575 V_R} \right)^2 W_{43}$$

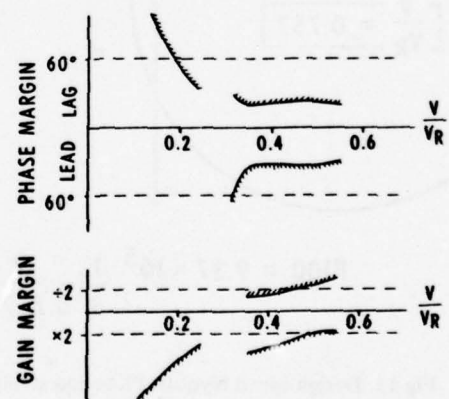
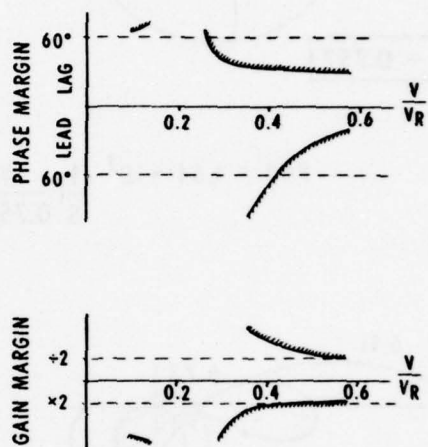
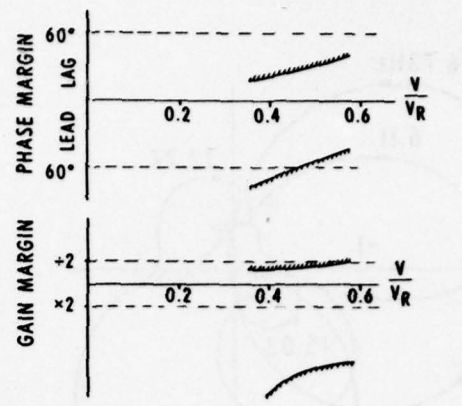
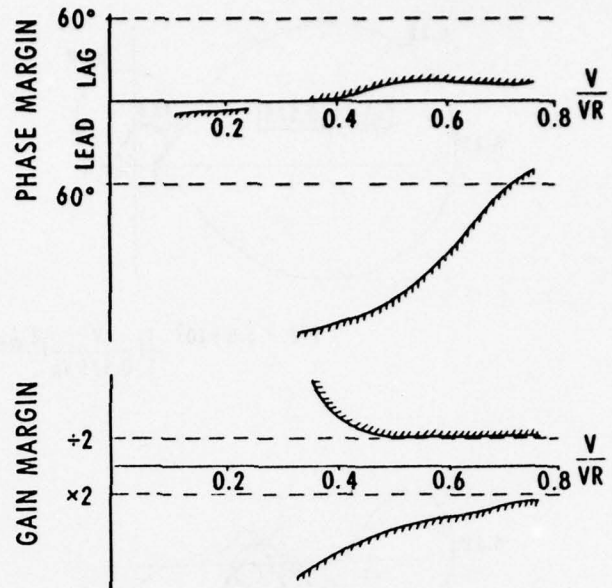
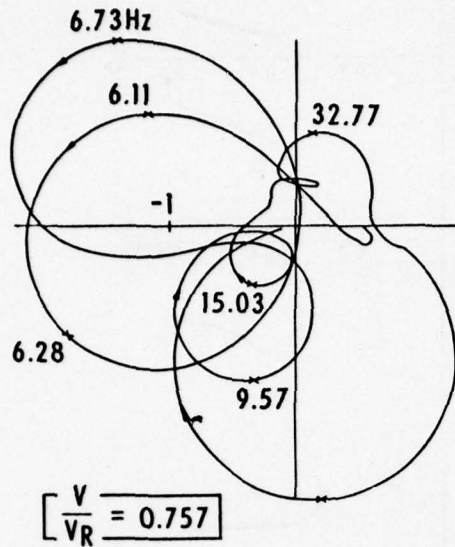
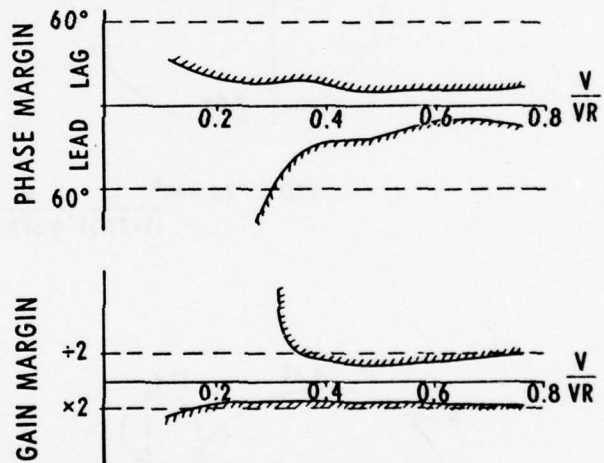
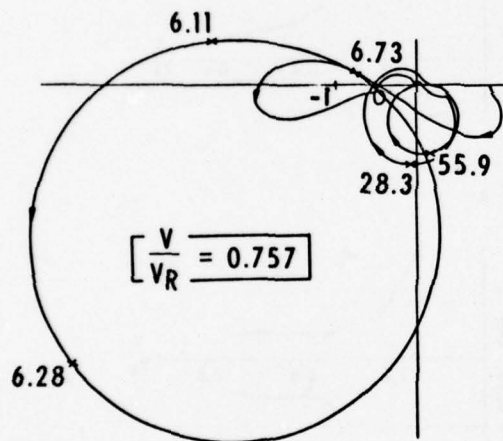


Fig.10 Design speed Nyquist Plots and stability margins. Best wing feedback systems – Case 2

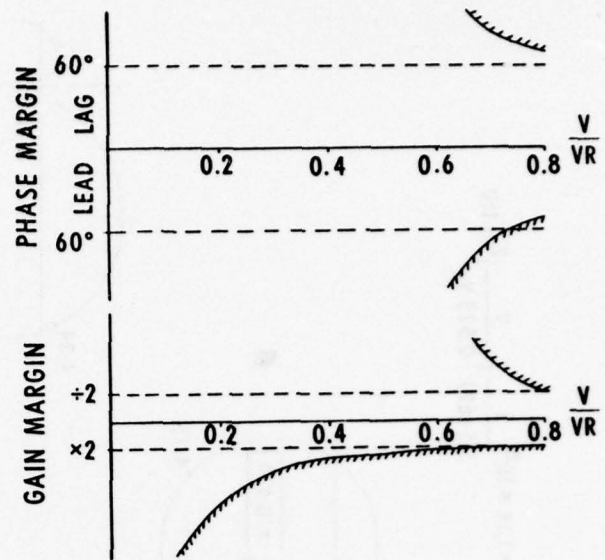
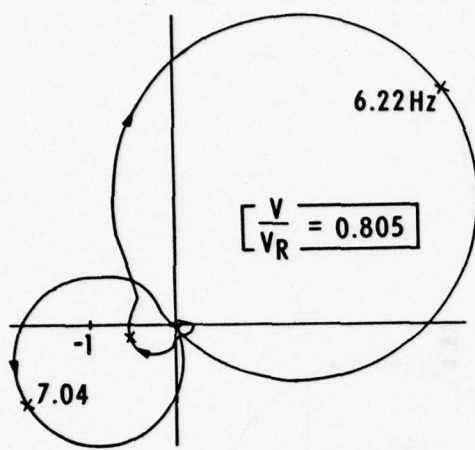


$$P_{90} = 1.64 \times 10^7 \frac{1}{s} \left(\frac{V}{0.757 V_R} \right)^2 W_1$$

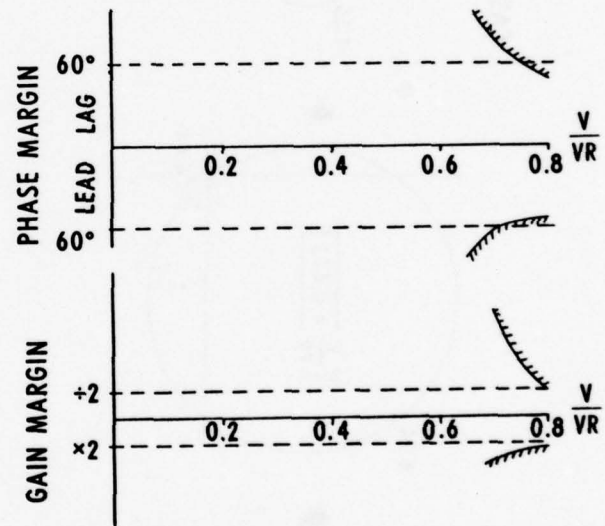
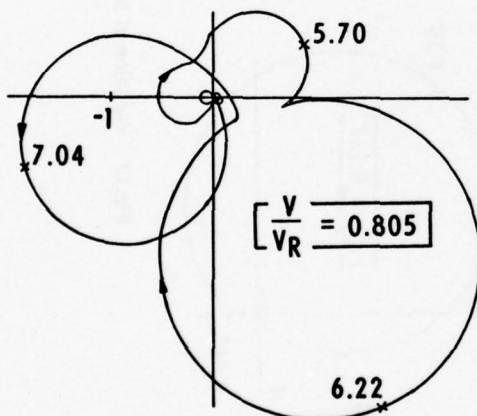


$$P_{100} = 9.37 \times 10^5 \frac{1}{s} \left(\frac{V}{0.757 V_R} \right)^2 W_{85}$$

Fig.11 Design speed Nyquist Plots and stability margins. Best wing feedback systems – Case 3



$$P90 = 5.11 \times 10^6 \frac{1}{(S+6)^2} \left(\frac{V}{0.805 V_R} \right)^2 \approx 114$$



$$P90 = -1.06 \times 10^8 \frac{1}{(S+6)^2} \left(\frac{V}{0.805 V_R} \right)^2 \approx 114$$

Fig.12 Design speed Nyquist Plots and stability margins. Best wing feedback systems – Case 4

CASE 1 — $P_{100} = -1.14 \times 10^8 \frac{1}{s(s+62)} \left(\frac{V}{0.575 V_R} \right)^2 \alpha 110$

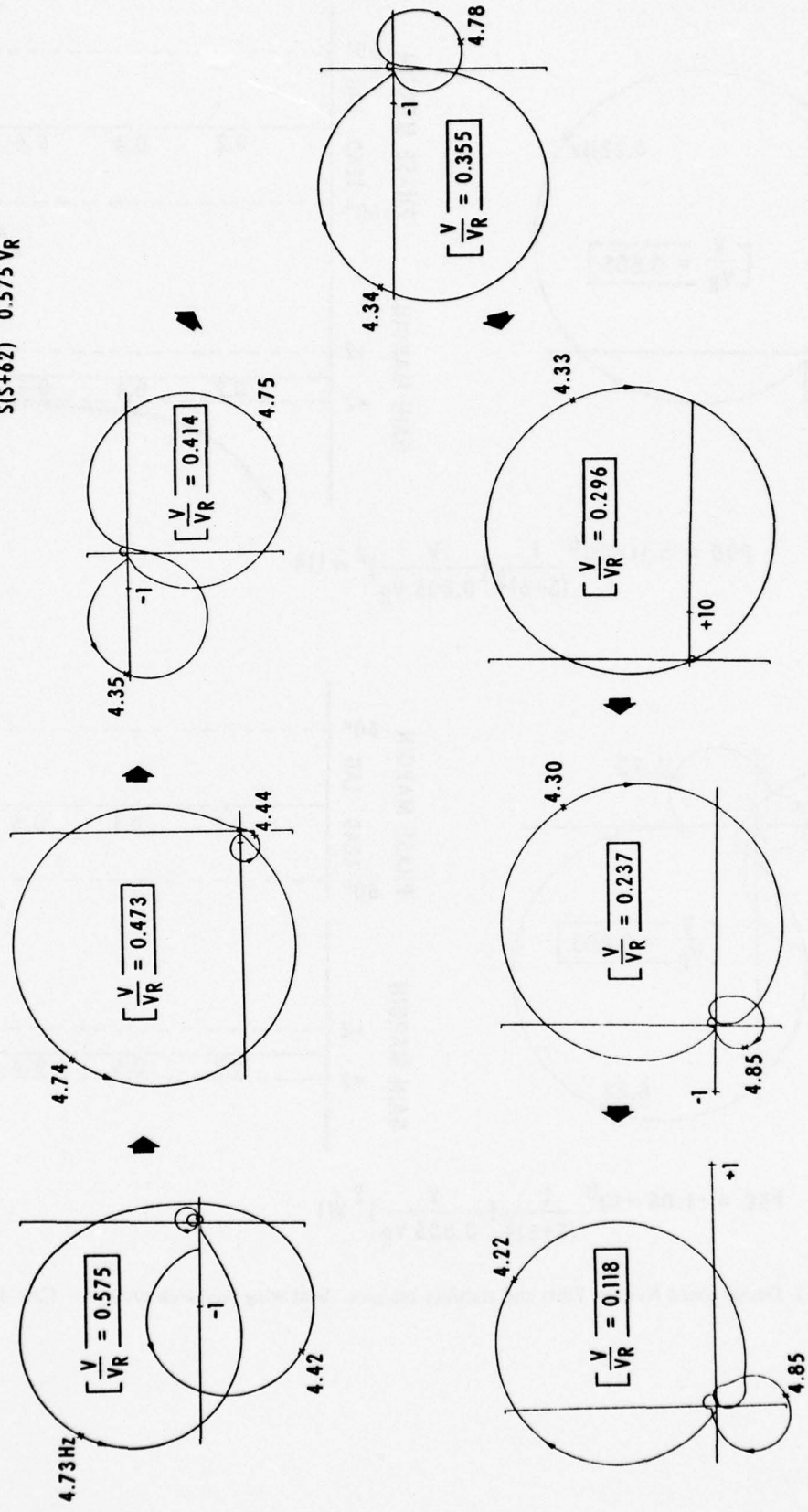
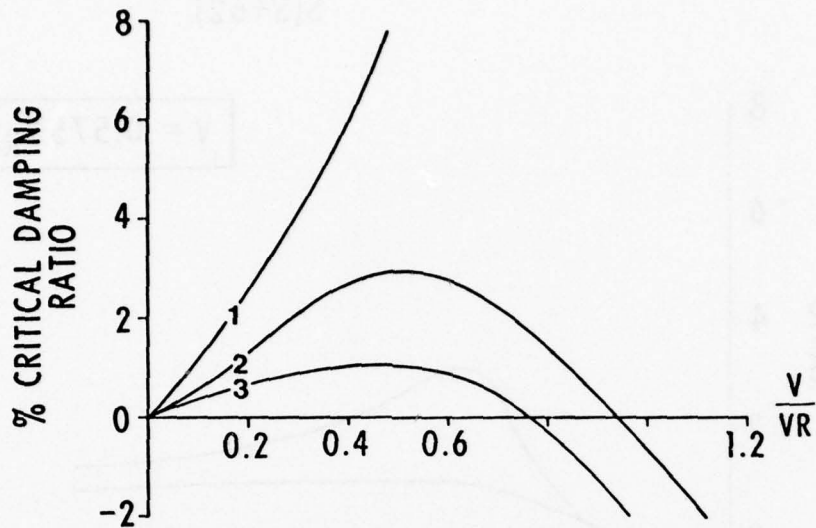


Fig.13 Variation of Nyquist Plots with speed

$$\text{CASE 1} - P_{100} = -1.14 \times 10^8 \frac{1}{S(S+62)} \left(\frac{V}{0.575 V_R} \right)^2 \approx 110$$



$\frac{V}{V_R}$	GAIN MARGIN		PHASE MARGIN	
	\times	\div	LEAD	LAG
0.575	3.1	2.0	34°	25°
0.473	4.7	2.7	40°	35°
0.414	6	3.1	42°	44°
0.355	6	6.3	45°	52°
0.296	4	∞	55°	55°
0.237	10	∞	59°	> 90°
0.118	12	∞	> 90°	> 90°

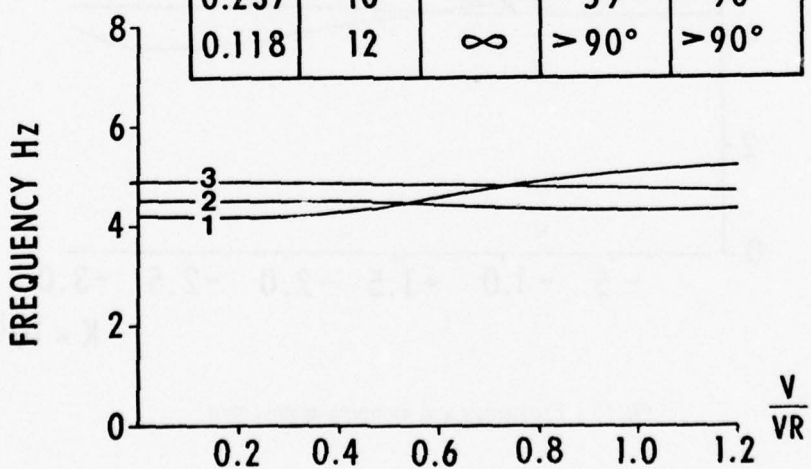


Fig.14 Frequency and damping against speed

CASE 1 — $P_{100} = K \frac{1}{S(S+62)} \dot{\alpha} 110$

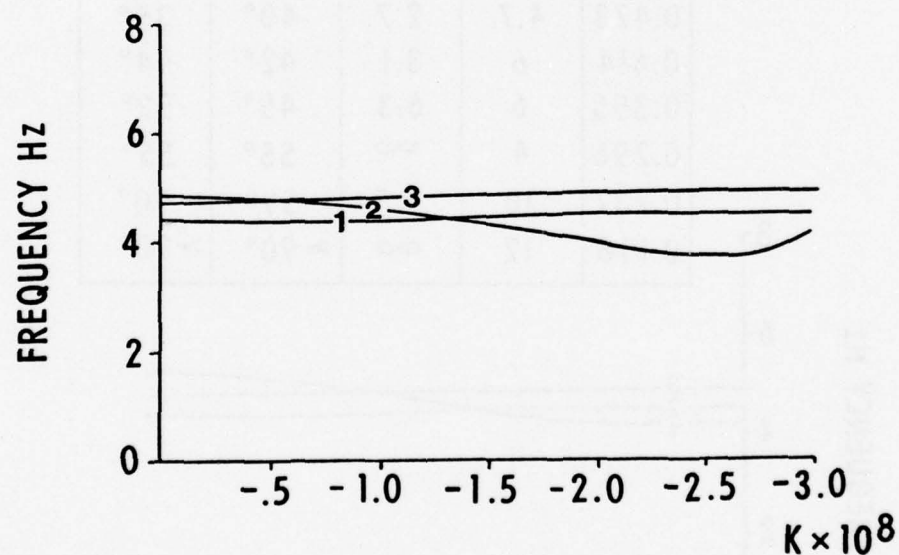
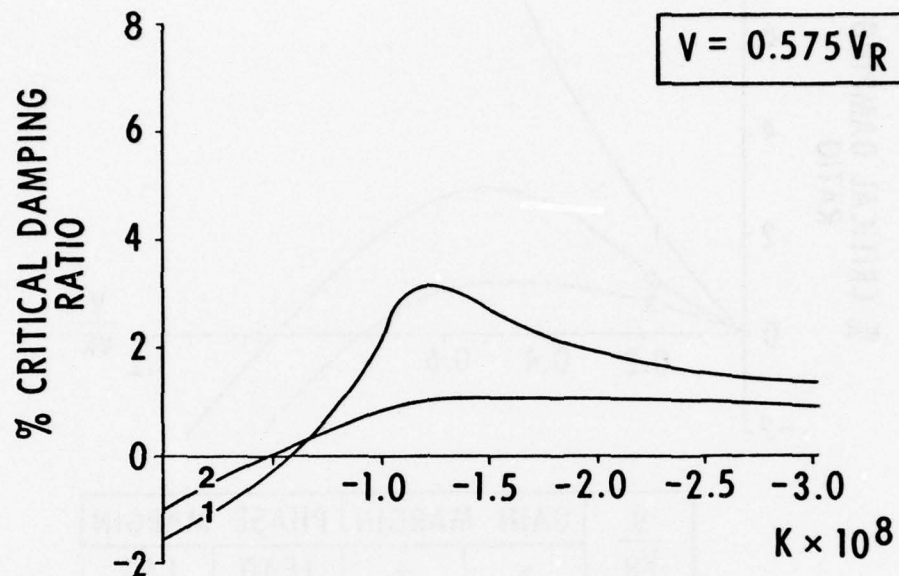


Fig.15 Frequency and damping against gain

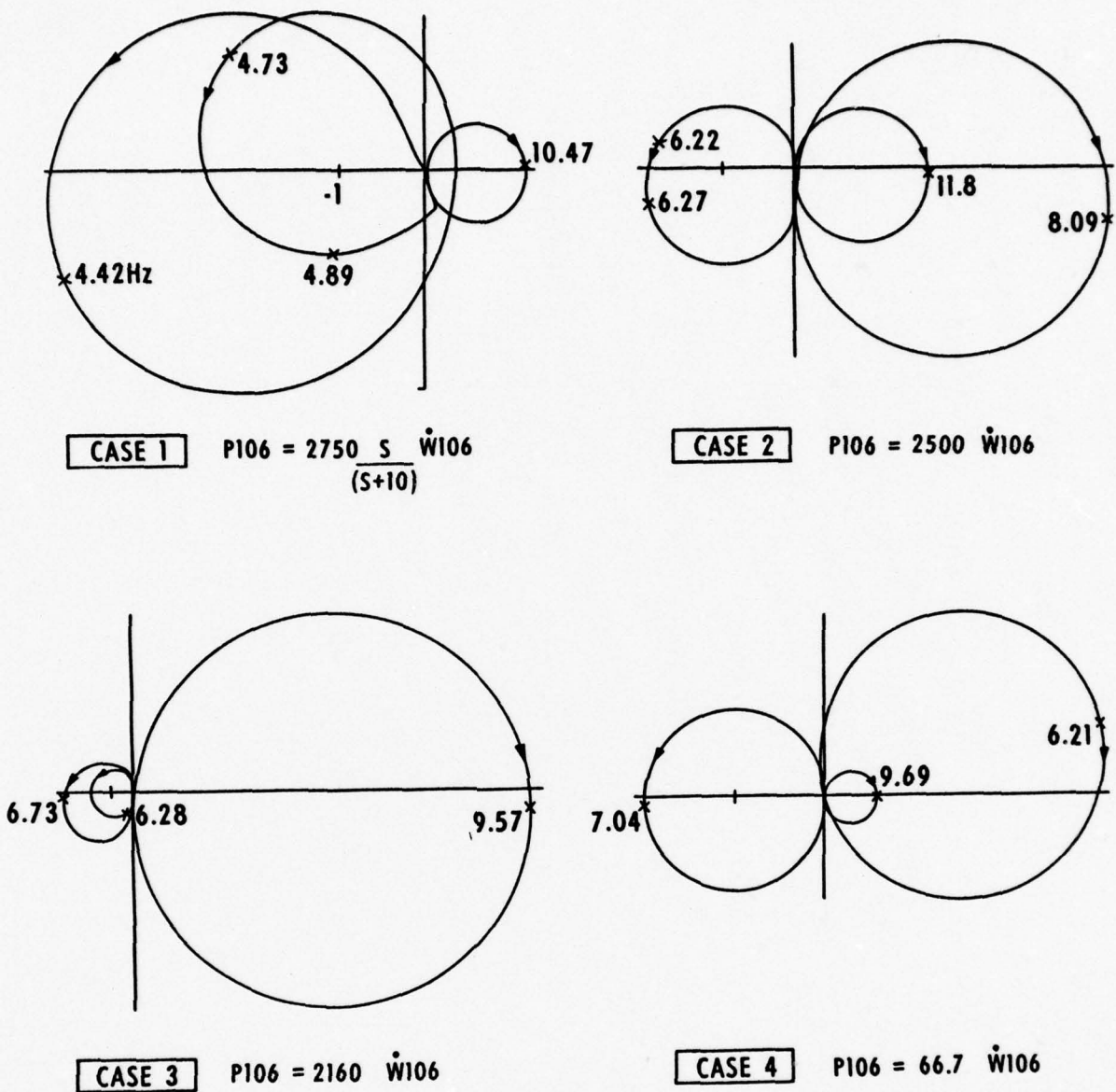


Fig. 16 Design speed Nyquist Plots. Force and transducer vertical on store front

**IMPACT OF A COMMAND AND STABILITY AUGMENTATION SYSTEM ON GUST
RESPONSE OF A COMBAT AIRCRAFT**

by

K.D. COLLMANN

VEREINIGTE FLUGTECHNISCHE WERKE - FOKKER GmbH.
2800 Bremen 1, Postfach 1206 - W.-Germany

and

O. SÈNSBURG

MESSERSCHMITT-BÖLKOW-BLOHM GmbH.
Unternehmensbereich Flugzeuge
8 München 80, Postfach 801160 - W.-Germany

INTRODUCTION

Calculations of transfer functions to predict the structural response of elastic aircraft to gust, manoeuvres, or landing impact excitation are becoming increasingly elaborate, and yet produce results which show only limited agreement with experimental results in return for extensive and time-consuming computation. The theoretical principles and their linearized versions required for these computations are well known. In order to reduce the discrepancies between theoretical and experimental results, input data, interim results, and part of the final results of the calculations are compared with corresponding experimental results and corrected to agree with those, Ref.[1], [2], [3].

To get reasonable results for gust response calculations it is necessary to introduce the elastic aircraft behaviour as well as the command and stability augmentation system (CSAS) into the mathematical model. Once these techniques are established they can be used for any kind of control law including CCV technologies.

In this paper it is demonstrated how calculation results are influenced by using aerodynamic interference air forces. In the second part the influence of the CSAS is presented. Considering that all important elastic degrees of freedom are used together with a CSAS-model and unsteady air forces are calculated with interference influence the analysis becomes very expensive and computer-time-consuming. To reduce this heavy work load it is necessary to find out negligible parameters and also highlight the influence of important ones.

The figures in this paper show that the influence of the CSAS on the dynamic response is of prime interest and often exceeds the influence of the elastic structure by far.

It is also shown that the unsteady aerodynamic forces should be determined with three-dimensional theories including interference and that corrections to match the steady derivatives measured in the wind tunnel should be made.

The impedance function, control loop transfer functions are highly nonlinear due to the nonlinearities of the hydraulic actuators. All these functions must be determined experimentally and introduced into the elastic aircraft equation. Response plots of the total system should be calculated and compared with results of so-called "structural mode coupling tests". If correlation is good a major part for the investigation of structural response of the aircraft due to various input functions is verified.

1. SYMBOLS

$\underline{A}(\omega)$	defined in equation (3)
\underline{D}	matrix of generalized structural damping
$\underline{H}(\omega)$	vector of frequency response function relating the response of generalized coordinates to a sinusoidal turbulence
$\underline{H}_o(\omega)$	vector of frequency response function relating the aircraft response to a sinusoidal turbulence
i	$\sqrt{-1}$
k	reduced frequency
\underline{K}	generalized structural stiffness matrix
\underline{M}	generalized mass matrix
N_0	number of zero crossings
\underline{q}	vector of generalized coordinates
\underline{q}^2_x	variance function or mean square
$\underline{T}_{\beta x}$	matrix of actuator transfer functions
$\underline{T}_{\beta \beta}$	matrix of control surface impedance
\underline{T}_{Rq}	matrix of frequency response functions of CSAS relating the actuator input to a sinusoidal displacement of the generalized coordinates
\underline{T}_{Sq}	matrix of frequency response functions of CSAS relating the actuator input to a sinusoidal displacement of the generalized coordinates
\underline{T}_g	matrix of frequency response functions relating the required aircraft response to sinusoidal generalized coordinates
$\underline{x}(t)$	vector of output functions
\underline{x}_e	actuator input displacement
$\underline{X}(\omega)$	vector of Fourier transformations for \underline{x}
$\underline{y}(t)$	vector of input functions
$\underline{Y}(\omega)$	vector of Fourier transformations for \underline{y}
$\underline{\beta}$	vector of control surface deflections
$\underline{\Phi}_x(\omega)$	input power spectral density
$\underline{\Phi}_y(\omega)$	output power spectral density
$\underline{\Omega}_M$	vector of generalized forces due to motion
\underline{Q}_M	matrix of generalized forces due to sinusoidal displacements of generalized coordinates

\underline{Q}_D	vector of generalized forces due to excitation
\underline{Q}_R	vector of generalized forces due to CSAS
ω	circular frequency

2. THE EQUATION OF MOTIONS OF A FREE ELASTIC STRUCTURE WITH CSAS

To describe the dynamical behaviour of an elastic structure that can move freely in the space the following assumption must be made:

- a) The elastomechanical behaviour can be described by linear equations. This assumes that the elastic deformations are small compared with the dimensions and the motions of a structure and it requires the validity of the Hooke's Law.
- b) The dynamical behaviour can be described by linear relations. This implies the applicability of the small perturbations method.
- c) The specific weight of a structure is invariant (for instance fuel consumption is not considered).
- d) The elastic structure having an infinite number of degrees of freedom will be replaced by a system with a limited number of degrees of freedom. For this idealization it does not matter whether the deformations are a finite sum of assumed modes or whether they are described by the motions of a finite number of discrete elements.

A system of linear equations can be written in a matrix form.

$$\underline{M}\ddot{\underline{q}} + \underline{D}\dot{\underline{q}} + \underline{K}\underline{q} = \underline{\bar{Q}}_M(\underline{\dot{q}}, \underline{\dot{q}}, \underline{q}) + \underline{\bar{Q}}_D(t) \quad (1)$$

The order of the quadratic matrices and the number of column of the vectors is determined by the number of rigid body and elastic modes which are considered. The elastic modes used are the primary vibration modes of the free-free elastic structure. This is a common but not necessary procedure. If the orthogonal coordinate system having its origin in the center of gravity is referred to the principal axes of the structure then the matrix of generalized masses \underline{M} and generalized stiffnesses \underline{K} is a diagonal matrix because the rigid body degrees of freedom as well as the elastic degrees of freedom fulfil the known orthogonality condition. For the elastic degrees of freedom the elements of matrix \underline{D} are the generalized structural dampings. The generalized forces on the right side of the equation are arising from motions (\underline{Q}_M) and from excitations (\underline{Q}_D).

This paper deals only with the solutions of the equations in the frequency domain, Ref. [4]. Choosing this method has the advantage that the important functions - actuator impedance, CSAS transfer functions and unsteady aerodynamic airforces - are available in the frequency domain. The PSD-Analysis to determine structure fatigue life is a direct result of this method. The Fourier transformation of equation (1) leads to

$$[-\omega^2 \underline{M} + i\omega \underline{D} + \underline{K} - \underline{Q}_M(\omega)] \underline{q} = \underline{Q}_D(\omega) \quad (2)$$

or

$$\underline{A}(\omega) \underline{q} = \underline{Q}_D(\omega)$$

with

$$\underline{A}(\omega) = -\omega^2 \underline{M} + i\omega \underline{D} + \underline{K} - \underline{Q}_M(\omega) \quad (3)$$

The transfer function of the elastic system can be determined from

$$\underline{H}(\omega) = [\underline{A}(\omega)]^{-1} \underline{Q}_D(\omega) \quad (4)$$

The frequency responses of other parameters like the total motions, the velocities, accelerations and of the forces, moments and stresses can be described by the transformation

$$\underline{H}_G(\omega) = \underline{T}_0 \underline{H}(\omega) \quad (5)$$

This transformation is usually replaced by other analysis methods for the sake of numerical accuracy, Ref. [4]. With any kind of deterministic excitation the response in the frequency domain can be calculated from

$$\underline{X}(\omega) = \underline{H}_G(\omega) \underline{Y}(\omega) \quad (6)$$

where $\underline{Y}(\omega)$ is the Fourier transform of the excitation. The response in the time domain is defined by the transformation

$$\underline{x}(t) = \int_0^\infty \underline{X}(\omega) e^{i\omega t} d\omega \quad (7)$$

For stochastic excitation the power spectral density of the response is obtained from

$$\Phi_x(\omega) = |\underline{H}_G(\omega)|^2 \Phi_y(\omega) \quad (8)$$

where $\Phi_y(\omega)$ is the power spectral density of the excitation. The variance or mean square values can be determined from

$$\bar{q}_x^2 = \int_0^\infty \Phi_x(\omega) d\omega \quad (9)$$

and the number of positive zero crossings from

$$N_{0i}^2 = \frac{1}{\bar{q}_{xi}^2} \int_0^\infty \omega^2 \Phi_{xi}(\omega) d\omega \quad (10)$$

In Fig. 1 the control system is shown. The aircraft is the system to be controlled. Responses of this system are the generalized coordinates \underline{q} .

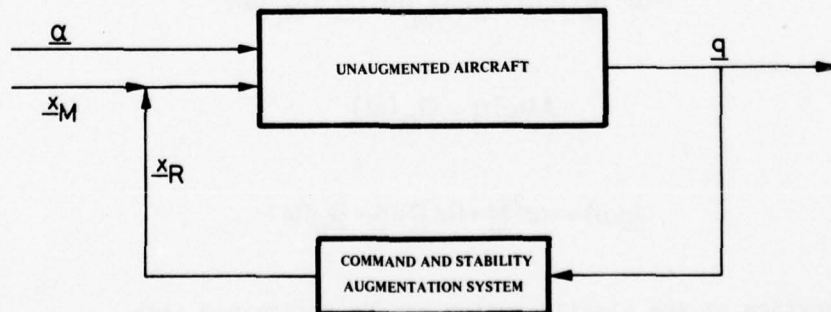


FIG. 1 BLOCKDIAGRAM OF THE AUGMENTED AIRCRAFT

The system is excited by gusts or buffeting (changes of the airplane angle of attack) or by manouevres (signals to the actuators of control surfaces). In addition to the external excitations the control system generates input signals to the actuators. The generalized excitation force of equation (2) can therefore be partitioned into the external excitation force and into the force produced by the control system.

$$\underline{A}(\omega) \underline{q} = \underline{Q}_D(\omega) + \underline{Q}_R(\omega) \quad (11)$$

The impedances of the hydraulic actuators are strongly frequency dependent. Calculation of frequencies and primary modes considering the actuator stiffnesses leads to an Eigenvalue problem with complex frequency dependent stiffnesses. It is not necessary to solve this problem if the normal modes are determined with infinitely stiff control surface attachments. The elastic deformation of the control surfaces must be contained in these modes. The degrees of freedom missing in these modes can be introduced later by additional attachment modes (secondary modes). It should be borne in mind that the orthogonality condition is no more fulfilled using primary modes and secondary modes. For this reason the mass matrix will have off diagonal elements.

The amplitudes of generalized coordinates for the primary modes will be described by the vector \underline{q} and for the control surface rotations (secondary modes) by the vector $\underline{\beta}$. Equation (11) can now be written down.

$$\begin{bmatrix} \underline{A}_{qq} & \underline{A}_{q\beta} \\ \underline{A}_{\beta q} & \underline{A}_{\beta\beta} \end{bmatrix} \begin{bmatrix} \underline{q} \\ \underline{\beta} \end{bmatrix} = \begin{bmatrix} \underline{Q}_{qD} \\ \underline{Q}_{\beta D} \end{bmatrix} + \begin{bmatrix} 0 \\ \underline{Q}_{\beta R} \end{bmatrix} \quad (12)$$

From the principle of the virtual-work it follows that the components of the amplitude vectors $\underline{Q}_{\beta R}$ are the moments of the control surfaces and these must be zero because the primary modes contain no control surface motions. The vector of the actuator moments shall be described by the following relation

$$\underline{Q}_{\beta R} = \underline{T}_{\beta X}(\omega) \underline{x}_e + \underline{T}_{\beta\beta}(\omega) \underline{\beta} \quad (13)$$

It is assumed that the dependence of the control surface moments from the actuator inputs can be described by linear transfer functions. The coefficients of the matrix $\underline{T}_{\beta\beta}$ are the control surface impedance which are the reaction moments of the actuators due to control surface motion. The second product of equation (13) is considered to be a part of $\underline{Q}_{\beta R}$. According to equation (11) $\underline{T}_{\beta\beta}$ is the matrix of control surface stiffnesses and therefore an additive term of matrix $\underline{A}_{\beta\beta}$.

Due to the motion of the airplane, input signals to the actuators of the control surfaces are generated. Since the motions of the elastic structure were developed in a finite number of rigid body modes and primary modes the input signals can be described as a function of generalized coordinates \underline{q} .

$$\underline{x}_e = \underline{T}_{Rq}(\omega) \underline{q} + \underline{T}_{Sq} \underline{q} \quad (14)$$

The coefficients of the matrix \underline{T}_{Rq} are the transfer functions of the control system including the sensors multiplied with the amplitudes of the primary modes at the sensor stations. The coefficients of the matrix \underline{T}_{Sq} are the input signals which for instance arise from mechanical inputs to the actuators due to different deformations of the structure and the control rods and are therefore determined by the vibration modes.

\underline{x}_e therefore only describes the actuator input signals introduced by the control system. Reactions of the actuator inputs due to control surface moments are not contained in \underline{x}_e . How to determine the matrix coefficients of equation (13) and equation (14) experimentally is described in Ref. [5], [6], [7] or the respective literature. If the control surfaces are not dependent upon each other then only the main diagonal elements of the matrixes of equation (13) and equation (14) are not zero. Equation (13) and equation (14) inserted in equation (12) give

$$\begin{bmatrix} \underline{A}_{qq} & \underline{A}_{q\beta} \\ \underline{A}_{\beta q} - \underline{T}_{\beta X}(\underline{T}_{Rq} + \underline{T}_{Sq}) & \underline{A}_{\beta\beta} - \underline{T}_{\beta\beta} \end{bmatrix} \begin{bmatrix} \underline{q} \\ \underline{\beta} \end{bmatrix} = \begin{bmatrix} \underline{Q}_{qD} \\ \underline{Q}_{\beta D} \end{bmatrix} \quad (15)$$

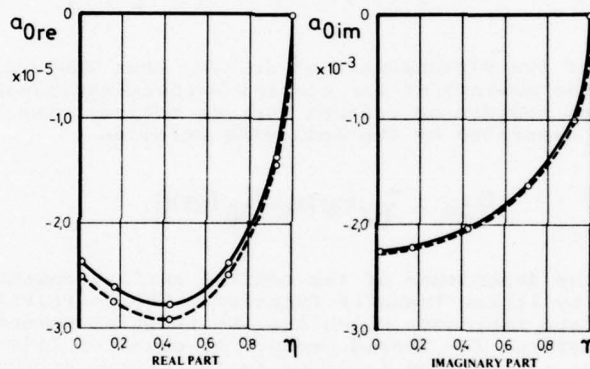
3. INTERFERING UNSTEADY AERODYNAMIC FORCES

The effect of interference between control surfaces of an aircraft in steady flow is well known and is introduced in flight mechanics by theoretical estimates and measurements. Neglecting these terms would lead to wrong flight mechanical results.

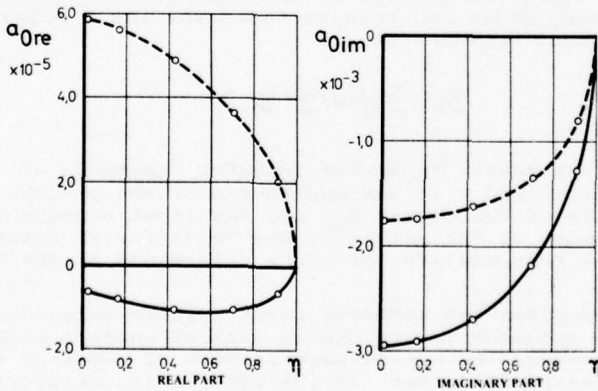
The aerodynamic interference is also important for unsteady flow. To estimate its impact is much more difficult considering that no corresponding unsteady measurements are available to aid these estimates. After a few flutter accidents especially on airplanes with T-tails the interference between harmonically oscillating surfaces was analytically investigated. The first topic which was investigated was the interference between tailplane and fin especially for the T-tail, Ref. [8], [9]. After instabilities created between tail and wing interference became known the theoretical investigation of interference between all surfaces was considered, Ref. [10]. A surface method was developed by B. Laschka which was used to create the results shown here, Ref. [11]. Experimentally the method was substantiated by J. Becker in Ref. [12]. The unsteady rudder air forces were calculated with the so-called equivalent slope method, Ref. [13]. Good correlation of these analytical air forces with experiment was presented in Ref. [14].

In earlier gust calculations without the complete consideration of the theoretical interference the downwash of the wing on the tailplane was estimated and considered by introducing a downwash factor for harmonical motion. This downwash (due to motion) depends upon the angle of attack of the wing and can be easily introduced for the heave motion ($\alpha = \text{constant}$) but for an arbitrary α -distribution on the wing a useful estimate is extremely difficult.

Fig. 2 shows analytical air force distributions in spanwise direction with and without interference for the symmetrical case (heave-motion) on the wing and on the tailplane. For the wing there is practically no interference effect whereas on the tailplane there is a considerable reduction of the air force and also a reversed phase.



AIR FORCE DISTRIBUTION ON THE WING DUE TO HEAVE MOTION



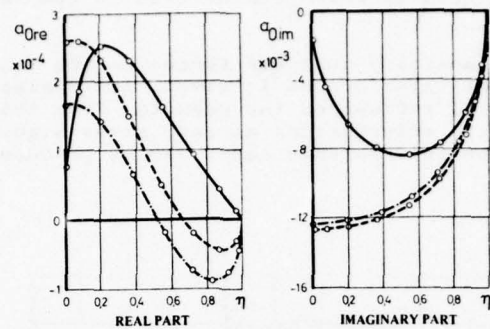
AIR FORCE DISTRIBUTION ON THE TAILPLANE DUE TO HEAVE MOTION

—○— WITH AERODYNAMIC INTERFERENCE
—●— WITHOUT AERODYNAMIC INTERFERENCE

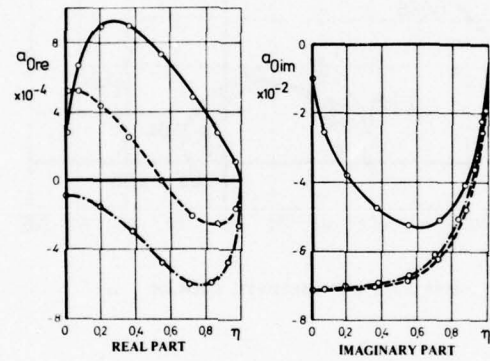
FIG. 2 AIR FORCE DISTRIBUTIONS ALONG THE SPAN DUE TO HEAVE MOTION ($k = 0.05$)

Fig. 3 shows corresponding results for antisymmetrical motion of fin and tailplane. The air force distributions on the fin show in addition to the results with and without interference the results of the calculation with a fin which is symmetrically extended. It is shown that this method almost gives the same results for the fin as the consideration of interference. For the tailplane there are considerable differences.

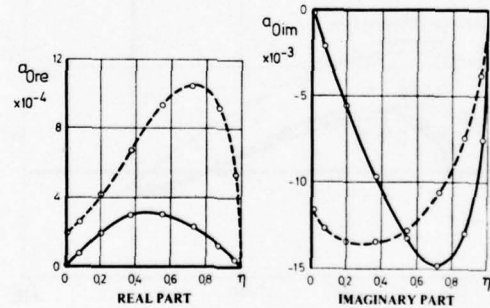
The last section of this chapter deals with the correction of analytically determined air forces by measured values. Between calculated and experimental air force distributions and their corresponding derivatives there are differences which cannot be neglected. There are various reasons of this differences like boundary layer thickness effects, fuselage interference etc. In general there are only test results for steady flow available, mainly derivatives for certain parts or for the total airplane.



AIR FORCE DISTRIBUTION ON THE FIN DUE TO LATERAL TRANSLATION



AIR FORCE DISTRIBUTION ON THE FIN DUE TO YAW MOTION



AIR FORCE DISTRIBUTION ON THE TAILPLANE DUE TO ROLL MOTION

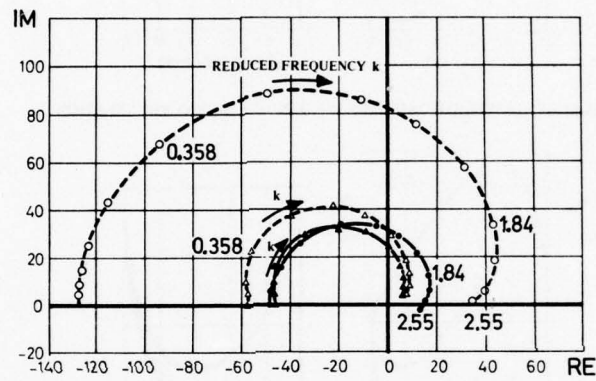
	} NO INTERFERENCE
	INTERFERENCE

FIG. 3 AIR FORCE DISTRIBUTIONS ON FIN AND TAILPLANE

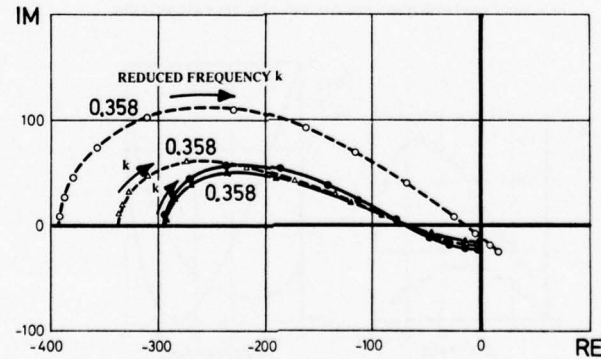
Unsteady pressure distribution measurements especially for elastic motions are very seldomly available so that a correction of theoretical air forces due to elastic motions is practically impossible.

For the rigid body modes a correction of the theoretical air force distribution and/or derivatives is possible and necessary because usually test results are available and the loads are mainly determined by rigid body modes. To adjust the theoretical derivatives to test results the analytically determined downwash is modified locally or globally depending whether a distribution measurement or measured derivatives for the rigid body modes are available. For that reason it is necessary to find a correspondence between the stationary flight mechanical and the unsteady aeroelastical method. For the stationary case ($k \rightarrow 0$) these relations can be found. It should be noted here that the two-dimensional unsteady theory is not applicable for some derivatives because there stationary values ($k \rightarrow 0$) become singular whereas the three-dimensional theory leads to useful results which can be used to complete the stationary derivatives.

In Fig. 4 a comparison of unsteady gust air forces on the tailplane and on the total aircraft with and without interference is given. It is also shown how a matching of the stationary values ($k = 0$) influences the results. From this picture one can deduce that the calculation with interference already gives a good match of the stationary values. Not considering the interference aerodynamics produces much bigger gust forces on the tailplane.



GENERALIZED GUST FORCE ON THE TAILPLANE



GENERALIZED GUST FORCE ON THE TOTAL AIRCRAFT

<ul style="list-style-type: none"> $\cdots\triangle\cdots$ WITH INTERFERENCE $\cdots\circ\cdots$ WITHOUT INTERFERENCE 	} UNCORRECTED
<ul style="list-style-type: none"> \blacktriangle WITH INTERFERENCE \bullet WITHOUT INTERFERENCE 	} CORRECTED WITH STEADY WIND TUNNEL DERIVATIVA

FIG. 4 GENERALIZED GUST FORCE

4. IMPACT OF AERODYNAMIC INTERFERENCE ON THE DYNAMIC RESPONSE

The dynamic response calculations were made using the unsteady airforces described as follows:

- a) not interfering (corrected)
- b) interfering (corrected)
- c) interfering (not corrected)

In Fig. 5 the root shear force on tailplane and wing is presented for discrete gusts with various length. Here it is shown that the influence on the wing is small compared with that on the tailplane.

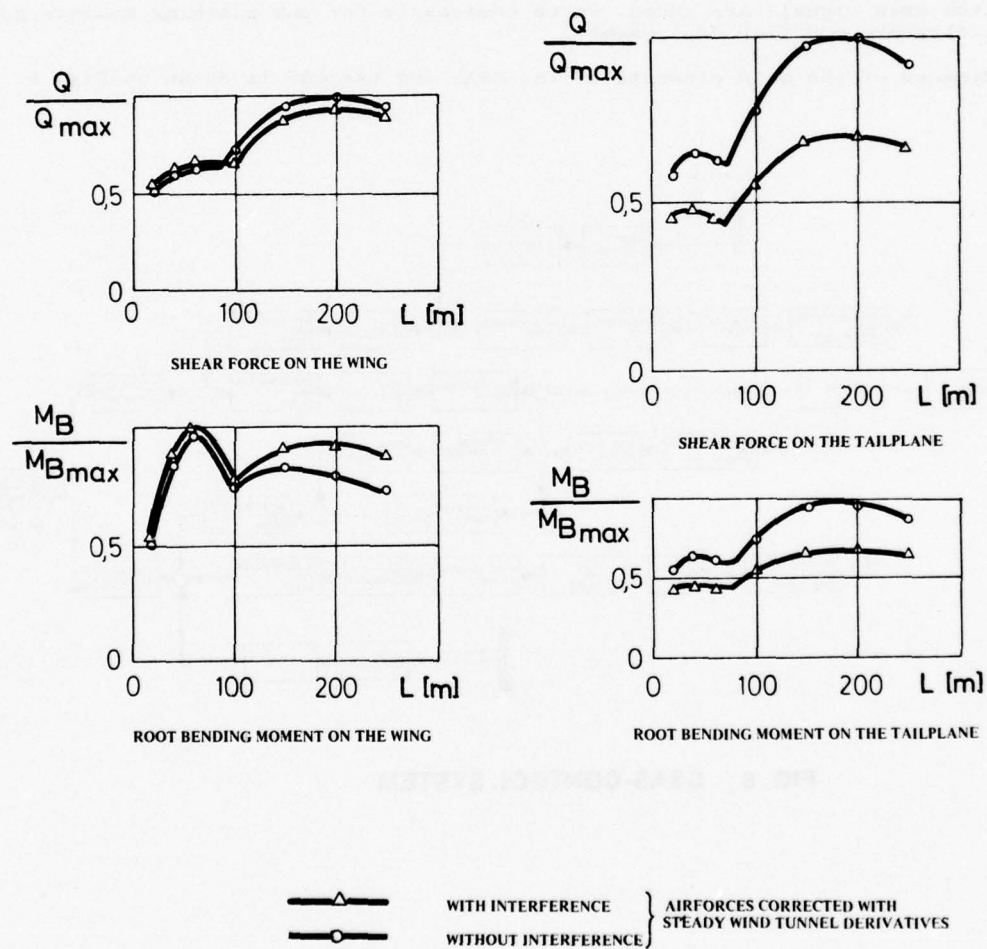


FIG. 5 SHEAR FORCE AND BENDING MOMENT AS A FUNCTION OF VERTICAL GUST LENGTH (ELASTIC AIRCRAFT)

5. DYNAMIC RESPONSE CALCULATIONS WITH AND WITHOUT CSAS

This chapter deals with the impact of the Command and Stability Augmentation System (CSAS) on the gust response.

The airplane we are discussing here is the first operational sweepable wing aircraft featuring a triplex analogue fly-by-wire control system, mechanical emergency control and automatic stabilization. The primary flight control system provides pitch, roll and yaw control by means of an all moving tailplane (taileron), a conventional rudder, and wing mounted spoilers. The tailerons operate in phase for pitch and differentially for roll control. The spoilers give augmented roll control at unswept and intermediate wing positions at low speeds, and also act as lift dumper after touch down.

The flying control surfaces are actuated by tandem hydraulic jacks. Two completely separate and independent hydraulic systems provide fully duplicated power for the primary and secondary flying controls. The control stick and rudder pedal movement is picked off by triplex electrical position sensors which generate the command signals to the CSAS.

The main sensors for feeding back the aircraft motion are rate gyros. Both, the command signals and the feedback signals are passed through appropriate gain schedulers and filters before they are fed to the control surface actuators. As main scheduling parameters dynamic pressure, wing sweep and a flap switch signal are used. For improving the rolling characteristics, especially turn entry and turn exit, a roll to rudder interconnect is implemented and scheduled with a pitch stick increment signal in addition to the aforementioned scheduling parameters.

In pitch axis signals are added, which compensate for the pitching moments generated by airbrake and flap deployment.

A block diagram of the main elements of the CSAS and the CAS is shown in Fig. 6.

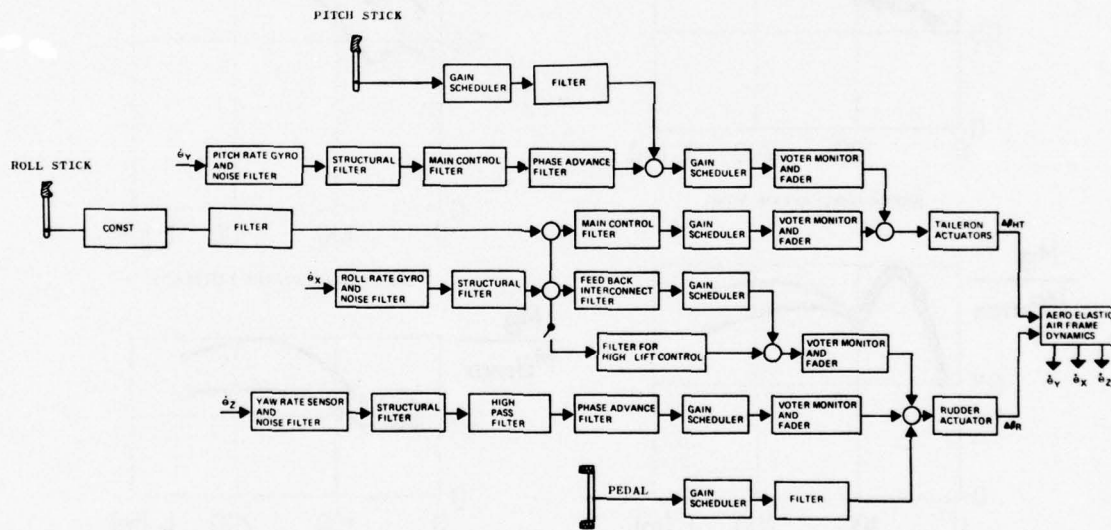


FIG. 6 CSAS-CONTROL SYSTEM

In Fig. 7 the wing root bending moment for vertical ($1-\cos$) gust is depicted. These bending moments are presented for the rigid and elastic mathematical model with and without CSAS. For the elastic mathematical model two rigid body modes - heave and pitch - together with 15 elastic modes of the free-free structure were used. The CSAS was considered by three degrees of freedom of the all moveable tail.

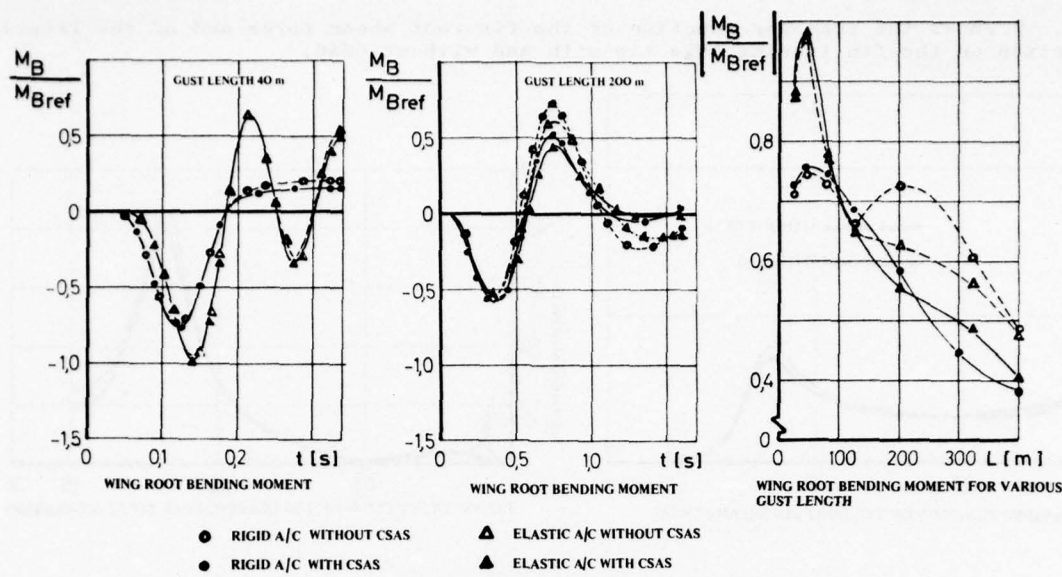


FIG. 7 WING ROOT BENDING MOMENT AS A FUNCTION OF VERTICAL GUST LENGTH

One can see that the considerable influence of the CSAS on the wing root bending moment is only apparent for the low frequency regime. This means that in the frequency regime of the elastic modes the influence of the CSAS is negligible whereas it must be introduced in the low frequency regime near the short period mode frequency to get realistic structural loads due to gusts.

Fig. 8 shows the bending moment, the shear force and the torsional moment on the fin root due to a lateral ($1-\cos$) gust. These results were also derived with a rigid and an elastic mathematical model with and without CSAS. For the antisymmetrical mathematical model three rigid body degrees of freedom - side translation, roll and yaw - together with 18 elastic modes were used. The CSAS was considered with four modes. Fig. 8 shows similar results for the fin root as Fig. 7 for the wing as far as the influence of the CSAS is concerned.

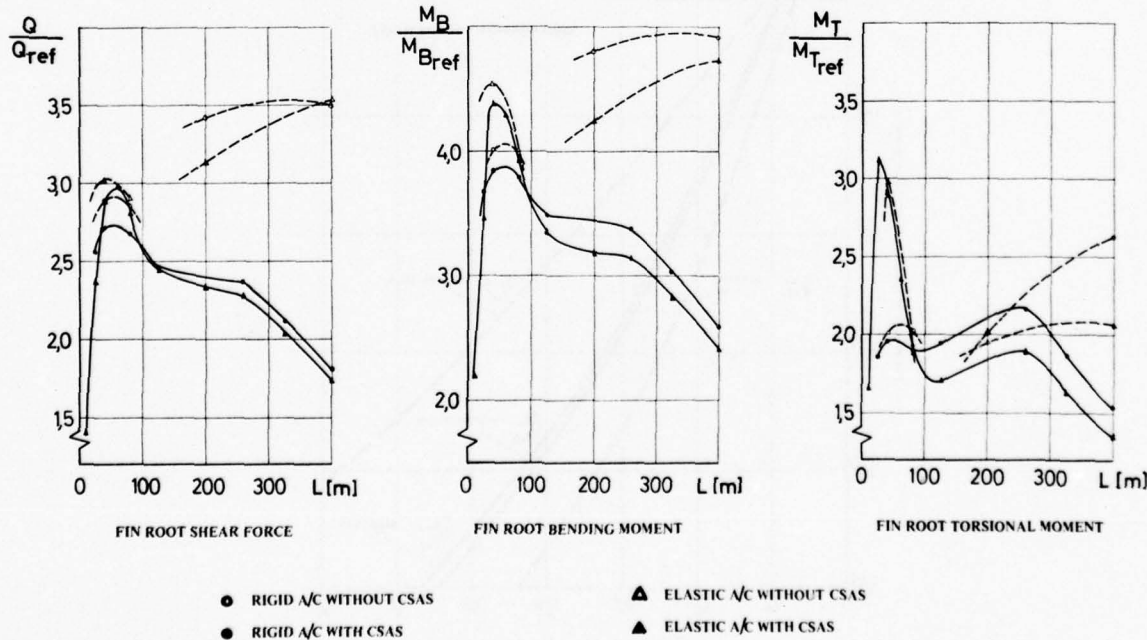


FIG. 8 FIN ROOT LOADS AS A FUNCTION OF LATERAL GUST LENGTH

Fig. 9 shows the transfer function of the fin root shear force and of the lateral acceleration on the fin leading edge tip with and without CSAS.

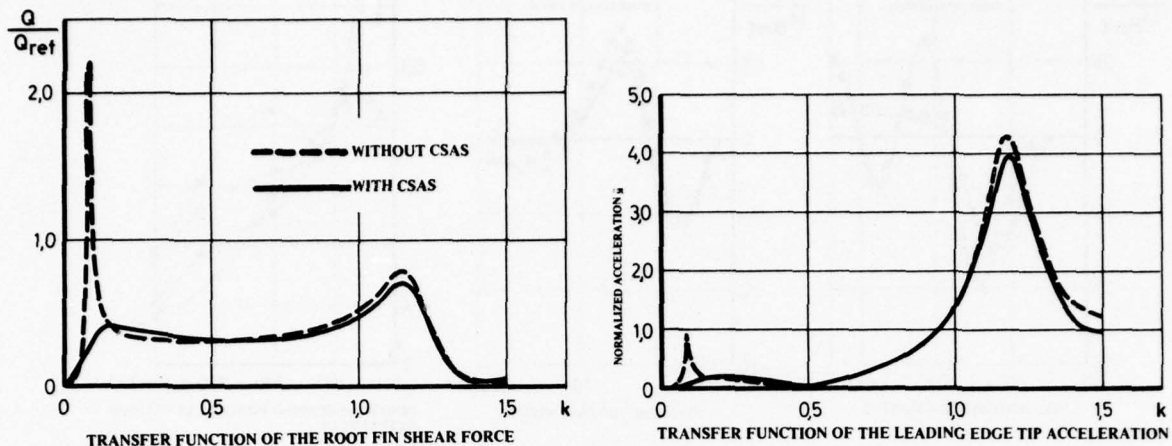


FIG. 9 FIN TRANSFER FUNCTIONS FOR LATERAL GUST

It can be seen from this picture, that there is a big influence of CSAS on Fin Shear Force is considerable. This can be explained by the fact that the gust spectrum (integral of equation 9) is mainly determined by the influence of the low frequency amplitudes.

In Fig. 10 the frequency of exceedance of the wing root bending moment due to vertical stochastic gust excitation and the shear force on the fin root due to lateral stochastic gust excitation is shown. These results were calculated with the mathematical model described for Fig. 7 and 8. The constants used for this calculation were taken from the US-Airforce Military Specification 8861 A (May 1960). The influence of the CSAS on the fin root shear force is considerable.

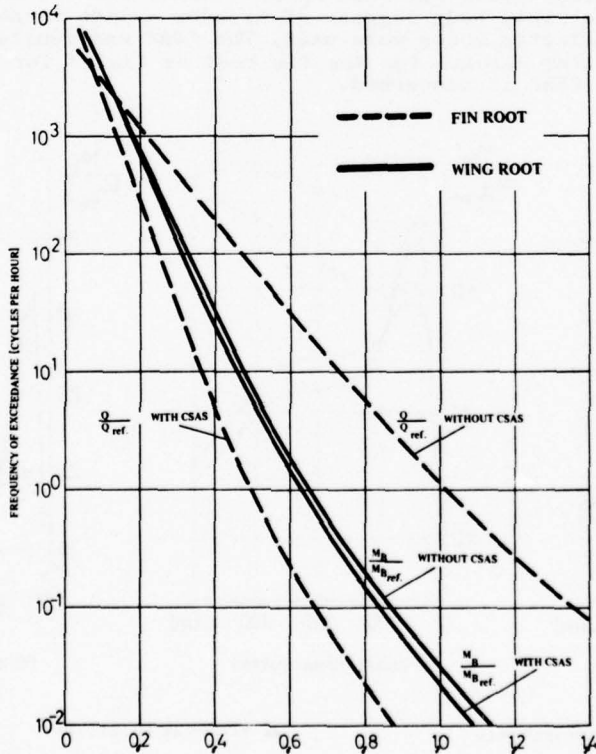


FIG. 10 FREQUENCY OF EXCEEDANCE OF WING ROOT BENDING MOMENT AND FIN ROOT SHEAR FORCE FOR GUST EXCITATION

The last part of this paper deals with the influence of CSAS on response calculations due to manoeuvre. In order to sort out the different influences three different kinds of tailplane movements were considered:

- the theoretical trapezoidal tailplane movement
- the trapezoidal tailplane movement multiplied with the actuator functions
- the trapezoidal tailplane movement multiplied with the transfer function of the command augmentation system (CAS) and the actuator.

These three tailplane motions are presented in Fig. 11.

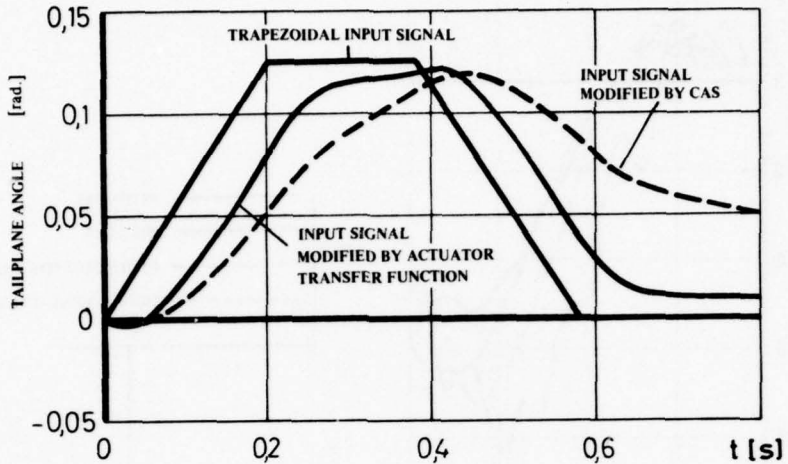


FIG. 11 TAILPLANE ANGLE INPUT SIGNAL

These three motions were introduced as tailplane manoeuvre input into the rigid and elastic mathematical model. In Fig. 12 the vertical acceleration of the center of gravity is depicted.

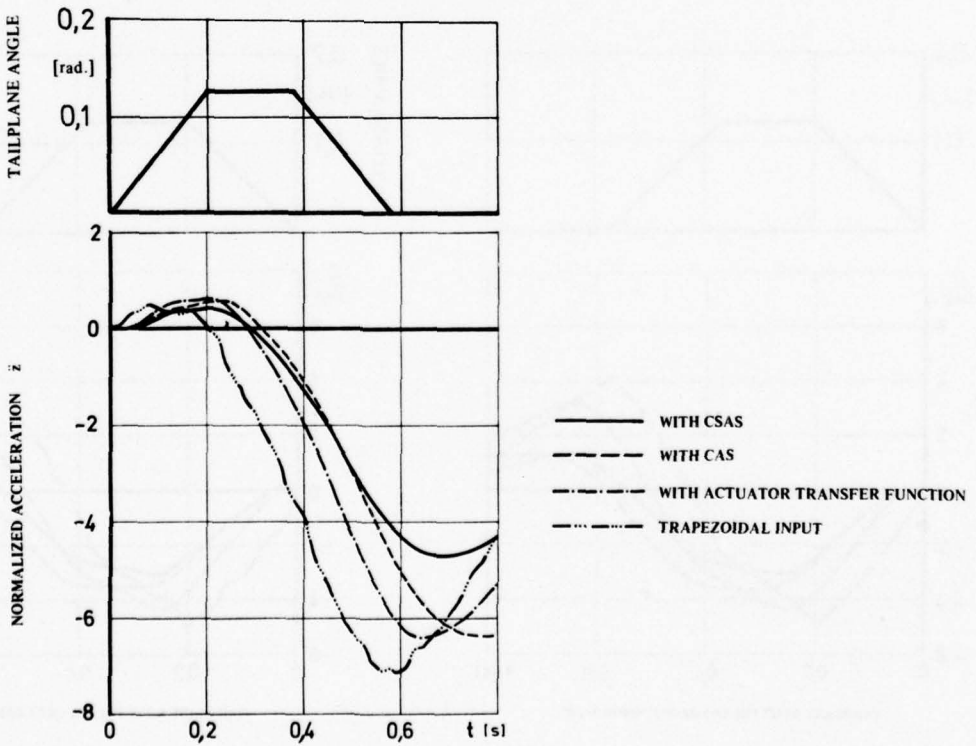


FIG. 12 A/C CENTER OF GRAVITY VERTICAL ACCELERATION DUE TO MANOEUVRE (ELASTIC A/C)

The corresponding vertical accelerations on the wing tip are presented in Fig. 13 and the tailplane root shear forces in Fig. 14.

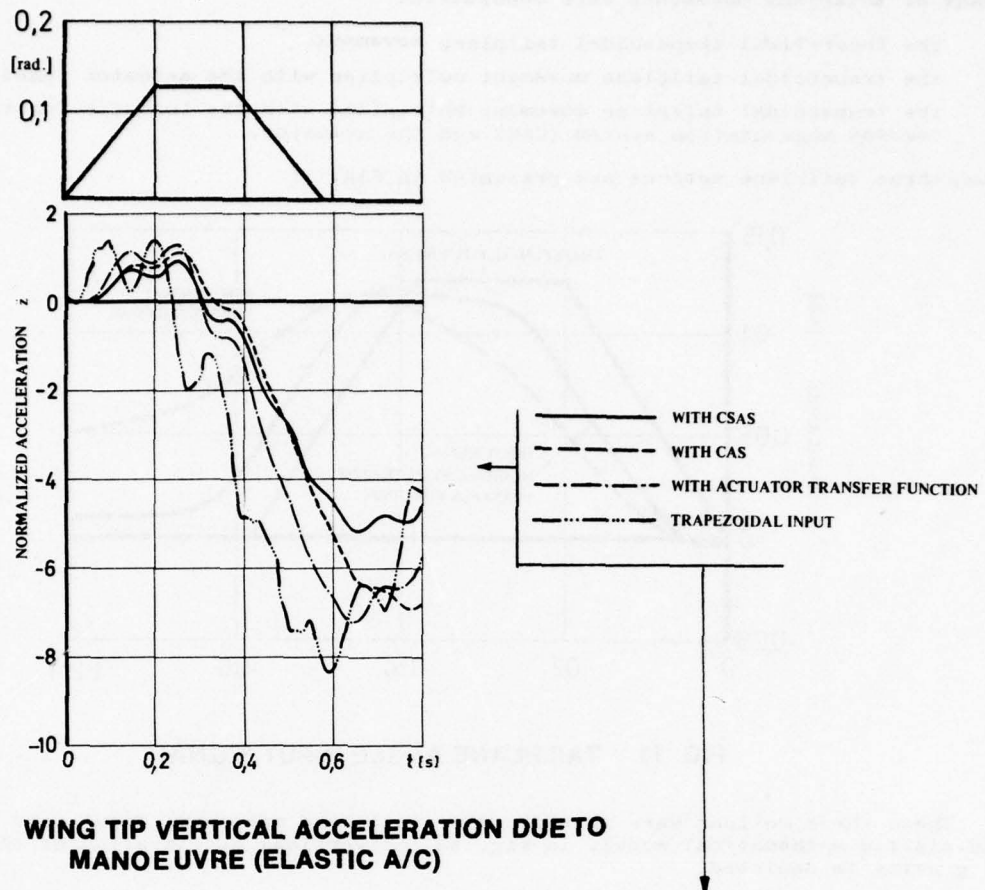


FIG. 13 WING TIP VERTICAL ACCELERATION DUE TO MANOEUVRE (ELASTIC A/C)

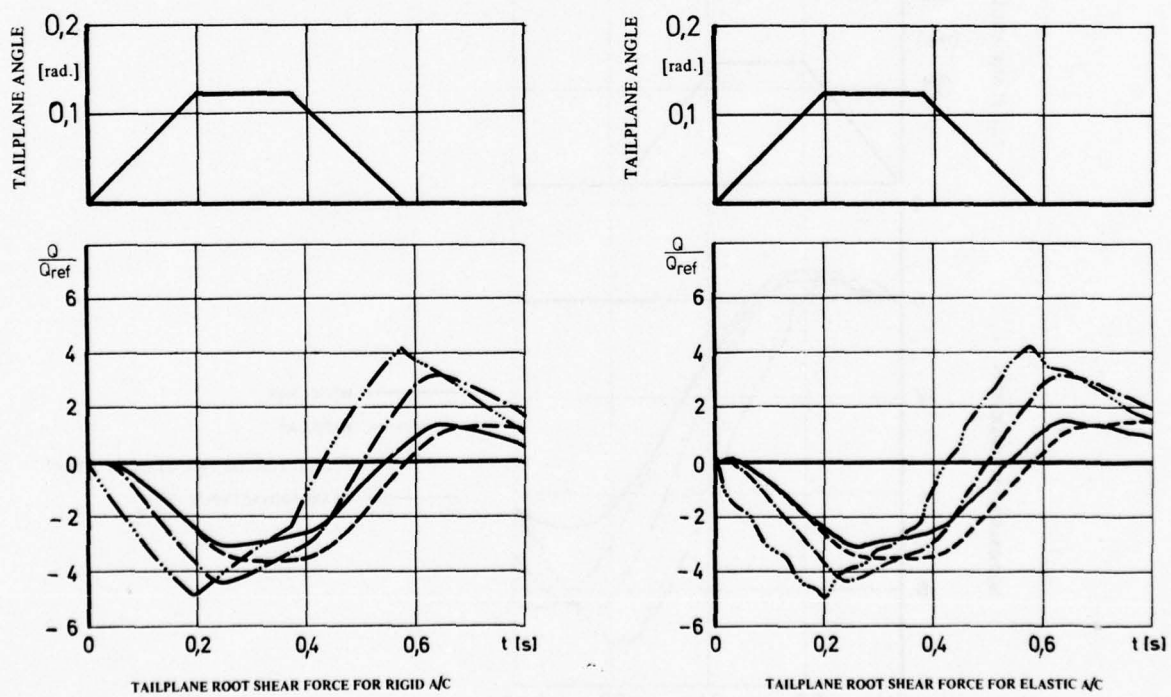


FIG. 14 TAILPLANE ROOT SHEAR FORCE DUE TO MANOEUVRE

Together with the responses of the uncontrolled aircraft for the three different tailplane modes in Fig. 12 to 14 the responses with the full CSAS are also plotted. The mathematical model used, was described for Fig. 7. Figs. 12 - 14 show that the consideration of the actuator transfer function reduces the vertical acceleration as well as the root shear force on the tailplane more than 10 %. The introduction of the CSAS gives only a time shift of the maxima of the plotted accelerations whereas the tailplane root shear force is reduced more than 20 %. The mathematical model with the full CSAS reduces the structural loads about 25 % - 35 % compared with the responses without CSAS and trapezoidal excitation.

A comparison of the responses for the elastic and rigid mathematical model shows that the influence of structural elasticity is small. A reasonable explanation for this small influence is the low excitation frequency having a big frequency distance to the first elastic mode. The responses for the trapezoidal excitation show for the elastic model that higher modes of the elastic structure are excited. This can be explained by the fact that this excitation cannot be steadily differentiated which does not occur for the other forms of excitation. Such an excitation of higher modes is therefore a result of a theoretical model of a tailplane motion which does not occur in flight.

An intensive study of all responses show that the CSAS must be very carefully introduced into the mathematical model to determine structural loads due to manoeuvres whereas the elastic behaviour can be neglected if there is enough frequency space between the main frequency of the existing manoeuvre and the frequency of the first elastic mode.

REFERENCES

[1] An Assessment of the P02 Clean Aircraft Ground Resonance Test.
MRCA-Report No. Ae/V/589, February 1974

[2] COLLMAND, K.D. Über den Nachweis für die Flatterfreiheit der VFW 614.
Entwicklungstechnische Berichte - VFW-Fokker, Band 4, 1975, S. 1-15

[3] Total Airplane Flutter Analysis -
Part I - Vibration Analysis
MRCA-Report No. M/FE1710/1240,
April 1974

[4] COLLMAND, K.D.
ZIMMERMANN, H. Bestimmung dynamischer Lasten an elastischen Strukturen auf Grund äußerer Erregungen.
ZfW 21, 1973, S. 225-234

[5] WITTMAYER, H. Flattergleichungen mit Berücksichtigung einer Servosteuerung und eines Flugreglers.
ZfW 22, 1974, S. 37-40

[6] FÖRSCHING, H. Einfluß servomechanischer Steuerungs- und Stabilitätssysteme auf das Flatterverhalten von Flugzeugen.
ZfW 21, 1973, S. 22-31

[7] LOTZE, A.
SENSBURG, O.
KÜHN, M. CSAS-Structural Mode Coupling on the Tornado Combat Aircraft.
Journal of Aircraft (April, 1977)

[8] BALDOCK, J.C.A. The Determination of the Flutter Speed of a T-Tail Unit by Calculation, Model Test and Flight Flutter Test.
AGARD-Report No. 221, Oct. 1958

[9] DAVIES, D.E. Calculation Methods for Unsteady Air Forces of Tandem Surfaces and T-Tails in Subsonic Flow.
AGARD-Conference Proceedings 80/71
"Symposium on Unsteady Aerodynamics for Aero-elastic Analysis of Interfering Surfaces"
Tonsberg/Norway, Nov. 1970

[10] SENSBURG, O.
LASCHKA, B. Flutter Induced by Aerodynamic Interference Between Wing and Tail.
Journal of Aircraft, Vol. 7, No. 4, July-August 1970

[11] LASCHKA, B. Interfering Lifting Surfaces in Subsonic Flow.
ZfW 18, Band 9/10, 1970

[12] BECKER, J. Interfering Lifting Surfaces in Unsteady Subsonic Flow/Comparison Between Theory and Experiment.
AGARD-Report No. 614
AGARD Manual of Aeroelasticity, Volume II,
Chapter 10

[13] RICHARDSON, J.R. The Application of the Multhopp-Garner Theory to the Evaluation of Control Surface Derivatives.
Techn. Office Report No. 135, 1954
- The Fairey Aviation Company -

[14] LODGE, C.
SCHMID, H. Unsteady Pressures due to Control Surface Rotation at Low Supersonic Speeds Comparison Between Theory and Experiment.
42nd Meeting of the SMP, Ottawa/Canada,
4-9 April, 1976

ACTIVE FLUTTER SUPPRESSION ON AN AIRPLANE WITH
WING MOUNTED EXTERNAL STORES

by

H. HÖNLINGER

MESSERSCHMITT-BÖLKOW-BLOHM GmbH.
Unternehmensbereich Flugzeuge
8 München 80, Postfach 801160,-W.Germany

1. INTRODUCTION

After a successful application of active flutter suppression on wing store and empennage flutter problems [1],[2],[3] in wind tunnels an extension of this technology to a full scale airplane was considered to be rewarding. The effort was focused on the flight test of a wing/store flutter suppression system (FSS) with store mounted vanes.

This program started in 1975 with the design of the system and the instrumentation of a FIAT G 91/T3 as flying test bed. Flight test was finished in Febr. 1977.

Test objectives of this study were:

- Provide first flight experience with FSS on external stores
- Substantiate and demonstrate a new method for flight flutter testing wing mounted external stores by use of this FSS (Automatic Mode Excitation System - AMES)

This work was carried out under the ZTL research contract for the German Ministry of Defense by the MBB structural dynamics group. The flight test was performed by BWB - LG IV 8 - and E 61 at the German Airforce Test Centre at Manching.

ACKNOWLEDGEMENT:

The author wants to express his appreciation for the E-Stelle and LG IV 8 who performed all the flight operations. Especially Herr Koark - LG IV 8 - was contributing a great deal to the successful performance of the program.

2. DESIGN OF THE FLUTTER SUPPRESSION SYSTEM

2.1 Selected Store Configuration

The G 91/T3 is flutter free within its flight envelope when carrying its external store inventory. Therefore trend studies were performed to evaluate a critical store configuration which can be simulated by a ballasted 520 ltr. tank (flutter tank). Fig. 1 shows the flutter calculation for the finally selected critical tank configuration.

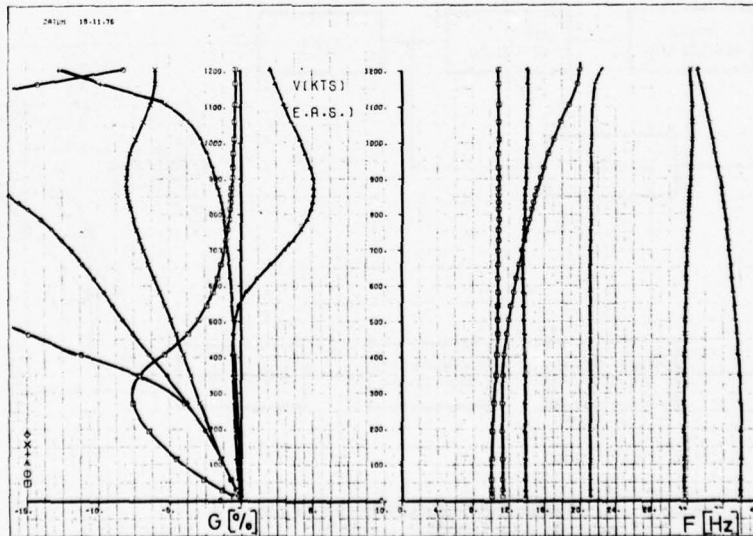


FIG. 1 FLUTTER SPEED VERSUS DAMPING AND FREQUENCY

Two modes, shown in Fig. 2, wing bending at 11.39 Hz and store pitch with wing torsion at 14.15 Hz are causing the flutter case which we intended to suppress.

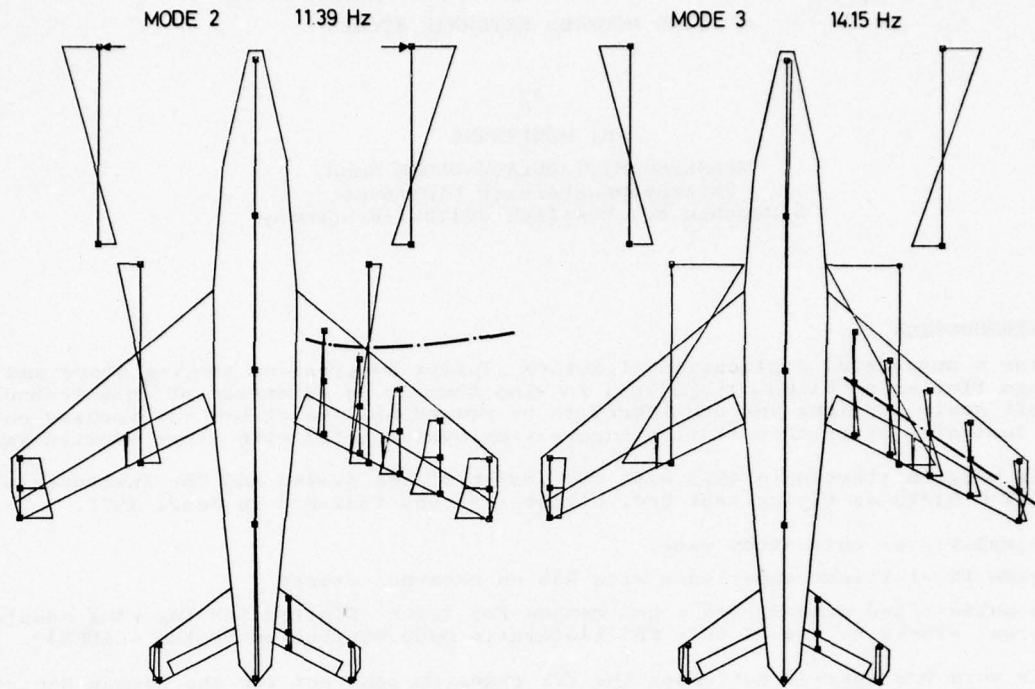


FIG. 2 VIBRATION MODE SHAPES

2.2 Control System

The damping of vibration or flutter modes of wing mounted stores by oscillating vanes creating aerodynamic forces was tested in the wind tunnel to be a very effective way and should now be applied on an airplane. The block diagram in Fig. 3 shows the control loop of the airplane with the FSS.

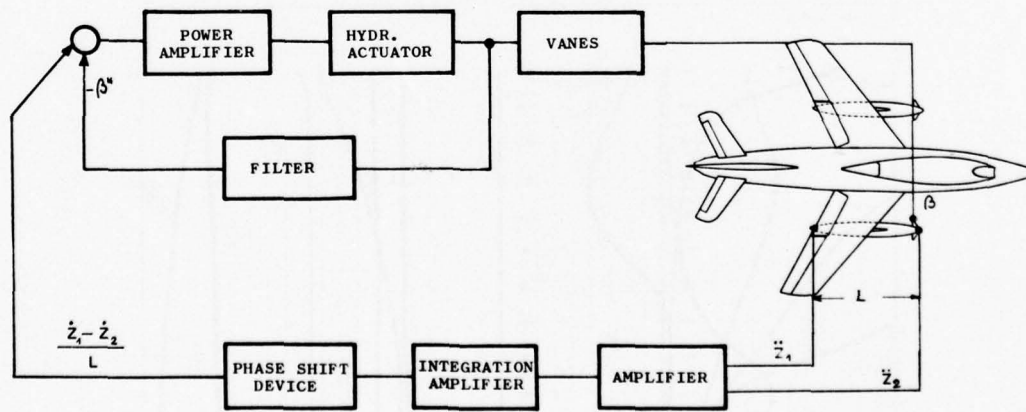


FIG. 3 FLUTTER SUPPRESSION SYSTEM
BLOCK DIAGRAM

The control signal is produced by two accelerometers located in the forward and rear part of the flutter tank. This signals were added and integrated to give the pitch angle of velocity of the flutter store which is used as input signal to the hydraulic actuators driving small vanes attached at the forward part of the store. The vanes oscillate in such a way that the generated airforces counteract the pitch motion of the store like a velocity proportional damper. The steady aerodynamic derivatives of the A/C were not influenced by these vanes and therefore no change in the flight mechanical behaviour was expected. For optimization of the phase between control signal and angle of attack of the vanes a manual phase shift device was provided in the control loop.

2.3 Analysis of the Control System

An analysis of the airplane with control system was carried out with a computer program developed at MBB[13]. This analysis predicted that the system could be successfully applied. An explanation of the applied Nyquist criteria is shown in Fig. 4.

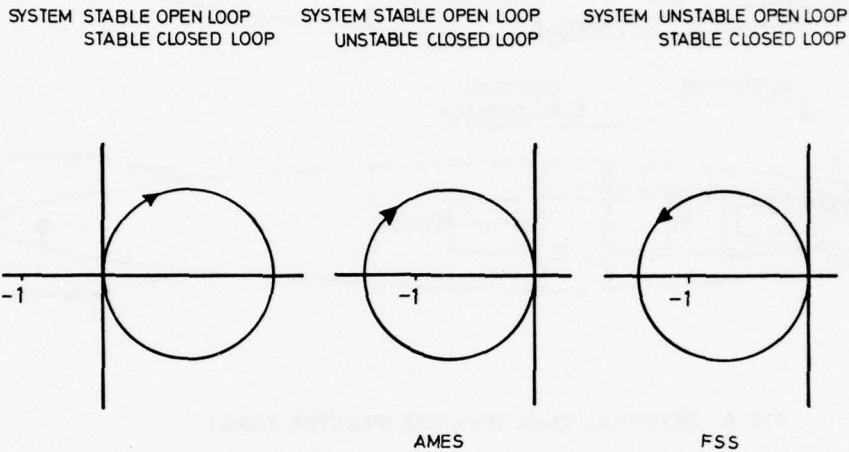


FIG. 4 NYQUIST STABILITY CRITERIA

In Fig. 5 the Nyquist diagram for $v = 500$ kts for the airplane with FSS is depicted. It shows that the mode to be controlled is stable. With the automatic mode excitation system (AMES) this mode becomes unstable. For $v = 600$ kts the system is fluttering and becomes stable only with the FSS.

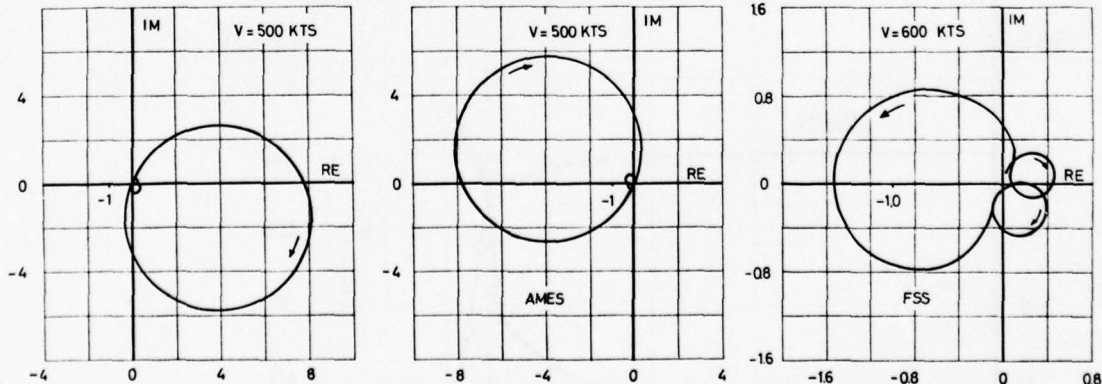


FIG. 5 NYQUIST DIAGRAM FOR THE FLUTTER SUPPRESSION (FSS) AND MODE EXCITATION SYSTEM (AMES)

2.4 Technical Realization of the FSS

As mentioned before the FSS had to be implemented into the two ballasted 520 ltr. tanks of the G 91. For the sake of redundancy one tank on each wing was installed. Each tank worked independently and only needed electrical power from the aircraft.

Fig. 6 shows a sketch of the installation of the FSS in the 520 ltr. tank. A frame was installed in the forward part of the tank to carry the vanes, the electro-hydraulic power package and control electronics. The ballast weight was clamped in the centre part of the tank.

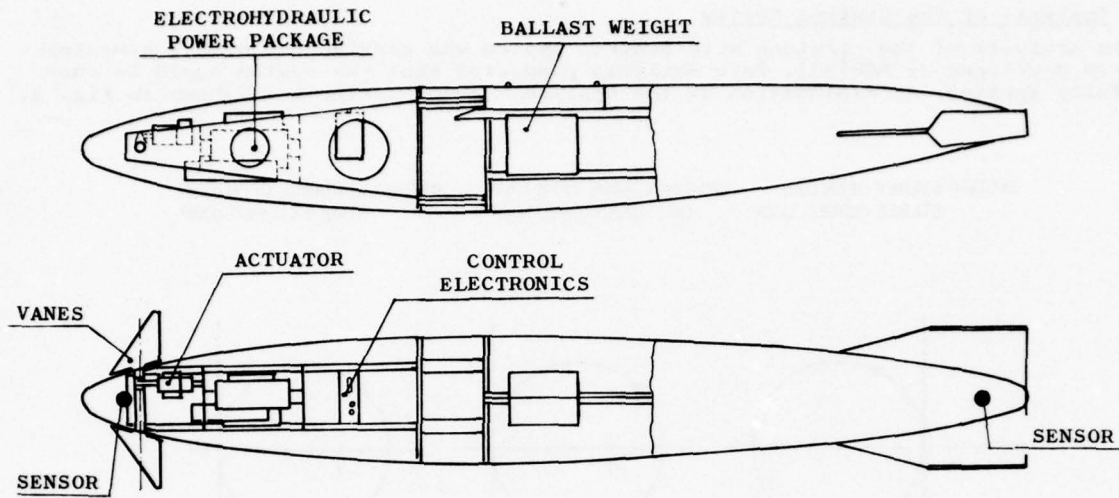


FIG. 6 EXTERNAL TANK WITH FSS (FLUTTER TANK)

The vanes were designed for transsonic flow (angle of leading edge 30° , axis of rotation at 35 % root chord).

Special fast vane actuators with a mechanical fixing device were developed. In Fig. 7 the transfer function of the actuator with vanes is given. The Bode plot shows ideal behaviour in the required frequency range (up to 14 Hz). There is only a small phase shift and the amplitudes remain constant up to 15 Hz. The max. torque the actuators produce is 2700 Ncm. The max. possible angle of attack of the vanes is $\pm 10^\circ$. The weight of the whole FSS in this test status is approx. 21 kg.

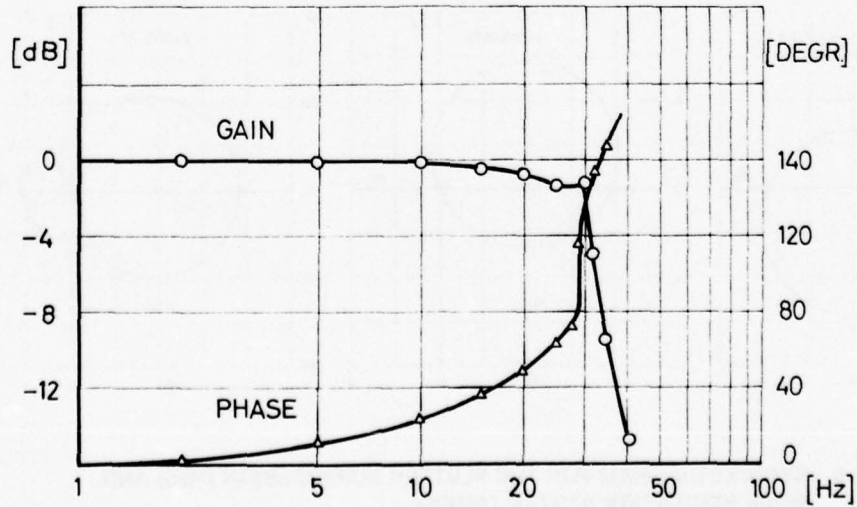


FIG. 7 ACTUATOR TRANSFER FUNCTION

Fig. 8 shows the flutter tank and the vanes on the aircraft.

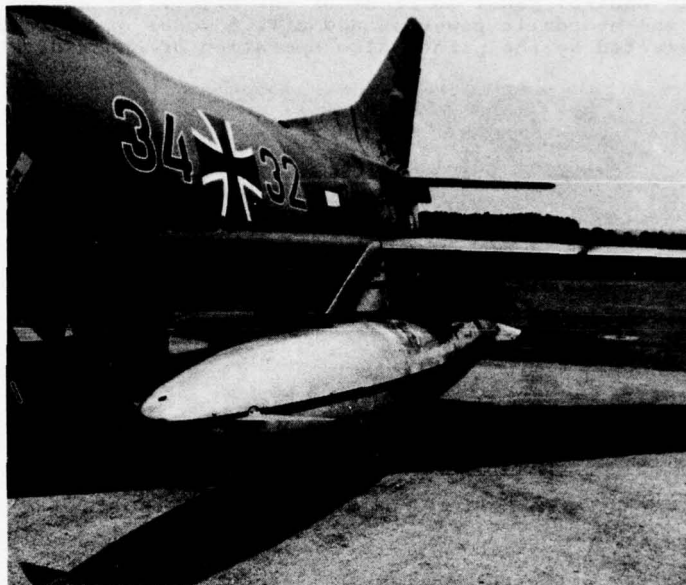


FIG. 8 FLUTTER TANK ON THE AIRPLANE

3. FLIGHT TEST INSTRUMENTATION

To perform the flight test of the FSS and to evaluate new methods for flight flutter tests special flight test equipment was installed in the airplane.

A frequency sweep generator was fitted which gives specified inputs into the control system (variable frequency sine wave). This input can be given in the open and closed loop mode as well.

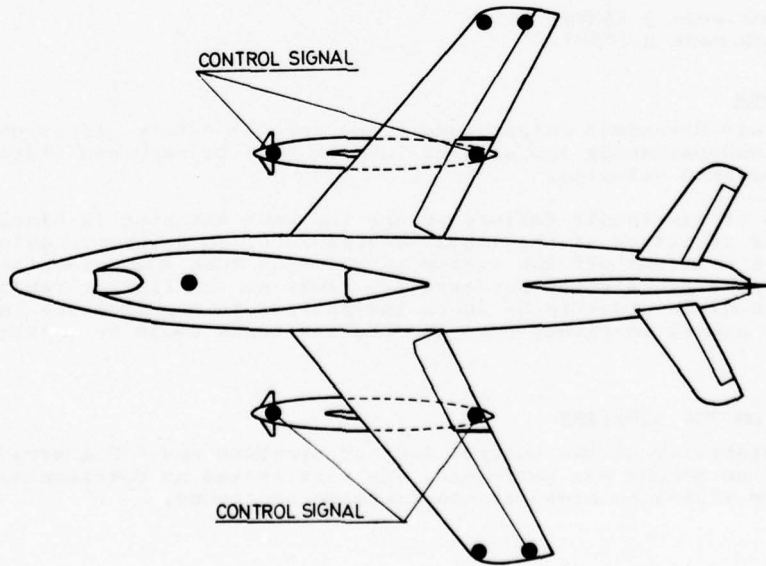


FIG. 9 ACCELEROMETER LOCATIONS

The acceleration pickup locations are shown in Fig. 9. 17 parameters could be recorded on tape and also telemetered for ground quick look inspection. The pilot was able to manually control the FSS with two control panels.

Fig. 10 shows the main control panel in front of the pilot. The second control panel was used to switch the hydraulic power on and off. 6 modes of operation of the flutter tanks could be selected by the pilot. Also operation of one side FSS was possible.

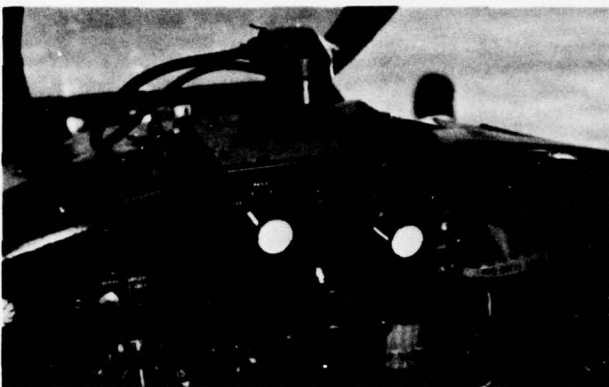


FIG. 10 MAIN CONTROL PANEL

In the open loop mode four different angles of attack of the vanes ranging from 1° to 4° could be chosen by the pilot. A warning light indicated failure or automatic cutoff of the system.

All operation modes could be started and cut off by the pilot pressing the trigger button on the stick. An emergency switch was also installed in the stick.

The operation modes of the flutter tanks were:

1. Open loop mode
(mode excitation by frequency sweep inputs)
2. Automatic flutter suppression (FSS)
3. Automatic mode excitation (AMES)
4. FSS with additional frequency sweep input
5. L/H flutter tank mode 1 (open loop excitation)
R/H flutter tank mode 2 (FSS)
6. L/H flutter tank mode 3 (AMES)
R/H flutter tank mode 2 (FSS)

Safety Installations

In order to avoid hazardous flight conditions special safety provisions were made. Both systems work independently and each of them is able to suppress flutter of the airplane up to a defined velocity.

If a hydraulic or electronic failure occurs the vane actuator is blocked mechanically and the angle of attack of the vanes becomes zero. An automatic cutoff device was installed which switches off the system in the open loop and automatic flutter excitation mode when a preselected acceleration limit on the flutter tanks or on the wing tips is exceeded. In order to be shock insensitive this system was integrating amplitudes. In the utmost emergency case the flutter tanks could be jettisoned.

4. GROUND TESTS ON THE AIRPLANE

To check the stability of the control loop of airplane and FSS a structural mode coupling test on ground was performed. The test showed no detrimental coupling of the FSS with the vibration modes of the airframe on ground.

5. FLIGHT TEST

5.1 Performance of Flight Test

From the beginning of Nov. 1976 till end of Febr. 1977 18 flights were performed. 17 parameters were monitored at the telemetry station during the flights.

After each flight the test data were analyzed with an HP 5451 Fourier Analyzer. Special programs were developed to calculate Nyquist diagrams and evaluate damping from the open loop tests with frequency sweep excitation.

5.2 Open Loop Tests in Flight

In order to check the stability and to optimize the phase of the FSS open loop tests in flight at various airspeeds were performed at the beginning of the flight test. Frequency sweeps were fed into the control system. The frequency increased according to a logarithmic law from 5 Hz to 25 Hz and then decreased to 5 Hz within 120 seconds.

Fig. 11 shows the response of the flutter tank to the frequency sweep excitation through the vanes. A good excitation of the flutter mode can be seen.

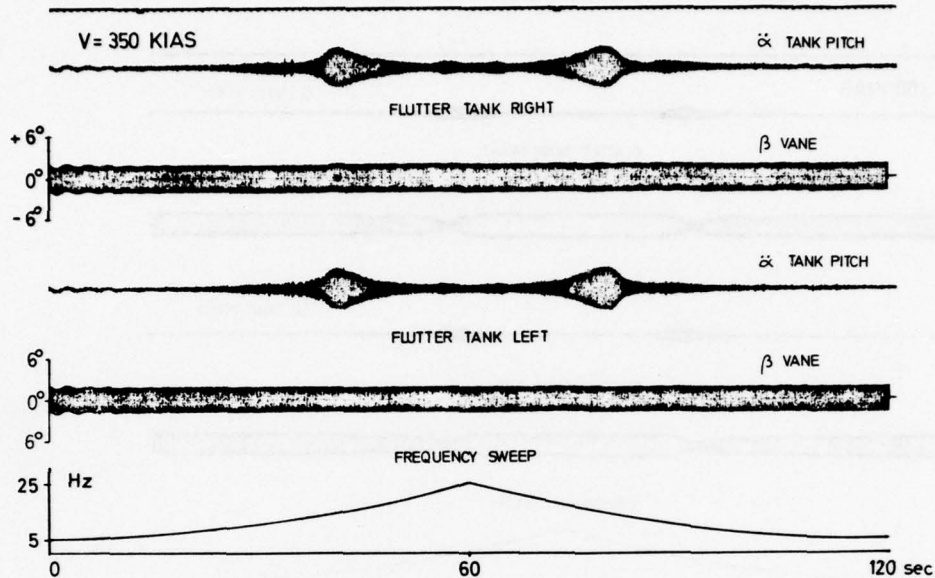


FIG. 11 TIME HISTORY OF FREQUENCY SWEEP EXCITATION (OPEN LOOP)

In Fig. 12 two Nyquist diagrams calculated from these frequency sweeps at $v = 350$ KIAS and $v = 450$ KIAS are presented. The phase of the flutter mode is not yet optimized. Comparing both plots the phase shift due to the unsteady air forces can be seen too.

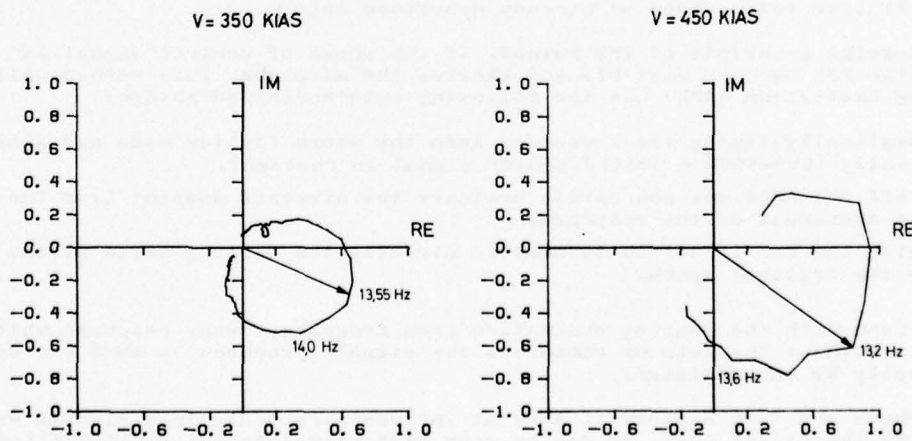
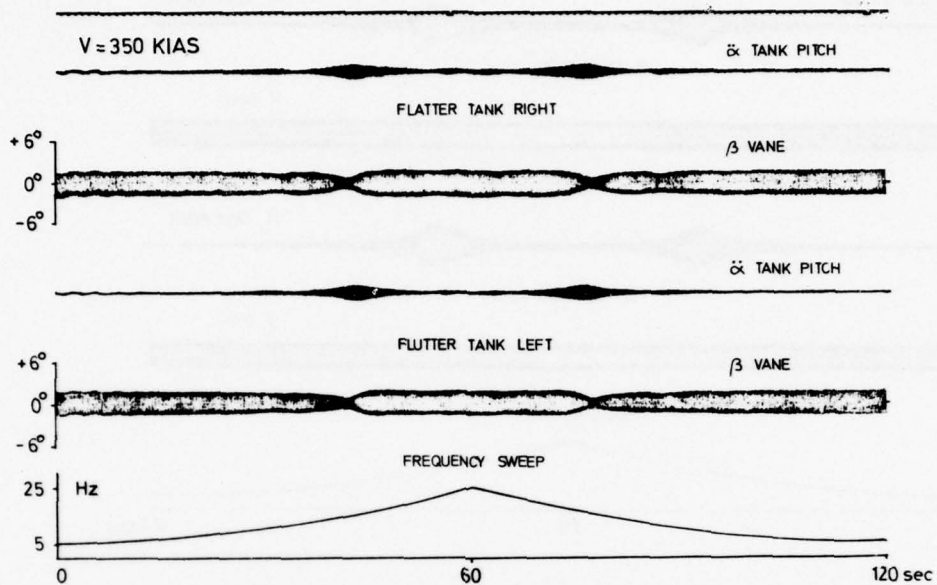


FIG. 12 NYQUIST PLOTS AT $v = 350$ KIAS AND $v = 450$ KIAS (OPEN LOOP)

5.3 Closed Loop Tests of the FSS

After having optimized the phase of the flutter mode and having checked the stability of the system within the whole flight range closed loop tests were performed. No valuable test data could be gained by excitation through stick jerks because the frequency content of those excitation signals is too low. The only method to check the closed loop condition is to feed an additional sinusoidal signal (frequency sweep) into the closed loop and analyze the response.

Fig. 13 shows the time history of a closed loop test with frequency sweep input. Comparing Fig. 12 with Fig. 11 one can see that the FSS reduces the vane angle at the frequency of about 14 Hz. The damping coefficient was also evaluated from these tests and is presented later in a summary plot.



**FIG. 13 TIME HISTORY OF FSS RESPONSE
DUE TO FREQUENCY SWEEP INPUT**

5.4 Tests to Substantiate a New Flight Flutter Test Method for Stores

The aim of this tests was to demonstrate that the modified FSS can be used for a new flight flutter test method as already described in [1].

Fig. 5 shows the principle of the method. If the phase of control signal is shifted 180° the FSS becomes unstable and excites the airplane. This method called Automatic Mode Excitation (AMES) has the following outstanding advantages:

- It is automatically tuning the frequency into the store flutter mode and excites it harmonically (provided a suited sensor signal is chosen).
- Switching off the AMES one can easily evaluate the aircraft damping from the logarithmic decrement of the response.
- Combined with the FSS it allows to measure directly the damping trend of the flutter mode above the critical speed.

In comparison with the damping evaluation from frequency sweep response which cannot be done without the help of computers the signals produced by AMES can be analyzed directly by the engineer.

Fig. 14 shows the time history of AMES at various airspeeds. These signals were produced during the flight test. As can be seen high signal to noise ratio allows an evaluation of the damping from the decay at once.

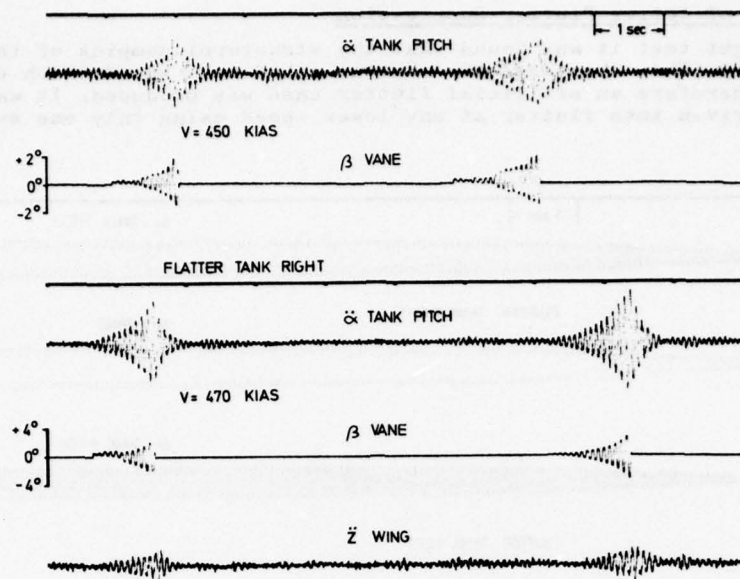


FIG. 14 TIME HISTORY OF AMES $v = 450$ KIAS AND $v = 470$ KIAS

The logarithmic increment of the increasing amplitudes shows the excitation of the stable system which can be turned into damping by shifting the phase 180° . The damping evaluated this way has to be added to the damping trend of the flutter mode to get the damping of the stabilized system. This is shown in Fig. 15.

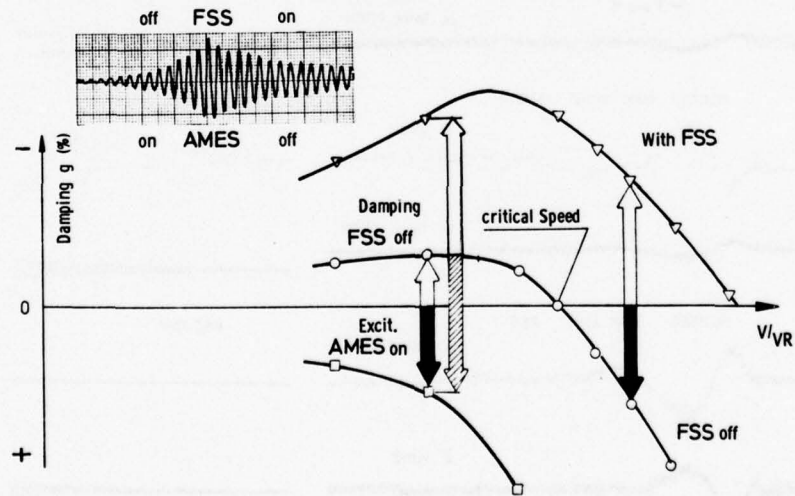


FIG. 15 RELATIONSHIP BETWEEN FSS AND AMES

5.5 Demonstration of Active Flutter Suppression

During the flight test it was found that the structural damping of the A/C was higher than expected. This increased the flutter speed to a speed which could not be reached anymore. Therefore an artificial flutter case was produced. It was found that the A/C could be driven into flutter at any lower speed using only one system in the AMES mode.

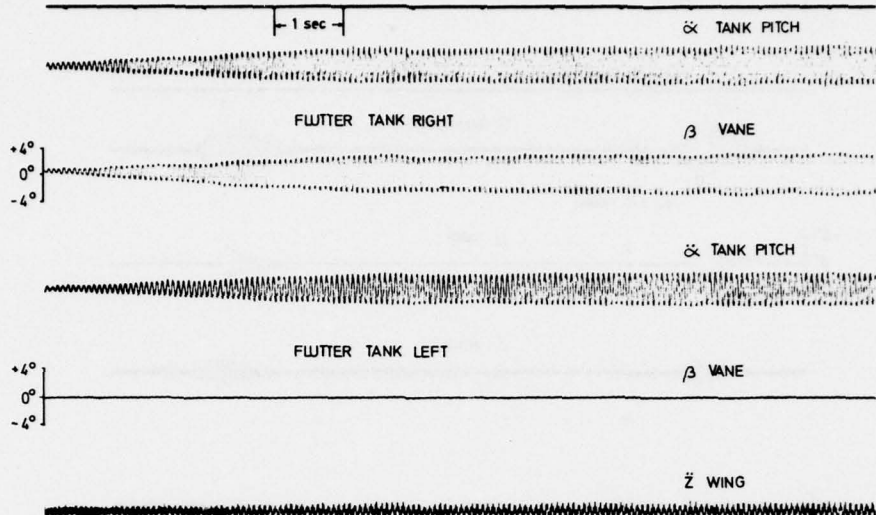


FIG. 16 TIME HISTORY OF THE UNSTABLE SYSTEM AT $v = 300$ KIAS

Fig. 16 shows the time history of an artificial flutter case at 300 kts. Using the other system in FSS-mode the unstable system became stable.

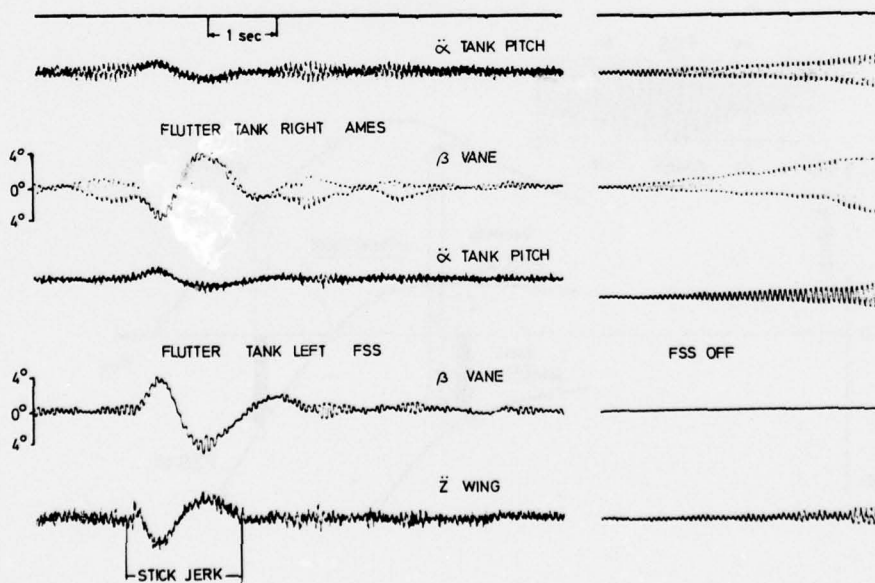


FIG. 17 TIME HISTORY OF STABILIZED SYSTEM AT $v = 300$ KIAS

This is demonstrated in Fig. 17. This figure shows the unstable and stabilized system. As can be seen, even additional excitation by stick jerks could not destabilize the system.

6. FLIGHT TEST RESULTS

All tests were performed in the high subsonic regime. Pronounced transsonic effects could not be evaluated.

6.1 Automatic Mode Excitation

The method described was found to be very powerful and promising. The main advantages of the AMES are:

- The possibility to measure the flutter speed directly if it occurs within the flight envelope of the A/C
- Improved extrapolation of the damping trend is possible
- The test results can be directly used by the engineer without the help of computers
- The flight flutter test of stores can be done with less flight hours and less risks for the A/C (one store configuration in one flight!)

In Fig. 18 damping trends of the aircraft with the flutter stores are presented. It can be seen that the damping evaluated from the frequency sweep response is slightly higher than the values found with AMES.

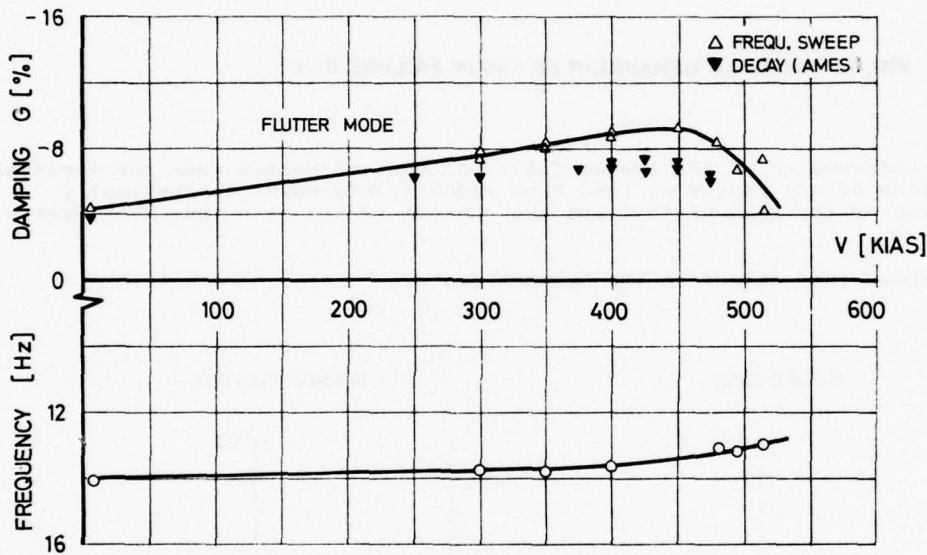


FIG. 18 MEASURED DAMPING AND FREQUENCY TREND

The most important feature for the system is a reliable automatic switch off of the AMES. Especially at higher frequencies and higher speeds it was found that in some cases the pilot will not be able to switch off manually the system quick enough.

6.2 Discussion of Results with the Flutter Suppression System

- Influence of the phase on efficiency of FSS:

The simple control system used for this test was optimized for one mode, the flutter mode.

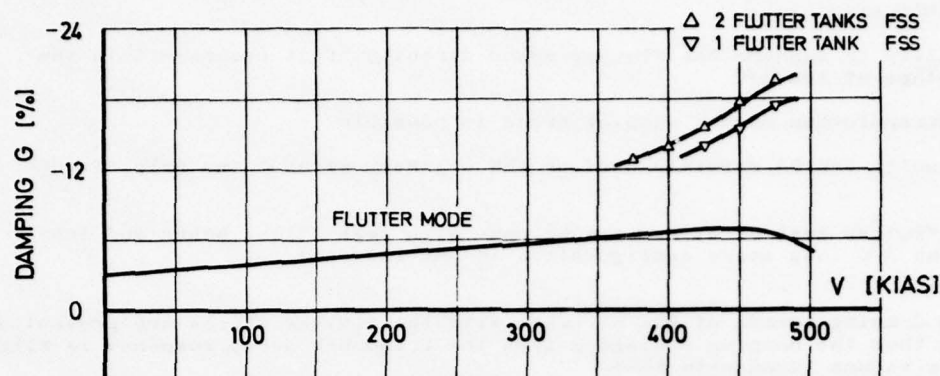
As can be seen from the open loop tests non optimized phase reduces the system efficiency with the cosine of the phase. Therefore the phase optimization needs no high precision. The control system however has to compensate the phase shift caused by the air forces on the flutter store (approx. 20° from 0 - 500 KIAS).

- Influence of the gain on the efficiency of the FSS:

The damping force produced by the FSS at constant airspeeds is proportional to the gain of the system.

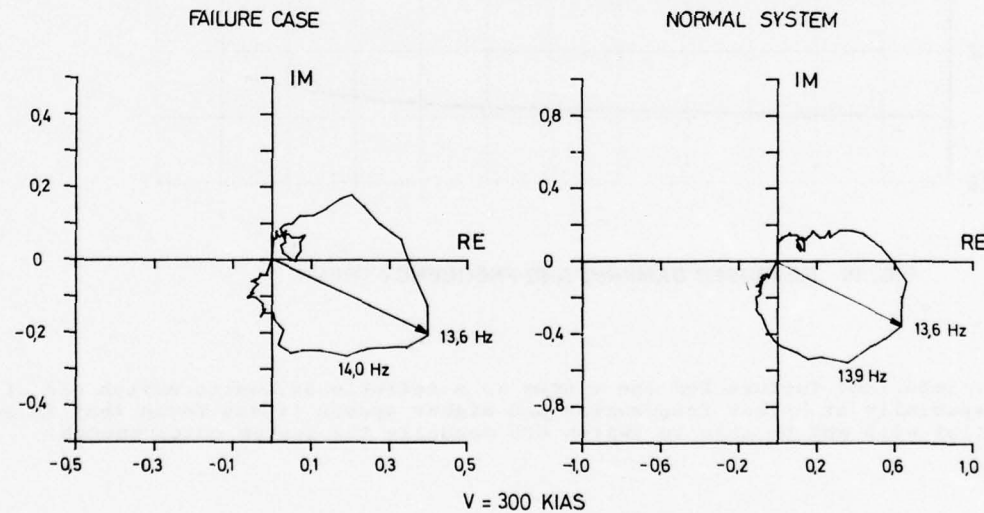
Testing of failure cases

In a failure case if only one flutter tank works as a damper the efficiency is reduced. In Fig. 19 this effect is shown. If the behaviour of the A/C is symmetrical this effect can be regarded as a gain reduction.

**FIG. 19 DAMPING BEHAVIOUR OF FSS IN FAILURE CASE**

If one accelerometer of the system fails the control system uses the vertical acceleration of one sensor as feed back signal. This means theoretically a reduction of the gain of 50 % and the control system is a true ILAF System [17].

Fig. 20 shows this effect on the Nyquist plots.

**FIG. 20 NYQUIST PLOTS FOR FAILURE OF ONE ACCELEROMETER**

These two tests have shown that assuming the A/C's behaviour is symmetrical this kind of FSS can be easily designed with high redundancies.

6.4 Estimated Increase of the Flutter Speed due to FSS

The increase of the real flutter speed could not be demonstrated in flight. In Fig. 21 the increase of the flutter speed is given by extrapolating the measured damping trends. In this picture a medium gain was used. One must keep in mind that the extrapolation given in Fig. 20 does not include the effects which may occur at high transsonic speeds. Stall of the vanes and saturation conditions of the actuator have to be avoided.

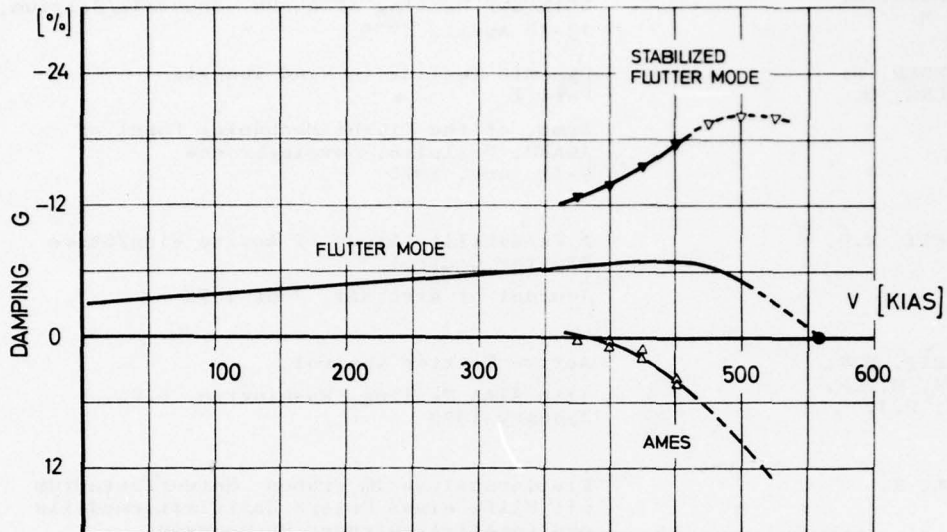


FIG. 21 EFFICIENCY OF FSS

7. CONCLUSIONS AND RECOMMENDATIONS

It was shown that a relative simple control system with store mounted vanes can be used for store flutter suppression. This FSS is very effective with relative small vanes which do not change the flight mechanical characteristics of the aircraft.

First flight experience with an AMES was made and the method was found to be promising.

REFERENCES

- 1 HIDL, G.
LOTZE, A.
SENSBURG, O.

Active Flutter Suppression on Wings with
External Stores
AGARDograph No. 175
- 2 SENSBURG, O.
HÖNLINGER, H.
KÜHN, M.

Active Control of Empennage Flutter
40th SMP Meeting of AGARD, Brussels/Belgium,
13-18 April, 1975
- 3 HÖNLINGER, H.
SENSBURG, O.

Dynamic Testing in Wind Tunnels
Part I

Symp. of the Flight Mechanics Panel of
AGARD, Valloire, Savoie/France
9-12 June, 1975
- 4 TRIPLETT, W.E.

A Feasibility Study of Active Wing/Store
Flutter Control

Journal of Aircraft, June 1972
- 5 TRIPLETT, W.E.
KAPPUS, H.P.F.
LANDY, R.J.

Active Flutter Control
11th AIAA Meeting, Washington, D.C.,
January 1973
- 6 SEIDEL, W.

Flatteranalyse im frühen Entwurfsstadium
mit Hilfe eines Unterschallflattermodells
und paralleliaufender Rechnungen

Jahrbuch 1967 der WGLR
- 7 SCHOEN, J.

Schwingungsuntersuchungen an Flugzeugmodellen
zur Unterstützung der Flatterrechnung
1974 VDI-Bericht Nr. 197
- 8 FÖRSCHING, H.

Einfluß servomechanischer Steuerungs- und
Stabilitätssysteme auf das Flatterverhalten
von Flugzeugen

ZfW 21, 1973, Heft 1
- 9 HÖNLINGER, H.

Entwurf und Erprobung eines aktiven Schwingungs-
und Flatterdämpfungssystems für Außenlasten
DGLR-Symp. "CCV-Technologien",
Munich/Germany, 17 September, 1976
- 10 OTNES, R.K.
ENOCHSON, L.

Digital Times Series Analysis
John Wiley & Sons/London
- 11 BENDAT, J.S.
PIERSOL, A.G.

Measurement and Analysis of Random Data
John Wiley & Sons Inc., 1966
- 12 SEIDEL, W.
SENSBURG, O.

Some recent Investigations on Flutter
31th SMP Meeting of AGARD, Tonsberg/Norway
November, 1970
- 13 SENSBURG, O.

Interaction between Aircraft Structure and
Command and Stability Augmentation System
42nd SMP Meeting of AGARD, Ottawa/Canada,
4-9 April 1976
- 14 BERKELEY, E.
KINEMANN

Flutter Analysis of Complex Airplane by
Experimental Methods

Journal of the Aeronautical Sciences,
Vol. 19, Sept. 1952

15 KUHN, M.
GARR, R.
LOTZE, A. Interaction of CSAS with Elastic Aircraft
Internal MBB-Report 17, Dec. 1974

16 SENSBURG, O.
LOTZE, A.
HAIDL, G. Wing with Stores Flutter on Variable Sweep
Wing Aircraft
39th SMP Meeting of AGARD, Munich/Germany
6-12 Oct. 1974

17 DAVIS, H.M.
SWAIM, R.L. Controlling Dynamic Response in Rough Air
AIAA Third Annual Meeting, Boston, Massachusetts,
29th Nov., 1966
AIAA Paper No. 66-997

**AIRPLANE MATH MODELING METHODS
FOR ACTIVE CONTROL DESIGN**

by
 Kenneth L. Roger
 The Boeing Company
 3801 S. Oliver
 Wichita, Kansas 67210
 U.S.A.

SUMMARY

Selected Analytical Methods are described which are useful and practical in math modeling for airplane active control system design. A technique for writing state equations is presented which is suitable for incorporating lifting surface aerodynamic solutions. An economical method of computing unsteady aerodynamic influence matrices is presented for line doublets and plate doublets, the latter usable at any Mach number. An economical way to analyze three-dimensional turbulence and a convenient way of using design criteria in n-dimensions are presented to aid in designing for statistical performance. Recommendations include the use of a single airplane math model for analysis of multiple performance parameters and the use of control hardware math modeling during preliminary design.

NOTATION

A	Aerodynamic influence matrix relating grid element force and boundary condition velocity (normal wash)
B	Matrix approximating function for the product $H_1^T A^{-1}$
B_K	One of the coefficient matrices used in defining B
b	An element of the matrix B
C_k	One of the coefficient matrices used in approximating F
e	Base of natural logarithms, 2.718...
F	Generalized aerodynamic influence matrix relating generalized forces and motions
f	Frequency, Hertz
G	Power spectral density; also a generalized aerodynamic influence matrix relating generalized forces and gust velocities.
H	Frequency response function relating an airplane response and a gust velocity
H_{1, 2, 3}	Modal matrices, relating generalized motion and grid element normal displacements: (1) linear at center of pressure, (2) angular and (3) linear at normal wash reference point.
i	Imaginary number $\sqrt{-1}$; Also an index
j	An index
K	A factor used in turbulence design criteria. Also a modified spherical Bessel function
k	An index
L	Scale of turbulence. Also, a randomly varying structural load
L-Steady	The average value of a random structure load
M	Mach number
n	The number of dimensions of a multiple-dimension variable
p	Scaled Laplace variable, s/U_0
Q	Vector (column matrix) of generalized aerodynamic forces

q	Generalized displacement vector (column matrix)
R	Correlation function, transform related to power spectral density
R_K	One of the coefficient matrices used in approximating G
S	Wing semi-span
s	Complex Laplace variable
T	Rectangular or diagonal matrix of gust penetration time delays (Laplace transformed) for grid elements or groups of grid elements
U_0	Airspeed
v_g	Lateral gust velocity vector (column matrix)
w_g	Vertical gust velocity vector (column matrix)
x	A superposition of responses (for example structural element stress). Also, the argument of the function $K_\nu(x)$
y	Spanwise coordinate. Also, a typical response (for example a bending moment)
α	Dummy argument of R . Also, a vector (column matrix) of points on a multiple dimension sphere
β	A denominator constant used in defining B and b
γ	A denominator constant used in approximating G
Γ	Mathematical gamma function, the generalized factorial
Δ	Difference operator, requires subtraction as $\Delta y = y_2 - y_1$
ν	The order of the function $K_\nu(x)$
σ^2	Variance of a random variable
τ	Time variable for the correlation function R
ω	Fourier variable or frequency, radians/second
Ω_1	Scaled turbulence frequency, $2\pi f/U_0$
Ω_0	Turbulence parameter = $\Gamma(1/2)\Gamma(5/6)/L \Gamma(1/3) = 1/1.339L$
{ }	A column matrix (vector)
[]	A rectangular or square matrix

1. INTRODUCTION

A description of analytical methods found useful and practical in math modeling for airplane active control system design and performance analysis is presented. The selection of methods, emphasizing lifting surface aerodynamic theory and statistical performance evaluation, was based not only on their current acceptance by engineering specialities but also on the existence of format or cost barriers which have prevented widespread use by control system designers. The adaptation, extensions and simplifications discussed in the following sections have been used in practical engineering problems requiring design of active flight control systems.

The need for compatible airplane math models for analysis of stability and control, flutter, structural integrity and comfort has been heightened by two factors: first, the ability to improve performance in each of these areas with active control systems, and second, the lack of frequency separation in large airplanes between these areas of concern which means all performance measures must be monitored to prevent inadvertent degradation. The experience basis for the chosen methods is outlined by the following: the development of measures of structural performance (Reference 1), the design and flight testing of an active control fatigue damage reduction system (Reference 2), development of the interface between stress analysis and statistical loads analysis (Reference 3), and the design and flight testing of active control load reduction and ride improvement systems (Reference 4) and a flutter suppression system (Reference 5).

The following paragraphs and appendices contain sufficient information for the techniques to be used by aeroelasticians and active control analysts. The primary intent is, however, to encourage the active controls designer to ask for and use math models which are adequate for simultaneous analysis of all airplane dynamic performance requirements.

2. LIFTING SURFACE AERODYNAMIC SOLUTIONS IN EQUATIONS OF MOTION

Generally useful equations of motion must be expressible in all user formats including differential equations, difference equations, Laplace transformed equations, Z-transformed equations and Fourier transformed equations. Linearity of the structural and aerodynamic theory is assumed, although linearity may be with respect to a nonlinear "steady-state" solution. This section is concerned with the aerodynamic part of the equations and the unsteady linear aerodynamics typified by the lifting surface theories. These are calculable by pressure series, doublet lattice, Mach box and other methods. This theory is not directly suitable for equations of motion since it cannot be represented by a finite number of state variables in the user's transform formats. Also, most current solution methods are limited to numerical evaluation of the Fourier transformed airloads for selected frequencies.

Given a set of Fourier transformed airloads covering the frequency range of inputs and structural modes, the use of an approximating function for the airloads is permissible and desirable. The function can fit the known solutions to any desired accuracy and can serve as an interpolator for other frequencies. This function must be physically realizable and stable (its time transform, the impulsive admittance of airloads to boundary normalwash, must be nonanticipative, real, and zero at time = infinity).

Such an approximating function, since it will not accurately fit all frequencies from zero to infinity, cannot be presumed to be universally usable. For example, a Laplace transform of the function would not be accurate in the vicinity of a zero or pole introduced by the approximating function.

The usefully accurate range for Laplace arguments is not obvious, although analytic continuity suggests that leaving the imaginary axis (small positive or negative damping) is comparable to interpolation along the imaginary axis. The region near the imaginary axis is of greatest physical interest.

Fourier transform lifting surface airloads, whether panel airloads, pressure coefficients or otherwise generalized airloads, are presumed equal to the product of an influence matrix and a matrix of local normalwashes. The latter matrix is due to gusts, control surface and airplane motions, and structural deformations. The approximating function must fit the elements of the influence matrix. Equations of motion used in References 4 and 5 were based on fitting each element of the influence matrix with a function of the form shown in Equation (1). The denominator constants are noncritical and are typically chosen as $\beta_k = \omega_{\max}/kU_0$. The numerator constants are selected to give the least square error for the values of ω at which b is known.

$$b \approx b(p) = b_0 + \sum_{k=1}^4 \frac{p}{p + \beta_k} b_k, \quad p = 0 + i\omega/U_0 \quad (1)$$

Appendix I provides the computations required to incorporate these approximating functions into equations of motion for generalized freedoms. For each generalized displacement, the aerodynamic plus structural terms require six state variables. The usefulness of this formulation is in regarding the imaginary variable p as a complex scaled Laplace variable, s/U_0 . When this is done, eigenvalues of the Laplace characteristic equation appear as in Figure 1. Airplane rigid body and vibration eigenvalues appear as expected. The four clusters of eigenvalues on and near the negative real axis are due to the approximating functions and therefore not physically meaningful. Q-R iteration with complex conjugate shifts (Reference 6) is adequate for this eigenvalue problem.

Equations of motion in the form shown in Appendix I are satisfactory for all types of aeroelastic analysis - open and closed loop flutter, divergence, gust response, maneuver response, stability and control and active control synthesis. It is sometimes useful to let the approximating function give linear piston theory results when the frequency approaches infinity; however, this is not required for low frequency analysis and it does not imply knowledge of high noninfinite frequency response.

The differential equations deduced from the Laplace equations are used for designing to criteria specified as time histories and analysis of control limiting and saturation and closed-loop limit cycles. Other forms of the equations are readily determined if the eigenvectors and eigenvalues of the Laplace equations are put in a real uncoupled, first-order form as illustrated in Section 9.67 of Reference 7. Eigenvectors corresponding to the approximating function eigenvalues may be deleted.

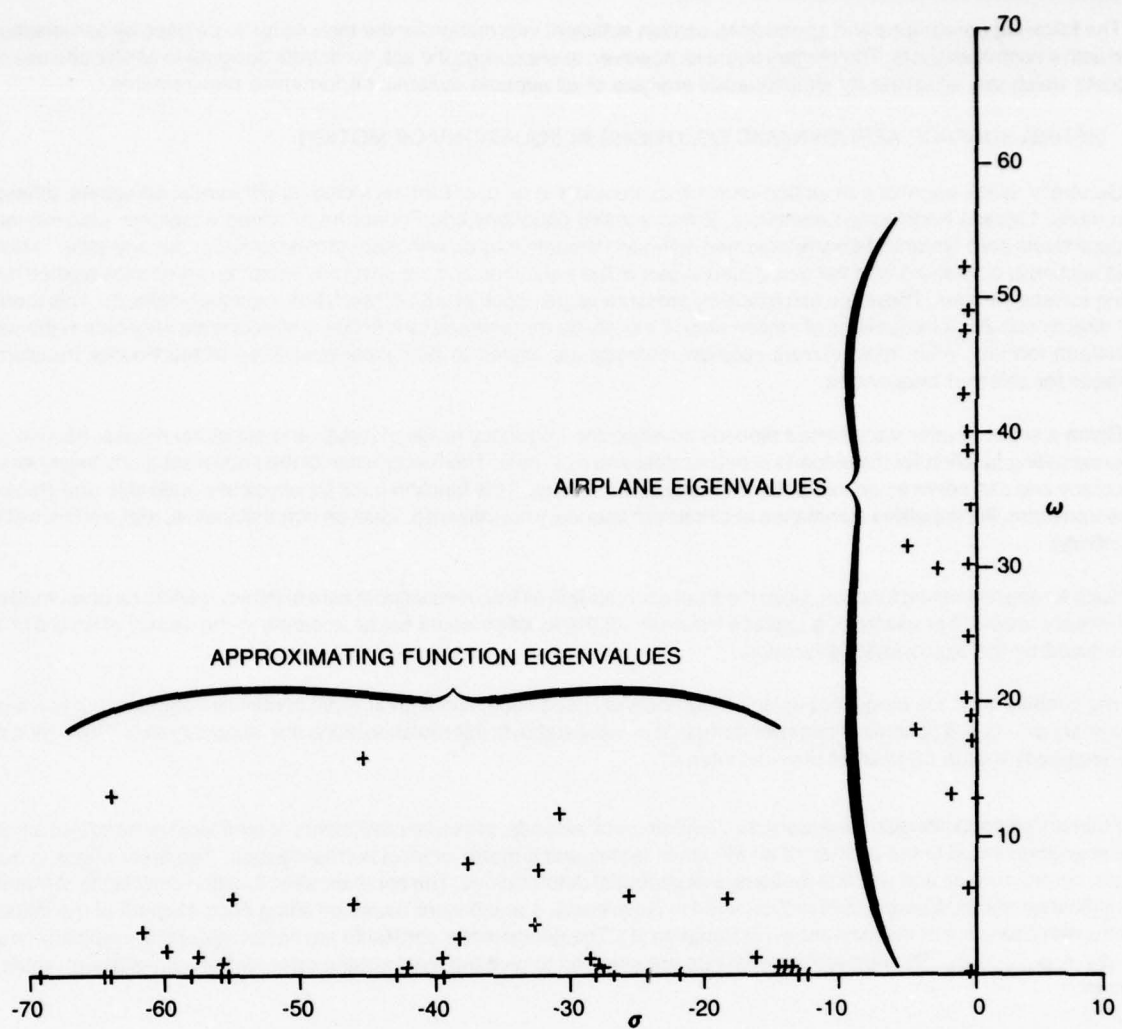


Figure 1. Typical Eigenvalues of the Laplace Characteristic Equation Using Approximating Functions

3. USE OF UNSTEADY AERODYNAMIC INFLUENCE MATRICES GENERATED FOR PLATE DOUBLET AERODYNAMIC MODELS

The use of active control surfaces on airplanes, especially several small surfaces, leads to complicated and expensive airplane math models. The following discussion concerns the use of lifting surface aerodynamic theory through finite element aerodynamic doublet modeling, the conversion of steady-state solutions to unsteady solutions, and the successful use of unsteady elements analogous to the Woodward steady-state trapezoidal element (Reference 8).

Lifting surface theory is derived from the acoustic wave equations. This theory is valid at any Mach number if the boundary conditions imposed do not require significant pressure perturbations compared with static pressure, or equivalently, do not require significant velocity perturbations compared with the speed of sound. When the solutions are presented in the Fourier transform domain, steady-state lifting surface theory appears as a special case when the frequency is zero. Another special case occurs when the boundary conditions on a region of the wing are constant for a radius large compared with the wavelength of the motion; then the solution of lifting surface theory for that region will be the same as that of linear piston theory.

Finite element aerodynamic solutions require dividing the airplane into a fine enough grid so that the user will need to specify only one boundary condition and compute only one aerodynamic force for each grid element. When each element influences every other element, a square influence matrix must be computed. Two well-known methods of computing the influence matrix are doublet lattice and Mach box, see (for example) Reference 9. The former method is suitable for subsonic flow only, the latter only for supersonic flow. The latter requires that grids must be Mach line oriented and changed for each new analysis Mach number.

A Kernel function (see Reference 10) giving velocity perturbations due to an aerodynamic force applied at a point can be readily computed at any Mach number. Hedman, in Reference 11, analytically integrated the steady-state Kernel along a spanwise line and constructed a subsonic influence matrix using these line elements (vortex lattice). Woodward, in Reference 8, integrated the Kernel over a trapezoidal "plate" element and showed the possibility of using a single element at

all Mach numbers. The authors of Reference 10 developed a practical unsteady form of the line element method (doublet lattice) and recommended an extension of the Woodward method to unsteady flow.

The author uses a simple scheme for converting vortex lattice influence matrices to doublet lattice. The ratio of the normal component of the unsteady Kernel to the steady Kernel is a well-behaved function that shows gradual changes in phase and amplitude over regions the size of doublet lattice elements. To calculate the unsteady (complex) normal wash, the author merely multiplies the integrated steady (real) normal wash by this ratio obtained at a point in the element near the normal-wash reference point. For practical size grid elements, this method is as accurate as numerically integrating the unsteady Kernel along a line and it is not erratic for high aspect ratio elements.

A similar scheme was successful for converting steady plate element influence matrices to unsteady, which permits the use of "plate doublet aerodynamic models." The point in the receiving element where the unsteady to steady Kernel ratio is computed is chosen as deep as possible within the Mach cone of the sending (pressure) element. It is likely that other popular steady-state solutions, including those for finite thickness wings, could be converted to unsteady solutions by the same method.

Three interpretations or restrictions of the Woodward solution were required. First, an influence matrix for a particular grid pattern is an entity in itself, independent of the aerodynamic element used to derive it, and consequently does not imply any particular location for the center of pressure within the element. When generalizing forces, the vortex lattice convention was used subsonically which places the center of pressure at the element quarter-chord, mid-span. When the element leading edge was supersonic, the center of pressure was placed at mid-chord, mid-span and the location was interpolated for in-between Mach numbers.

Second, the location of the normalwash reference point within the element was always 0.8808 chord, mid span, where $0.8808 = 1/2 + 1/2 (e^2 - 1)/(e^2 + 1)$. This value was chosen so a single isolated rectangular element of aspect ratio approaching infinity would have a subsonic lift coefficient of $2\pi/\sqrt{1-M^2}$. The supersonic lift coefficient of such an element will be $4/\sqrt{M^2} - 1$ regardless of the normalwash location. A similar analysis of the line-doublet element will show the subsonic normalwash location, if at mid-span, must be one-half chord aft of the pressure line, but that no (real) supersonic location is possible.

Third, although the Woodward scheme may be readily programmed for trapezoidal elements, only parallelogram elements are consistently satisfactory. In calculating the steady influence matrix, the trapezoidal grid element is replaced by a parallelogram pressure element which has the same chord at mid-span and the same sweep at mid-chord.

Results of sample computations are presented in Figure 2 for the AGARD supersonic planform. These are compared with the Mach box results published in Reference 12. This method gives reasonably close answers for coarse grids and converges smoothly and quickly for finer grids. Subsonic solutions are equivalent in accuracy to doublet lattice. Solutions at any Mach number cost about the same as doublet lattice. The grid chosen can be used at all Mach numbers without change and solutions are available at all transonic Mach numbers. Planar doublet aerodynamic models are recommended for active control design and performance evaluation.

4. THREE-DIMENSIONAL TURBULENCE

The basic concepts of dynamic analysis for multiple random inputs are well understood and, given a suitable mathematical model of the input, the designer of active control systems does not have difficulty with design synthesis. In the important case of atmospheric turbulence, adequate math models exist but are cumbersome and not widely applied. A convenient and inexpensive method is presented for modeling three-dimensional turbulence, developed from the work of Sawdy in Reference 13.

The most noticeable improvement in analyses that use three-dimensional turbulence is in calculation of the variance of generalized mode velocities and accelerations, and therefore in the calculation of zero-crossing and maxima rates. The reason for change is that parallel components of turbulence in a plane perpendicular to the flight path are only partially coherent in three-dimensional turbulence. For example, the vertical component of turbulence across the span of a straight wing airplane will at any particular instant have some random variation instead of being identical as in one-dimensional turbulence analysis. The coherence between a vertical gust at the left wing tip and a vertical gust at the right wing tip decreases rapidly as frequency increases. If this decrease is neglected, most airplane math models will predict infinite zero-crossing rates for generalized freedoms.

The spectral density of a response to the vertical component of turbulence is given (see Reference 14, eq. 3.178) in Equation (2) where $G_{W_i W_j}$ = cross spectral density of the i th and j th vertical gust as shown in Figure 3, and where H includes the time delay caused by gradual penetration of the gust.

$$G_{YY}(f) = \sum_i \sum_j H_{Yw_i}(f) G_{W_i W_j}(f) H^*_{Yw_j}(f) \quad (2)$$

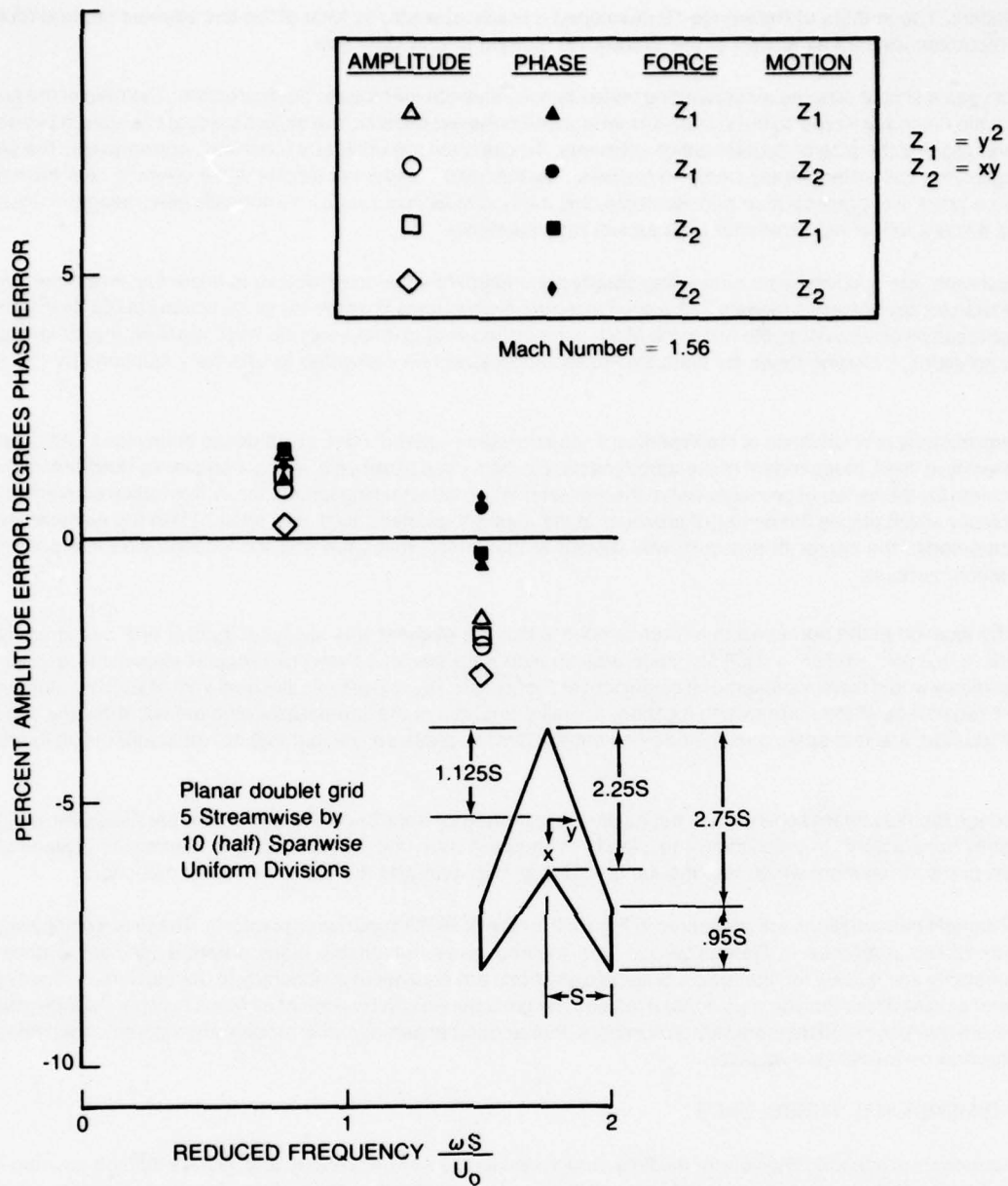


Figure 2. Comparison of Mach Box and Plate Doublet Force Coefficients for the AGARD Supersonic Wing

The summation is used as an approximation of the spanwise integration shown in Reference 13. The summation extends across the full span of the airplane and vertical gusts excite both symmetric and antisymmetric modes. Since the gust penetration time delays are included in the frequency response functions, the gust cross spectral densities are real. They are given for a unit standard derivation by the correlated spectra equation (A31) of Reference 13. Sawdy's equation is repeated here as Equation (3).

$$\begin{aligned}
 G_{w_i w_j}(f, \Delta y) = & \frac{(2)^{7/6} L}{U_0 \Gamma(5/6)} \left\{ \frac{(\Delta y \Omega_0)^{11/6} K_{1/6} \left(\Omega_0 \Delta y \sqrt{1 + (\Omega_1 / \Omega_0)^2} \right)}{[1 + (\Omega_1 / \Omega_0)^2]^{11/12}} \right. \\
 & + \left. \frac{[1 + 8/3(\Omega_1 / \Omega_0)^2] (\Omega_0 \Delta y)^{5/6} K_{5/6} \left(\Omega_0 \Delta y \sqrt{1 + (\Omega_1 / \Omega_0)^2} \right)}{[1 + (\Omega_1 / \Omega_0)^2]^{17/12}} \right\} \tag{3}
 \end{aligned}$$

BOUNDARY CONDITIONS DETERMINED BY
 w_j AND PENETRATION TIME DELAY

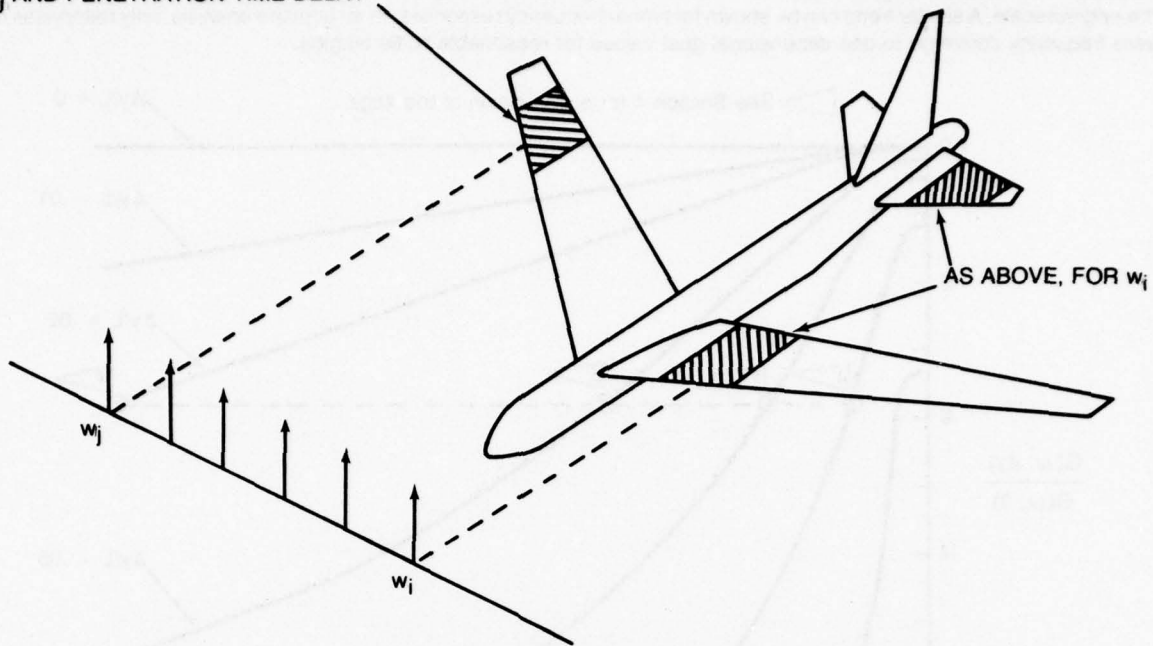


Figure 3. Spanwise Variation of Vertical Gust

In Equation (3), Δy is the spanwise separation distance. Using the limit shown in Equation (4), the special case of zero spanwise separation reduces to the familiar expression in Equation (5).

$$\lim_{x \rightarrow 0} K_\nu(x) = 1/2 \Gamma(\nu) (2/x)^\nu \quad (4)$$

$$G_{w_i w_j}(f, \alpha) = \frac{2L}{U_0} \frac{[1 + 8/3(\Omega_1/\Omega_0)^2]}{[1 + (\Omega_1/\Omega_0)^2]^{11/6}} \quad (5)$$

The gust cross spectral density may be identified alternately as in Equation (6),

$$G_{w_i w_j}(f, \Delta y) = 2 \int_0^\infty R_{w_i w_j} \left(\sqrt{\left(\frac{\tau U_0}{L}\right)^2 + \left(\frac{\Delta y}{L}\right)^2} \right) \cos(2\pi f\tau) d\tau \quad (6)$$

where $R_{w_i w_j} = \frac{\tau U_0}{L}$ is the von Karman autocorrelation function for vertical gusts and is given in Equation (7). The τ symmetry is apparent in this form and is the reason the cross spectral density is real.

$$R(\alpha) = .5925 \left(\frac{\alpha}{1.339} \right)^{1/3} \left[K_{1/3} \left(\frac{\alpha}{1.339} \right) \cdot 1/2 \left(\frac{\alpha}{1.339} \right) \times K_{2/3} \left(\frac{\alpha}{1.339} \right) \right] \quad (7)$$

Equation (6) is not recommended for evaluating G_{ww} because of computing cost. However, the equation is valuable for illustrating an alternate derivation and the significance of the forms from Reference 13. A rapid method for calculating the modified spherical Bessel functions in Equation (3) is presented in Appendix II.

In Figure 4, which is based on Equation (3), the cross spectral density of two gusts at points with spanwise separation Δy has been normalized by the gust autospectral density ($\Delta y = 0$). Flag 1 is plotted at $\Delta y/L = .2$ and $\omega L/U_0 = 4$ and is representative of the turbulence which drives large airplane low frequency modes at low altitudes ($L =$ approximately 150 m.). If the scale of turbulence "L" were doubled, the point would be replotted at Flag 2, but it does not move appreciably

upward toward the 1-D gust value. If the scale of turbulence were four times the original, the point would be at Flag 3. If the scale were ten times the original, the point would be at Flag 4, where the spectral ratio is still not significantly higher than for the original scale. A similar trend can be shown for higher frequency responses. In an airplane analysis, only responses near zero frequency converge to one dimensional gust values for reasonable scale lengths.

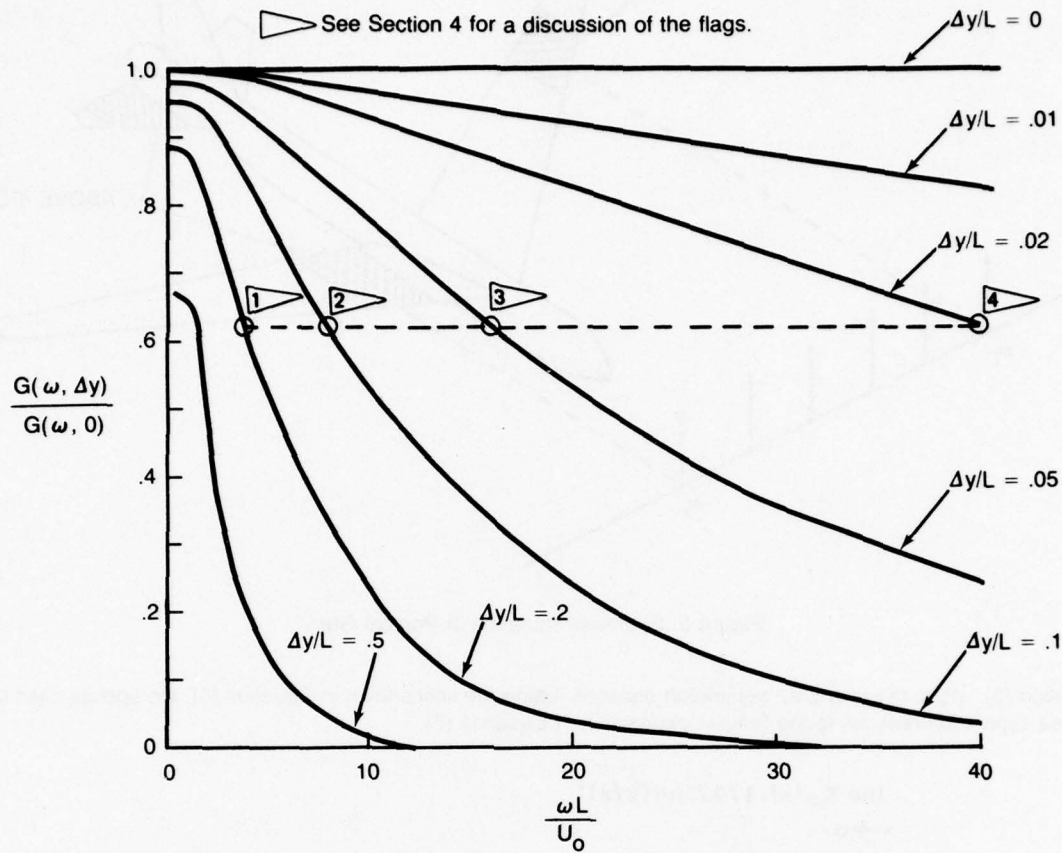


Figure 4. Effect of Spanwise Separation on Vertical Gust Cross-Spectral Density

5. MULTIDIMENSIONAL STATISTICAL PERFORMANCE CRITERIA

The use of multidimensional structural performance criteria is further complicated when those criteria are statistical. The structures analyst must be concerned with "Where does the active control system designer stop?" For example, does he need to know the damage-to-stress relationship, or the stress-to-load relationship, or even the load-to-state variable relationship? The answer depends on the criteria. The following is offered as a tool since such criteria sometimes are selected at the convenience of the analyst.

If X , consisting of $X_{\text{steady}} + \Delta X$, is any superposition of "n" responses (each consisting of $L_{\text{steady}} + \Delta L$), the design criteria for X is that $(\Delta X)^2$ be less than a factor times its variance in unit variance turbulence, as in Equation (8).

$$(\Delta X)^2 < K \sigma_x^2 \quad (8)$$

Then all points on the design surface in space L are mappable using Equation (9a). In Equation (9a), σ_{LL}^2 is a square symmetric matrix of covariances of the responses, L , and any of its symmetric square roots is acceptable. The matrix $\{\alpha\}$ contains the coordinates of a point on the surface of an n -dimensional sphere obtained by solving Equation (9b). Thus, the control system designer can work in the space L to define its covariance matrix, knowing the X - to - L relationship can be designed later in such a manner that X can meet its criteria.

$$\{L\} = \{L_{\text{STEADY}}\} + K \left[\sigma_{LL}^2 \right]^{1/2} \{\alpha\} \quad (9a)$$

$$\alpha_1^2 + \alpha_2^2 + \cdots + \alpha_n^2 = 1 \quad (9b)$$

Equation (9) was developed in Reference 3 to provide a design loads/design stress interface. Other procedures for more complicated criteria are outlined in the same reference and could be adapted to more general active control design use. Figure 5 illustrates a two-dimensional case, shear and bending moment, mapped for a mission-weighted exceedance criteria. This figure was developed without knowledge of the stress-to-load relationship. Using this figure, engineers can design structure which has acceptable stresses for load combinations on and within the envelope shown.

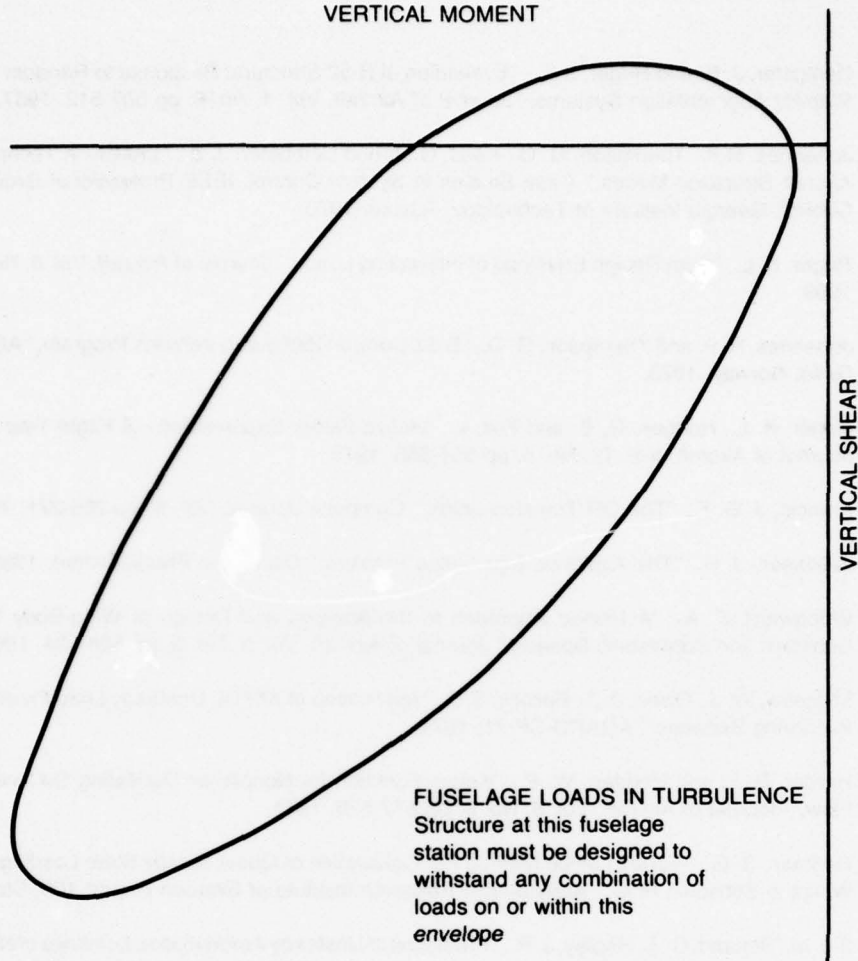


Figure 5. Example Presentation of Two-Dimensional Design Envelope for Statistical Criteria

6. RECOMMENDATIONS

The implementation of active controls in flight hardware and the flight attainment of predicted airplane structural benefits are achievable with today's analytical methods and technology. Successful design is based on first predicting the characteristics of feasible hardware and structure and the flight environment and then synthesizing control systems. Minimum requirements for the math models are summarized below.

Control hardware math models should include a nonlinear simulation of the preliminary design actuator. If realistic tolerances for backlash and hysteresis prevent attainment of performance goals, smaller control surfaces with larger amplitude motions should be considered. Control system math models should permit the designer to trade electrical versus mechanical functions. For example, the low-pass characteristics of an actuator may be less desirable than those of a specially designed electronic circuit. Low-pass filtering must be completed within the range of validity of truncated mode math models.

Airplane math models should be available which are adequate for analysis of flutter, dynamic loads, and stability and control. The active control designer must synthesize his system using these math models at the preliminary design stage. The use of simplified models and optimization procedures is not precluded, but a system should not be considered a preliminary design until its performance is adequate on complete math models. Providing such math models to the active control designer in a form he can use has been the subject of previous sections.

The author recommends the adoption of state-variable equations by all analysts involved with airplane dynamics as a standard interface and means of information exchange. Improvements in math modeling theory then become as transferable as data updates. When a common format is established, the economy and convenience of more complete math models will be self-evident.

REFERENCES

1. Dempster, J. B. and Roger, K. L., "Evaluation of B-52 Structural Response to Random Turbulence With Stability Augmentation Systems," *Journal of Aircraft*, Vol. 4, No. 6, pp 507-512, 1967.
2. Johannes, R.P., Thompson, G. O., Kass, G. J. and Dempster, J. B., "LAMS - A Technology to Control Aircraft Structural Modes," *Case Studies in System Control*, IEEE Professional Group on Automatic Control, Georgia Institute of Technology, Atlanta, 1970.
3. Roger, K. L., "Gust Design Envelope of Interesting Loads," *Journal of Aircraft*, Vol. 6, No. 4, pp 380-381, 1969.
4. Johannes, R. P. and Thompson, G. O., "B-52 Control Configured Vehicles Program," AGARD-CCP-137, Geilo, Norway, 1973.
5. Roger, K. L., Hodges, G. E. and Felt, L., "Active Flutter Suppression - A Flight Test Demonstration," *Journal of Aircraft*, Vol. 12, No. 6, pp 551-556, 1975.
6. Francis, J. G. F., "The QR Transformation," *Computer Journal*, Vol. 4, pp 265-271, 1961.
7. Wilkinson, J. H., "The Algebraic Eigenvalue Problem," Clarendon Press, Oxford, 1965.
8. Woodward, F. A., "A Unified Approach to the Analysis and Design of Wing-Body Combinations at Subsonic and Supersonic Speeds," *Journal of Aircraft*, Vol. 5, No. 6, pp 528-534, 1968.
9. Mykytow, W. J., Olsen, J. J., Pollock, S. J., "Application of AFFDL Unsteady Load Prediction Methods to Interfering Surfaces," AGARD-CP-71, 1971.
10. Harder, R. L. and Rodden, W. P., "Kernel Function for Nonplanar Oscillating Surfaces in Supersonic Flow," *Journal of Aircraft*, Vol. 8, No. 8, pp 677-679, 1971.
11. Hedman, S. G., "Vortex Lattice Method For Calculation of Quasi Steady State Loadings on Thin Elastic Wings in Subsonic Flow," *Aeronautical Research Institute of Sweden Report 105*, Stockholm, 1966.
12. Ji, J. M., Borland, C. J., Hogley, J. R., "Prediction of Unsteady Aerodynamic Loadings of Non-Planar Wings and Wing-Tail Configurations In Supersonic Flow," AFFDL-TR-71-108, Part I, 1971.
13. Sawdy, D. T., "On the Two-Dimensional Atmospheric Turbulence Response of an Airplane - The Description of Homogeneous and Isotropic Turbulent Fluid Flow, Ph.D. Thesis, Appendix A, University of Kansas, 1967.
14. Bendat, J. S. and Piersol, A. G., "Measurement and Analysis of Random Data," John Wiley & Son, New York, New York, 1966.
15. Anon., "Handbook of Mathematical Functions," National Bureau of Standards, U. S. Government Printing Office, Washington, 1968.

APPENDIX I - GENERALIZED EQUATIONS OF MOTION WITH APPROXIMATING FUNCTIONS

The generalized forces are defined in Equation (I-1a, b, c) for the interpolating variable "p". The influence matrix $[A(p)]^{-1}$

$$\{Q(p)\} = [F(p)] \{q(p)\} + [G(p)] \begin{Bmatrix} w_g(p) \\ v_g(p) \end{Bmatrix}, p : 0 + i \frac{\omega}{U_0} \quad (I-1a)$$

$$[F(p)] = [H_1]^T [A(p)]^{-1} ([H_2] + p[H_3]) \quad (I-1b)$$

$$[G(p)] = [H_1]^T [A(p)]^{-1} [T(p)] \quad (I-1c)$$

and the gust penetration matrix $[T(p)]$ are known only for discrete values of p . Define an approximating function as in Equation (I-2),

$$[H_1]^T [A(p)]^{-1} \approx [B_0] + \sum_{k=1}^4 \frac{p}{p+\beta_k} [B_k] \quad (I-2)$$

which is the matrix equivalent of Equation (1), where the $[B_k]$ are chosen for a least square error fit of the known values, and where the β_k are preselected as in Section 2. Substituting Equation (I-2) in Equation (I-1b) gives Equation (I-3a, b, c, d).

$$[F(p)] \approx p[C_1] + [C_0] + \sum_{k=1}^4 \frac{p}{p+\beta_k} [C_k] \quad (I-3a)$$

$$[C_1] = ([B_0] + [B_1] + \dots + [B_4]) [H_3] \quad (I-3b)$$

$$[C_0] = [B_0] [H_2] \quad (I-3c)$$

$$[C_k] = [B_k] ([H_2] \cdot \beta_k [H_3]), k=1, 4 \quad (I-3d)$$

The gust coefficient, Equation (I-1c) may be fitted with a separate approximating function as in Equation (I-4a, b), in which $[R_1, 2, \dots]$ provide a least square error fit. The author lets the penetration matrix

$$[G(p)] \approx [R_0] + \frac{p}{p+\gamma_1} [R_1] + \frac{p}{p+\gamma_2} [R_2] + \dots \quad (I-4a)$$

$$[R_0] = [B_0] [T(0)] \quad (I-4b)$$

$[T(p)]$ represent local groupings of aerodynamic elements with the time delay to the leading edge of the grouping being supplied at solution time.

APPENDIX II - NUMERICAL EVALUATION OF BESSEL FUNCTIONS IN CROSS-SPECTRAL MATRIX FOR VON-KARMAN TURBULENCE

The use of Equation 3 in Section 4 requires evaluation of a large number of modified spherical Bessel functions of fractional order. The following procedure is an acceptable compromise of speed and accuracy for the range of orders and arguments significant in turbulence analysis.

One of the integral representations of the function shown in Equation (II-1) is chosen according to the values of the order and argument. These are better suited for numerical integration than the integral in Equation (6), Section 4. These formulas were selected from those published in Reference 15, Paragraph 9.6. The integration is accomplished numerically using 15-point Laguerre weighting factors and abscissas (see Reference 15, Table 25.9).

$$K_\nu(x) = \int_0^\infty e^{-xt} \cos h(t) \cos h(\nu t) dt, \nu \leq 1/2 \text{ or } x \geq 1/2$$

$$= \frac{\Gamma(\nu + 1/2)}{\pi^{1/2}} \left(\frac{2}{x}\right)^\nu \int_0^\infty \frac{\cos(xt) dt}{(1+t^2)^{\nu + 1/2}}, \nu > 1/2 \text{ AND } x < 1/2 \quad (II-1)$$

CONSISTENCY IN AIRCRAFT STRUCTURAL AND FLIGHT CONTROL ANALYSIS

Robert C. Schwanz
 Flight Control Division
 Air Force Flight Dynamics Laboratory
 Wright-Patterson Air Force Base, Ohio 43433

ABSTRACT

Military Specifications (MILSPECs) are often employed by the USAF procuring authority as guidelines for design, development, acceptance testing and mission application of military aircraft. The MILSPECs must usually be satisfied by formulations of the aerodynamic and dynamic analyses that are consistent, or equivalent if not identical. When control configured vehicle considerations are involved, however, inconsistencies resulting from analysis expediency or previous engineering convention may occur. In this paper YF-16, C-5A, B-52E and large transport aircraft design studies and flight tests provide data for a discussion and numerical illustration of these inconsistencies. It is concluded that they may be minimized or avoided altogether if flight control specialists become more familiar with restrictions of present-day unsteady aerodynamic theory, and structural specialists increase their knowledge of modern dynamics and control theory.

1.0 INTRODUCTION

Several recent flight test programs sponsored by the Flight Control Division of the Air Force Flight Dynamics Laboratory (AFFDL) have demonstrated the possibility of improving aircraft performance thru less inhibited use of the flight control system. Within the USAF and much of the aerospace industry this technological development has been given the acronym CCV, the Control Configured Vehicle. One advantage of the CCV concept is that several of the structural design problems may be solved with high-gain, redundant, automatic control systems, rather than redefining the structure or redistributing mass. In fact CCV implies that the shape of the aircraft may in some cases be determined by the control systems required to meet mission goals.

A number of CCV concepts have been demonstrated in flight, both in part and as a whole for selected aircraft configurations; a substantial research effort to develop tools for CCV analysis is in progress. It will therefore be assumed in this paper that CCV is, or soon will be, a practicable aircraft design option and will indicate flight control systems that purposefully alter:

- Static stability and other handling qualities (8785B)
- Maneuver loads (8860A, 8861A)
- Fatigue life (8866A, 9490D)
- Ride quality (9490D)
- Flutter mode damping (8870A, 9490D)

The numbers in parentheses refer to selected Military Specifications (Refs. 1-6) that include considerations of interaction of the control system and structure.

An examination of these MILSPECs as design guidelines, with CCV in mind, shows that each recognizes the cross-disciplinary nature of these control systems. A partial listing of relevant paragraphs (Table 1), shows the degree of consideration to vary from specific phase- and gain-margin requirements, in MILSPECs 8870A and 9490D, to more general statements that leave interpretation of a particular flight vehicle to the discretion of the contractor and the procuring authority. Clearly, it is the intent of the MILSPECs to guarantee to the procuring authority that interaction of the flight control system with the structure of conventional and CCV aircraft is properly considered in design, development, acceptance testing, and mission application.

It is not the objective of this paper to delve into the origin and background of the MILSPECs, nor to address a specific redundancy or omission in current specifications. Its purpose is to indicate several problems of analysis consistency that arise as the individual flight control and structural engineering disciplines complete their tasks in fulfillment of design guidelines such as the MILSPEC requirements. These inconsistencies in aerodynamic and dynamic formulations occur in practice because each engineering discipline introduces different mathematical approximations and because analyses require certain expediencies.

Inconsistency in aerodynamic formulation appears to occur primarily because each of the disciplines has a different responsibility in aircraft design. The problem is particularly acute as it pertains to interaction between the control system and the structure. The flight control specialist, who is charged with responsibility for control system synthesis, employs the unique insight afforded by aerodynamic approximations in the frequency, Laplace, and time domains. Recent design studies of CCV configurations indicate that in the future, time domain aerodynamic approximation will assume added importance as very complex multi-loop control systems are synthesized via modern control theory. The structural specialist, who is accountable primarily for control system analysis, and not synthesis, employs most commonly aerodynamic approximations in the frequency domain. There, an application of classical control theory is often adequate to demonstrate compliance with design guidelines. It is clear that analysis inconsistencies can occur if each discipline individually utilizes its own approximation of the aircraft aerodynamics in these various mathematical domains.

Inconsistency in the dynamical description of the aircraft, given a common aerodynamic formulation, usually arises from (1) procedures used to reduce the number of elastic degrees of freedom (DOF); (2) deletion of the initial condition of state in the perturbation-dynamics equations; and (3) exclusion of the forward-speed degree of freedom. Studies of single-input/multiple-output CCV control systems (e.g., flutter mode control alone) have not adequately pictured the overall system dynamics problems, particularly those involving handling qualities and several CCV concepts. Also, previous studies of multi-input/multiple-output CCV control systems, intended for conventional aircraft, have not highlighted the aforementioned dynamics problems because of the inherent natural aerodynamic stability of the aircraft and the conventional dynamic approximations in the case of a relatively large frequency separation between the mean-axis-system modes (rigid body modes) and the structural dynamic modes.

The approach followed herein is to review briefly the CCV analysis and synthesis task, in section 2.0, prior to discussing in sections 3.0 and 4.0 the inconsistency that arises in aerodynamic and the dynamic formulations. The review is considered in order to define a general, modern control, state space terminology which will condense the description of CCV aircraft into a compact set of matrix differential equations that may then be subsequently referred to in the discussion. Classical and modern control theories are assumed to be well understood so that emphasis may be placed on detailed, numerical aircraft design or flight test results for the B-52E, C-5A, YF-16, and a large transport-category aircraft. These numerical results are presented graphically in terms of Bode, Nyquist, root locus and time history data plots. Section 5.0 contains concluding remarks. Throughout this discussion, one of the main goals of the Conference Committee on the Structural Aspects of Active Controls should be recalled:

.... to consider what the make up or ingredients should be for good and appropriate criteria and specifications."

2.0 BACKGROUND: CONTROL-SYSTEM ANALYSIS AND SYNTHESIS

The synthesis of a CCV or of a conventional control system may be accomplished by classical control theory, modern control theory, or more likely a blending of the two, since performance criteria are specified in both frequency and time domains. In synthesis, the problem is the development of a control system guaranteeing that relative stability, steady-state accuracy, transient response and frequency response of the control system are adequate to satisfy the performance criteria. In analysis the control system already exists and analytical or experimental methods are employed to measure the performance of the controlled dynamical system. A cursory review of design guidelines such as the MILSPEC paragraphs in Table I indicates that, for the most part, the structural specialist presently acts as an analyst who is supplied a control system as a portion of his dynamical system. If the structural specialist finds a structural problem induced by the control system, the only practical options are (1) to send the control system back to the flight control staff for redesign (synthesis); (2) to alter structural layout or mass distribution to compensate for the controller; or (3) to alter the control system himself. If the two disciplines develop identical or equivalent aerodynamic and dynamic formulations for the unaugmented aircraft, the first choice is the logical course of action. If it is determined that the formulations differ, the second two options might seem viable; they are certainly not advisable because the control system design is likely to diverge.

2.1 Definition of Problem

Specifically, in synthesis the goal is to establish a relationship between measurements, \underline{y} , and controls $\underline{\delta}$, of the form $\underline{\delta}(t) = K^* \underline{y}(t)$ where K^* is a matrix of control system gains. The measurements and responses are related algebraically to a first order, ordinary differential equation defining the states, \underline{x} , that is, in the modern control, state space form:

$$\text{State equation: } \dot{\underline{x}}(t) = A \underline{x}(t) + B \underline{\delta}(t) + \underline{n}_1(t) \quad (1a)$$

$$\text{Measurement equation: } \underline{y}(t) = M \underline{x}(t) + \underline{n}_2(t) \quad (1b)$$

$$\text{Response equation: } \underline{r}(t) = C \underline{x}(t) + D \underline{\delta}(t) \quad (1c)$$

$$\text{Control equation: } \underline{\delta}(t) = K^* \underline{y}(t) \quad (1d)$$

Here the matrix equations may be nonlinear, with time-varying coefficients in the matrices A, B, C, D, M, and K^* . Typically, the states, \underline{x} , consist of reference-axis-system motions, \underline{x}_r , kinematics, \underline{x}_k , elastic deformations, \underline{x}_u , and other variable associated with specifics of the control system and its modelling, \underline{x}_c . The controls consist of aerodynamic control surface motions, engine thrust and other means of purposefully inducing forces and moments on the aircraft. The measurements, \underline{y} , consist of accelerations, rotation rates, air data, inertial planform data and other sensed quantities. The responses, \underline{r} , usually consist of structural moments, shears and stresses, model following errors, control rates, tracking errors and other outputs of the system. The term $\underline{n}_1(t)$ is process noise associated with atmospheric gusts and turbulence or pilot commands, and $\underline{n}_2(t)$ is measurement error induced by the electronics or mechanics of the sensors.

It is assumed that equation (1) defines a dynamical, controlled system that is analog (or continuous). A state-space form of equation (1) also exists for a discrete-data digital system; it will not be discussed as most modern control theory applies equally well to digital control systems, and because many digital control systems result from "digitization" of previously designed analog systems. For all future discussions it will be assumed that equation (1) has constant coefficients and has been linearized in the independent variables of state, \underline{x} , and controls, $\underline{\delta}$. It should be recognized that the linearized, constant-coefficient problem, although the most common in the literature, is only a portion of the total CCV analysis and synthesis task. In actual design a substantial amount of engineering time must be spent in accounting for non-linearities in aerodynamics, structure, and dynamics and control; these non-linearities are not discussed herein. It is also assumed that the structural and the flight control specialists have agreed upon the significant terms constituting the control equations, but that each may have a different approximation of the state, measurement and response equations owing to differences in aerodynamic or dynamical formulation.

2.2 Classical Control Theory

In classical control theory determination of the control equation and K^* consists of a trial-and-error application of analysis procedures until the performance criteria are satisfied. The procedures are largely a graphical portrayal of Bode, Nyquist, and root locus stability criteria for open-loop and closed-loop systems. The measurement noise is usually ignored in all but specialized studies.

- Bode and Nyquist. The Bode graphical method determines relative stability information. The Nyquist method is particularly useful in that it treats stability of both minimum and non-minimum phase system. In both graphical procedures the open-loop transfer function is considered, and the phase and gain margins (the design criteria found in MILSPEC 8870) are determined from a plot of the amplitude and the phase angle of the transfer function, with frequency, ω , varying from zero to infinity. One advantage of these methods is that they may be used with frequency-dependent, unsteady aerodynamic forces. A disadvantage is that a multiple-input/multiple-output system (typical of CCV) must be analyzed one loop at a time for its stability characteristics; thus, a change in a compensating control element requires reanalysis of all the loops. Once the system is designed to be stable, Nichol's chart may be used to convert the open-loop magnitude and phase relationship to closed-loop frequency-response characteristics.
- Root Locus. This method is also graphical and requires that the analyst define his system [equation (1)] in the Laplace domain. Both the open- and closed-loop characteristics of a multiple-input/multiple-output system may be determined. Much of the information contained in the Bode, Nyquist, and Nichol's chart may be calculated directly from the root locus definition of the dynamical system. The advantages of the method are substantial in that closed-loop stability can be directly determined by working with the open-loop transfer functions of the overall system. Transient responses and steady state accuracy may also be easily determined by an inverse Laplace transform to the time domain. The effect on the stability of the dynamical system of a gain change in one loop of the control system may be determined directly. In addition, a root locus on the dynamic pressure, on sensor location or type and on the physical parameters of the system (such as those shown and discussed subsequently in Figure 11) make the method ideally suited to synthesis by reanalysis. The method requires that unsteady aerodynamic information in equation (1) be expressed as constant coefficient, ordinary differential equations in the Laplace domain. This disadvantage is discussed subsequently in section 3.0.

2.3 Modern Control Theory

In modern control theory synthesis of a CCV control system proceeds more directly than in classical control theory. That is, the trial-and-error analysis and reanalysis calculations are at a minimum. It is first necessary that equation (1) and the desired performance criteria be expressed as responses, \underline{r} , in the time domain. Before the gains, K^* , may then be determined, an index of performance, $J(\underline{r}, t)$, is minimized to determine the optimal gains, K , subject to constraints on the states, \underline{x} , and controls, $\underline{\delta}$. In CCV synthesis studies sponsored or conducted by the AFFDL, the specific form of J most commonly used has been the quadratic performance index:

$$J(\underline{r}, t) = E \left[\int_0^\infty \underline{r}^T Q \underline{r} dt \right]$$

where Q is a weighting matrix selected a priori and E is the expectancy operator required for systems with nondeterministic inputs, $n_1(t)$. More specifically, the process employed to determine optimal gains, K , that relate the controls $\underline{\delta}$ to the states, \underline{x} , involves an iterative solution for the Lagrange multipliers, P , using the matrix Riccati equation expressed by:

$$\begin{aligned} 0 &= \bar{A}^T P + P \bar{A} + \bar{Q} - P \bar{E} P \\ \text{where } \bar{A} &= A - B (D^T Q D)^{-1} D^T Q C \\ \bar{E} &= B (D^T Q D)^{-1} B^T \\ \bar{Q} &= C^T Q C - C^T Q D (D^T Q D)^{-1} D^T Q C \end{aligned}$$

then, knowing P ,

$$K = -(D^T Q D)^{-1} [D^T Q C + B^T P]$$

and finally,

$$\underline{\delta} = K \underline{x}$$

Only in the simplest systems, e.g., rigid aircraft, is it possible to measure the states \underline{x} as feedback. In general the measurements, \underline{y} , include a combination of mean-axis-system motions as well as structural deformations and for this reason a second set of gains, K^* , using the realistic measurements, \underline{y} , are then calculated. The procedure for doing this varies and is dependent upon the experience of the flight control engineer. One method used at the AFFDL consists of augmenting the measurement equation with states not directly measurable, and then inverting the measurement equation to arrive at a relationship between states, \underline{x} , and augmented measurements, \underline{y} . This new relationship is substituted in the response equation and the index of performance in order to arrive at the second optimization problem. Finally, an incremental gradient algorithm based upon the previously-determined weighting matrix, Q , and optimal gains, K , is applied. The process of arriving at the best practical gains, K^* , is partially trial-and-error due to numerical stability problems that develop if the incremental gradient method begins too far from the global minimum of the problem.

The advantages of optimal control are substantial since a stable, multiple-input/multiple-output

CCV control system can be designed directly in the optimal sense with a relatively small manpower investment. This means a particular component of the responses, r , such as wing root bending moment, can be treated without aggravating other responses such as those associated with handling qualities or flutter. One of the disadvantages of optimal control methods is that it is difficult, in a stable numerical sense, to enforce state, control and measurement constraints except by a trial-and-error method involving Q. Also it is necessary that the unaugmented system be stable at the beginning (usually easy to accomplish) and it is not generally possible to enforce relative stability, frequency domain stability margins even though the system is guaranteed stable in an absolute sense. Additionally, all aerodynamic information must be expressed in the time domain.

The importance of maintaining consistency in the aerodynamics and dynamics formulations is clearly illustrated. The optimal or suboptimal control system that evolves depends upon all the information presented in the state, measurement and response equations. If the flight control specialist accomplishes its synthesis, $\underline{\delta} = K^{\underline{u}} \underline{y}$, using one set of numerical values for A, B, C, D, and M, and the structural specialist then uses other numerical values to analyze this CCV aircraft according to MILSPEC requirements, the resulting design is sure to be erroneous.

3.0 AERODYNAMIC FORMULATIONS

The right-hand sides of equations (1a), (1b), and (1c) contain terms associated with aerodynamic forces that act upon the vehicle. These forces are known to be proportional to the mean-axis-system motion, x_r , elastic deformations, x_u , controls, $\underline{\delta}$, and the atmosphere, n_1 . There are numerous theoretical, semiempirical and experimental approximations of those aerodynamic forces reported in the literature. The Woodward method, vortex lattice, strip theory, doublet lattice, Rho's method, kernel function, piston theory, spline aerodynamics, etc., are just some of the highly specialized aerodynamic methods that are employed in CCV analysis and design. Of these, the steady aerodynamic methods employed to calculate initial values of the states, measurements and responses do not at present appear to introduce consistency problems because a great deal of experimental data and user experience have been accrued.

On the other hand, theoretical computation of the unsteady aerodynamic forces that are very important to the CCV dynamic analysis and synthesis problem appears to present the designer with two choices that may not enforce consistency between the methods of the structural and flight control staffs. With one choice, the unsteady aerodynamics are estimated in the frequency domain, resulting in frequency-dependent-coefficient, ordinary differential equations that are most suitable for analysis via classical control methods. This means absolute and relative stability and frequency response of the open- and closed-loop system may be estimated, thus satisfying many of the structural design MILSPEC requirements cited in Table 1. With the second choice, unsteady aerodynamic forces are estimated in the Laplace domain; the resulting linearized equations are then transformed to the time domain where control system analysis and synthesis via modern control theory may be accomplished. The transformation of these constant-coefficient, linearized equations from the Laplace to the frequency domain is well known. However, frequency-dependent-coefficient equations in the frequency domain may not be transformed to the Laplace and time domains without some approximation. The approximation involved in passing from frequency to Laplace and time domains introduce consistency problems between the methods of structural and flight control specialists.

One means of identifying potential inconsistency is to consider recent CCV-related examples in which the aerodynamic methodology is isolated and its impact on CCV studied: Four recent studies come to mind:

- Cunningham (Ref. 7) investigated the problem of extending frequency dependent aerodynamics to the Laplace and time domain of analysis; the objective was development of an unsteady aerodynamic methodology compatible with linear-systems root locus analysis and nonlinear-system time history analysis. The procedure is to fit frequency-dependent generalized aerodynamic forces with Tschebychev polynomials, then Fourier transform to the time domain to get indicial functions, approximate the indicial function by a second series of Tschebychev polynomials, and finally Laplace transform that series. The result is a polynomial with terms having first order polynomials in the Laplacian variable as their denominators. One problem arising from this procedure is that a large number of poles are introduced for each retained dynamic degree of freedom; for instance, in one application a total of 68 poles result when three mean-axis degrees of freedom and one structural mode degree of freedom are retained and unsteady aerodynamic force indicial functions are approximated by a five term polynomial. The large number of poles introduces numerical error when the roots of the equation are determined for root locus studies; the practical upper limit for acceptable numerical accuracy is 100-150 complex number roots. The test of this method on the YF-16 missiles-on roll-loop stability, discussed in section 4.1, indicate that the root-locus classical method predicts instability at 6.1 Hz, and at a lower roll-loop gain than the 6.50 Hz instability observed in flight test. The root locus analysis, however, matches the results of previous analytical analyses in the frequency domain.
- Roger (Ref. 8) approximated the frequency-dependent aerodynamic forces of the doublet lattice method as a rational polynomial function of the Laplace variable subject to the restrictions that (1) it must have complex-conjugate symmetry; (2) the denominator roots must lie in the left half of the complex plane; and (3) it must approximate the values of the complex coefficient when $s = 0 + j\omega$ for those values of ω analyzed using the doublet lattice theory. The B-52E CCV program analysis and synthesis tasks employ this method. Another paper in the conference discusses the method in more detail.
- Brune (Ref. 9) modified the steady aerodynamic method, developed at the Boeing Company by Woodward et al, to include a first-order, reduced-frequency, unsteady aerodynamic approximation to be used in the frequency, Laplace and time domain. This approximation is applicable to general three-dimensional configurations at subsonic and supersonic speeds (such as swept-wing aircraft idealized in Figure 1). The method is theoretically valid for reduced aerodynamic frequencies, $k = \omega_c/2\bar{u}_1$, of order much less than 1.0, much less than $[(1-M^2)/M^2]$ at subsonic speeds, and much less than $[(M^2-1)/M^2]$ at supersonic speeds. In contrast, doublet lattice and other unsteady aerodynamic

methods are theoretically valid for a reduced frequency of the order $[(1-M^2)/M]$ at subsonic speeds and of the order $[(1-M^2)/M^2]$ at supersonic speeds. A numerical quantitization of these boundaries, as well as a brief summary of the Woodward approach to the aerodynamics, is presented in Figure 2. When pressure distributions estimated by doublet lattice theory for various aspect ratio, wing-alone configurations are compared to similar data estimated by this low frequency approximation, boundaries of applicability may be established (Ref. 9). These boundaries for aspect ratio (AR) 2 and 8 wings at subsonic Mach numbers are shown in Figure 2. Note that the method is most theoretically valid for slender, low aspect ratio configurations. If the reduced frequency required for a 0 Hz to 10 Hz flight control system for the C-5A or B-1 are plotted on Figure 2, several important points would be noted. First, from a theoretical standpoint alone it would appear that most methods are barely adequate at subsonic speeds and are inadequate at transonic speeds. Also, the low frequency approximation, although of questionable accuracy at subsonic speeds when compared with other theories, may be adequate for CCV analysis and synthesis at supersonic speeds. Here, low aspect ratio and low reduced frequencies are the rule.

The most exhaustive study of the low frequency method for CCV applications has been on an aspect ratio 6.96 wing-alone configuration with the structure and (Mach number 0.80) aerodynamics representative of a large transport aircraft. This study, conducted by Kroll and Miller (Ref. 10), is limited to an investigation of frequency characteristics of unsteady aerodynamic terms in transfer functions that relate responses and measurements to vertical turbulence and inboard aileron harmonic motion. The data are presented as power spectral density plots and linear-amplitude Bode plots of the unaugmented aircraft transfer functions. The reference-axis-system motion states, \underline{x}_r , are reduced and then transformed to be the inertial coordinate states: vertical displacement, z , and rotation about the center of mass, θ . Six invacuum modes are retained in the states, \underline{x}_u . In this truncated modes formulation the initial conditions are wings-level flight, parallel to the flat earth; also, gravity terms are neglected. The aerodynamic methods employed are:

1. Woodward method
2. Woodward method, modified by Kussner/Wagner $[\psi(\omega)/\phi(\omega)]$ functions.
3. Woodward method, modified by low frequency corrections on the states $[\underline{x}(\omega)]$.
4. Woodward method, modified by low frequency correction on states $[\underline{x}(\omega)]$, gusts $[\underline{z}_g(\omega)]$ and controls $[\underline{\delta}(\omega)]$.
5. Strip theory method corrected with Kussner/Wagner $[\psi(\omega)/\phi(\omega)]$ functions.
6. Rho kernel-function unsteady aerodynamic method.
7. Vortex spline kernel-function unsteady aerodynamic method.
8. Doublet lattice unsteady aerodynamic method.

Figure 3 contains selected results of the study for flight in vertical turbulence. In this analysis of wing-tip vertical acceleration, a_z , and wing-root bending moment, the vortex spline, doublet lattice, and Rho methods provide nearly identical results; thus, the comparisons are not presented here. However, when the various formulations of the Woodward methods and the strip theory method are compared with the Rho method, the differences are moderate to large, with the largest discrepancies occurring at frequencies greater than 2 Hz. Possible reasons for this are a poor, low frequency approximation of the more exact unsteady aerodynamic theories, or the introduction of inaccuracies when the Kussner/Wagner functions are applied to the states of a three-dimensional wing. The results of the report concerning control surface transfer functions should be reviewed with some care, as the Woodward methods were not carefully "tuned" to control power calculations as the doublet lattice method, and because the strip theory method includes empirical corrections while the other methods do not.

- Disney, Hargrave, and Hollenbeck (Ref. 11) analyzed and synthesized in-part the Active Lift Distribution Control System (ALDCS) for the C-5A using a semi-empirical, unsteady aerodynamic strip theory method. Good correlation with flight test data is achieved and indicated by the Bode amplitude plot (Fig. 4) of the aileron open-loop transfer function of the ALDCS aircraft. Schwanz and Stockdale (Ref. 12) employed the low frequency correction to the Woodward method to analyze this same transfer function at another C-5A mass distribution; the results are compared with the strip theory method in Figure 5. Here it is seen that reasonable correlation in phase and amplitude exists up to 4.5 Hz ($k=0.5$); above 4.5 Hz the two methods approximate structural dynamics differently. The computer method used by Schwanz and Stockdale is the FLEXSTAB program (Ref. 9); the aileron unsteady aerodynamic forces, $\delta(\omega)$, are neglected, but care has been taken to correct the aerodynamic forces of the control surfaces to match experimental data.

From this discussion it may be inferred that an unsteady aerodynamics method that is theoretically exact in the Laplace domain of analysis would help to enforce consistency between the methods of the structural and flight control analysts. To be of greatest utility, the new theory should possess characteristics permitting exact transformations of the linearized form of equation (1) between the frequency, Laplace and time domains of analysis. Until a solution is found, flight control engineers must continue to question and test the unsteady aerodynamic approximations they employ in design, and structural specialists must continue to appreciate the role of unsteady aerodynamics in the special synthesis problem that the flight control specialist solves for the CCV aircraft.

4.0 DYNAMICAL SYSTEM FORMULATION

Experience within the Flight Control Division at the AFFDL has indicated that the crux of the inconsistency problem in dynamic system description, when the aerodynamic formulations are consistent, is the

formulation and approximation of the equations of motion contained in equation (1a). These equations of motion relate the states, \underline{x}_r , \underline{x}_k and \underline{x}_u to measurements, responses, controls and inputs. In order to subsequently explore these possible inconsistencies in the formulation and application of the equations of motion, it is best to express them in linearized, second-order, ordinary differential equation form. This form separates aerodynamic terms from the inertial, damping and stiffness terms. Using the non-inertial, mean axis as the body-fixed, reference axis system and the notation of References 9, 13 and 14, these equations may be written as:

$$\underline{M}^* \ddot{\underline{x}}_r + \underline{M}_1^* \ddot{\underline{x}}_r + \underline{M}_2^* \ddot{\underline{x}}_k = \dot{\phi}^T \underline{f}_{AP}(\underline{x}_r, \underline{x}_u, \underline{\delta}, \underline{n}_1, t) \quad (2a)$$

$$\underline{m} \ddot{\underline{u}} + \underline{d} \dot{\underline{u}} + \underline{k} \underline{u} = \dot{\phi}^T \underline{f}_{AP}(\underline{x}_r, \underline{x}_u, \underline{\delta}, \underline{n}_1, t) \quad (2b)$$

$$\dot{\underline{x}}_r = \underline{f}(\dot{\underline{x}}_k, \underline{x}_k) \quad (2c)$$

$$\text{where } \underline{x}_r^T = [u \ w \ q \ v \ p \ r]$$

$$\underline{x}_k^T = [\theta \ \phi \ \psi]$$

$\underline{x}_u^T = [\dot{u} \ \dot{w} \ \dot{q} \ \dot{v} \ \dot{p}]$ and \underline{u} are the time-dependent modal amplitudes.

$$\underline{M}^* = \begin{bmatrix} M_S & 0 \\ 0 & M_A \end{bmatrix}, \quad M_S = \begin{bmatrix} M_1 & 0 & 0 \\ 0 & M_1 & 0 \\ 0 & 0 & I_{yy} \end{bmatrix}, \quad M_A = \begin{bmatrix} M_1 & 0 & 0 \\ 0 & I_{xx1} & -I_{xz1} \\ 0 & -I_{xz1} & I_{zz1} \end{bmatrix}$$

$$\underline{M}_1^* = \begin{bmatrix} 0 & M_1 Q_1 & M_1 W_1 & -M_1 R_1 & 0 & -M_1 V_1 \\ -M_1 Q_1 & 0 & -M_1 U_1 & M_1 P_1 & M_1 V_1 & 0 \\ 0 & 0 & 0 & 0 & A & B \\ M_1 R_1 & -M_1 P_1 & 0 & 0 & -M_1 W_1 & M_1 U_1 \\ 0 & 0 & C & 0 & D & E \\ 0 & 0 & F & 0 & G & H \end{bmatrix}$$

$$A = 2P_1 I_{xz1} + R_1 (I_{xx1} - I_{zz1})$$

$$B = -2R_1 I_{xz1} + P_1 (I_{xx1} - I_{zz1})$$

$$C = -P_1 I_{xz1} + R_1 (I_{zz1} - I_{yy1})$$

$$D = -Q_1 I_{xz1}$$

$$E = Q_1 (I_{zz1} - I_{yy1})$$

$$F = R_1 I_{xz1} + P_1 (I_{yy1} - I_{xx1})$$

$$G = Q_1 (I_{yy1} - I_{xx1})$$

$$H = Q_1 I_{xz1}$$

$$\underline{M}_2^* = \begin{bmatrix} c\theta_1 & 0 & 0 \\ s\theta_1 c\phi_1 & c\theta_1 s\phi_1 & 0 \\ 0 & 0 & 0 \\ s\theta_1 s\phi_1 & -c\theta_1 c\phi_1 & 0 \\ 0 & 0 & 0 \\ 0 & 0 & 0 \end{bmatrix} M_1 g$$

Here the subscript 1 denotes initial value, while

c_{01} , is cosine θ_1 , etc.

s_{01} , is sine θ_1 , etc.

M_1 , is the total mass.

I_{jj1} is the total moments and products of inertia about the non-inertial axis system.

Ψ ($= \psi_1 + \psi$), Ω ($= \omega_1 + \theta$), Φ ($= \phi_1 + \phi$) are the Euler angles in the rotation sequence of Reference 14.

U ($= U_1 + u$), V ($= V_1 + v$), W ($= W_1 + w$) are the components of axis-system translation.

P ($= P_1 + p$), Q ($= Q_1 + q$), R ($= R_1 + r$) are the components of axis-system rotation rate.

Φ is the matrix of mean-axis system modes.

ϕ is the matrix of invacuum modes.

f_{AP} are the distributed aerodynamic forces due to changes in state, controls or atmospheric gusts and turbulence.

4.1 Reduction in Elastic Deformation States

An examination of equation (2) indicates than it can consist of a very large number of second-order equations for y . Common sense, augmented by theoretical and numerical accuracy considerations, dictates that equation (2) should be reduced in size to its absolute minimum. Typically, in this reduction process the analyst first determines the frequency range over which the CCV control system will be required to solve design problems, e.g., from 0 Hz to 20 Hz. In this example, the problem of state reduction then simplifies to eliminating higher frequency states while maintaining reasonably correct dynamics from 0 Hz to 20 Hz excitation frequencies, and appropriate asymptotic behavior as excitation frequency exceeds 20 Hz and approaches infinity. There are three state reduction procedures reported in the literature:

Residual flexibility - the invacuum mode shapes representing the elastic motion are separated into "retained" and "deleted" modes. The deleted modes are purged dynamically but retained statically as static elastic corrections to the remaining states. The correction factors are related to the retained invacuum modes and the flexibility matrix or stiffness matrix of the structure.

Truncated modes - the deleted modes of the residual methods are not represented by the static elastic correction factor. This is the most common method reported in the literature.

Static elastic or quasi-static - the motions of the structure relative to the mean axis are assumed to be in phase with the axis system motions.

Only recently have these state reduction procedures been tested numerically on realistic CCV hardware design cases:

- Schwanz and Stockdale (Ref. 12) studied the C-5A ALDCS design problem using equation (2) as mechanized in the FLEXSTAB computer software of Reference 9. Figure 6 presents the effects of residualization and truncation on the short period and phugoid dynamics of the unaugmented C-5A aircraft. Actual data points are noted at 3, 7, and 13 retained structural modes; the straight lines are drawn only to facilitate visualization of the trend. As shown, the residual formulation predicts the mean-axis-system dynamic characteristics nearly independently of the number of modes retained while the truncated formulation does not. Also note that the residual formulation correctly covaries to the static elastic formulation for zero retained modes, while the truncated formulation does not. The reason for the improved accuracy is that in the residual formulation, the generalized aerodynamic forces as well as the mean-axis-system stability derivatives are numerically dependent upon the number of modes retained, whereas in the truncated formulation these assume a constant value independent of the number of retained modes. As an example, Figure 7 presents the stability derivatives that are used in the 3, 7, and 13 retained structural mode study summarized in Figure 6.
- Konar, Mahesh, Stone, and Hank (Ref. 15) investigated the effect of residualization and truncation upon the design of an optimal ALDCS control system for the C-5A. Of interest here is the effect of residual and truncation mathematical formulations upon the time-domain responses of the closed-loop dynamical system. These data are calculated by first updating the FLEXSTAB math model of the C-5A (Ref. 12) with experimental data to match flight test results as closely as possible. Then, an optimal ALDCS control system is designed (as discussed in section 2.0) for the residual flexibility case in which 24 unaugmented aircraft states are retained. Finally, given that control system, time histories of selected responses are calculated for the case in which only the sensor equations and then the sensor plus state equations are truncated. Typical responses are presented in Figures 8 and 9. As shown, the pitch rate of the center of mass and the wing-root bending moment are more sensitive to sensor truncation than to state truncation.
- Peloubet, Haller, Cunningham, Cwach, and Watts (Ref. 7) analytically studied the effect of residualization and truncation on a flight-test observed instability in the YF-16 handling qualities augmentation system. The problem, mentioned previously in section 3.0 was corrected in the YF-16 in 1974, but is of continuing research interest because it is difficult to theoretically predict the phenomena. Tables 2 and 3 present selected results from Reference 7. Here the analysis is in

the frequency domain with experimentally-corrected, doublet lattice theory providing the unsteady aerodynamics information. As shown in Table 2, the low frequency ($\omega = 0.153$ Hz), residual flexibility measurements for sensors near the center of mass of the unaugmented aircraft have a magnitude and phase angle nearly independent of the number of retained structural degrees of freedom. In contrast, the truncated modes formulation provides transfer function amplitudes and phases that are dependent upon the number of retained states. In the truncated formulation of the unaugmented YF-16 dynamics, it takes six elastic degrees of freedom to approach the residual flexibility formulation results for only one retained structural degree of freedom. When the lateral-directional handling qualities augmentation system is included in the analysis the results are somewhat mixed. In the case of yaw-loop closed and roll-loop open for the wing-tip missiles-on (Table 3a), the residual formulation solution for the phase-crossover gain-margin converges much more rapidly than does the truncated modes formulation. Based upon convergence alone, the missiles-off configuration (Table 3b) also appears to be best represented by the residual flexibility formulation.

From these results, it may be concluded that the truncated and the residualized forms of equations (1) and (2) describe different system dynamics for the unaugmented and augmented aircraft. Of course, the difference between the two formulations may be large or small depending upon the aircraft and its mission. A review of the literature indicates that the structural specialist currently prefers the truncated formulation, while the flight control specialist may employ both formulations. Clearly, inconsistencies may arise if each discipline approaches the design requirements with its own formulation of the dynamics.

4.2 Representation of Initial Conditions

It is standard practice in the flight control studies to represent the dynamics of the mean-axis-system by states \underline{x}_r and \underline{z}_k , as indicated in equation (2). In contrast, structural specialists most often approximate these states as the so-called "rigid body modes":

$$\underline{z}_r^T = [x z y \dot{\psi}]^T, \text{ where } x, y, \text{ and } z \text{ are inertial coordinates.}$$

An inspection of the terms in equation (2) indicates that initial conditions of motion (quantities that are subscripted with "1") play a prominent role in the numerical calculations. Of further interest then is the consideration of initial conditions in state equations with independent coordinates \underline{z}_r .

This consideration of initial conditions is best approached by observing the kinematic expression in equation (2c) provides a partial transformation between \underline{x}_r and \underline{z}_r , namely (Ref. 14):

$$\begin{Bmatrix} P \\ Q \\ R \end{Bmatrix} = \begin{bmatrix} 1 & 0 & -s\theta \\ 0 & c\phi & \cos\phi \\ 0 & -s\phi & c\theta c\phi \end{bmatrix} \begin{Bmatrix} \dot{\phi} \\ \dot{\theta} \\ \dot{\psi} \end{Bmatrix}$$

If equation (2c) is augmented by an additional kinematic expression between u , v , w and \dot{x} , \dot{y} and \dot{z} , a complete expression may be developed to transform (2) from \underline{x}_r , \underline{x}_k , and \underline{u} space to \underline{z}_r and \underline{u} space. This additional kinematic expression is the well known trajectory equations used in stability and control ("flight-path" equations of Reference 14):

$$\begin{Bmatrix} \dot{x} \\ \dot{y} \\ \dot{z} \end{Bmatrix} = \begin{bmatrix} c\theta c\psi & s\theta s\phi c\psi - c\phi s\psi & c\phi s\theta c\psi + s\phi s\psi \\ c\theta s\psi & s\theta s\phi s\psi + c\phi c\psi & c\phi s\theta s\psi - s\phi c\psi \\ -s\theta & s\phi c\theta & c\theta c\phi \end{bmatrix} \begin{Bmatrix} u \\ v \\ w \end{Bmatrix}$$

These kinematic expressions may be combined to yield the desired transformation of state (Ref. 16):

$$\underline{x}_r = \begin{bmatrix} c\theta c\psi & -s\theta & 0 & s\psi c\theta & 0 & 0 \\ s\theta c\phi c\psi & c\phi c\theta & 0 & s\theta s\psi c\phi & 0 & 0 \\ +s\phi s\psi & & & -s\phi c\psi & & \\ 0 & 0 & c\phi & 0 & 0 & s\phi c\theta \\ s\phi c\psi s\theta & s\phi c\theta & 0 & s\theta s\phi s\psi & 0 & 0 \\ -s\psi c\phi & & & +c\phi c\psi & & \\ 0 & 0 & 0 & 0 & 1 & -s\theta \\ 0 & 0 & -s\phi & 0 & 0 & c\theta c\phi \end{bmatrix} \underline{z}_r \quad (3)$$

Note that the transformation contains both initial conditions of motion as well as perturbation values. Once the initial conditions are specified in \underline{x}_r space, the general form of the transform becomes:

$$\underline{x}_r = T_1 \underline{z}_r + T_2 \underline{z}_r \quad (4)$$

where T_1 and T_2 may be nonlinear in the kinematic states, \underline{x}_k .

As examples:

- The transformation for the case of steady, straight, wings-level, climbing flight is defined using stability axis ($w=0$) variables by setting $v_1, P_1, Q_1, R_1, \phi_1, \psi_1$ equal to zero in equation (3);

U_1 and O_1 are nonzero constant values. In this case $T1$ and $T2$ are independent of \dot{x}_k and sparse:

$$\begin{aligned} u &= \dot{x} \\ w &= \dot{x}s_0 + \dot{z}c_0 + U_1\theta \\ q &= \dot{\theta} \\ v &= \dot{y} - \psi U_1 c_0 \\ p &= \dot{\phi} \\ r &= \dot{\psi} \end{aligned} \quad (5)$$

- The transformation for the case of steady, wings-level, lg straight and level flight has only U_1 nonzero. Thus, for stability axes:

$$\begin{aligned} u &= \dot{x} \\ w &= \dot{z} + U_1\theta \\ q &= \dot{\theta} \\ v &= \dot{y} - U_1\psi \\ p &= \dot{\phi} \\ r &= \dot{\psi} \end{aligned} \quad (6)$$

Conventional and CCV flight control systems are designed to provide satisfactory performance for many initial conditions besides steady, level, lg climbing flight. This is accomplished using equations of motion such as indicated in equation (2). However, it has been the convention of many structural dynamicists to demonstrate compliance with certain of the MILSPECs using equations of motion in Z_r and u space that apply only to steady lg straight and level flight. This formulation can be visualized by first equating all initial conditions in equation (2a) to zero except U_1 and then transforming using equation (6). It should be clear that the solution of equations (2) for the states, measurements and responses of the unaugmented aircraft will be different for flight control and structures staffs unless great care is taken to account for the initial conditions in a consistent fashion.

Consider the importance of initial conditions on the horizontal tail torsion due to a frequency sweep by the outboard aileron as presented in Figure 10. These data presented in the form of Bode logarithmic amplitude and linear phase angle plots, are estimated theoretically for an unaugmented B-52/L7 aircraft configuration using the Woodward method corrected for the low frequency aerodynamics on the state only. The FLEXSTAB computer program defined in Reference 9 is the computer mechanization of equation (2). The transfer function that is presented is typical of a response that might be considered in designing a maneuver load control system for the wing. As indicated in Figure 10, the horizontal tail torsion for these two initial conditions is substantially different in both phase and amplitude at low frequencies of the order of the phugoid where a reduced static stability or handling qualities control system might be required.

4.3 Forward-Speed Degree of Freedom

It is often apparent in structural analyses, particularly those associated with flutter, that the structural dynamicist has neglected the forward-speed degree of freedom, u (or \dot{x}), while the flight control specialist has not. The neglect of forward-speed effect means that the first equation in (2a) is eliminated. This, affecting consistency of analysis between structural and flight control specialists, was justified in the past on the basis that there is a large frequency separation between the phugoid and short period modes; it was sufficient for the structural dynamicist to represent only the short period dominated motions, w and q (or \dot{z} and $\dot{\theta}$). However, reducing the static longitudinal stability can cause a coalescence of short period and phugoid motions into two aperiodic modes plus a third oscillatory mode, a phenomenon that can not be realistically approximated if the speed terms are neglected.

In order to illustrate numerically the importance of the speed degree of freedom, a root locus on C_{m_x} (the measure of longitudinal static stability) of an unaugmented B-52E/L7 configuration is calculated for the lg wings-level flight case discussed in Figure 10. In Figure 11 the data are presented for a variation of C_{m_x} from $-0.017/\text{deg.}$ (statically stable) to $+0.017/\text{deg.}$ (statically unstable). Retention of the forward-speed degree of freedom results in the presence of the phugoid mode. As C_{m_x} is varied this mode first moves to the real axis and then coalesces with the aperiodic short period mode to form the third oscillatory mode and an unstable aperiodic mode with a very small time-to-double amplitude. If the forward-speed degree of freedom is neglected, the coalescence of modes to form the third oscillatory mode would not occur and the unstable short period aperiodic mode would possess a different dynamic characteristic. A reduced static stability or other handling qualities control system is of course sensitive to all these modes. It is also influenced by and alters other higher frequency dynamic modes owing to (1) structural feedback through the control surface actuator; (2) sensor measurement of higher frequency structural modes; and (3) eigenvector coupling between states of the compensating control system and invacuum structural modes.

5.0 CONCLUDING REMARKS

The intent of design guidelines to enforce consistency in structural and flight control analysis and synthesis has been discussed. As indicated, CCV-type control systems are multiple-input/multiple-output systems in most applications, requiring that the aerodynamic formulation be expressed in the frequency, Laplace and time domains in order to demonstrate compliance with MILSPECs and similar guidelines. Also, as shown, the mathematical formulation describing the dynamical system, particularly the equations of motion of unaugmented aircraft, must not possess unjustifiable or unproven approximations and must define

the system from very low to moderately large frequencies. In order to enforce consistency in structural and flight control analyses it is apparent from the examples given that the flight control specialist should become increasingly familiar with unsteady aerodynamic theories and computerized methods. In addition, it is evident that the structural specialist should become equally familiar with the more precise system dynamical formulations that the flight control specialist uses matter-of-factly.

Ingredients for good and appropriate criteria, one goal of the Conference Committee on Structural Aspects of Active Controls, may well be found in the state space form of the equations describing the controlled dynamical system, e.g., equations (1a - 1d). This formulation, expressed in the time domain, enforces consistency between flight control and structural specialists' analyses by clearly defining technical responsibility for each state, measurement, response and control equation. The solution of these equations provides, simultaneously, direct and indirect numerical evaluations of significant parameters that are of interest to the specialists who must currently interpret the existing MILSPECs and other guidelines. Thus, the state-space equations are a numerical realization of the design guidelines that interrelate separate disciplines in the CCV analysis and synthesis task.

6.0 REFERENCES

1. MIL-F-8785B (ASG), Interim Amendment-1 (USAF), 31 March 1971.
2. MIL-A-008860A (USAF), Used in Lieu of MIL-A-8860 (ASG), 31 March 1971.
3. MIL-A-008861A (USAF), Used in Lieu of MIL-A-8861 (ASG), 31 March 1971.
4. MIL-A-008866A (USAF), Used in Lieu of MIL-A-8866 (ASG), 31 March 1971.
5. MIL-F-9490D (USAF), Superseding MIL-F-9490C (USAF), 6 June 1975.
6. MIL-F-008870A (USAF), Used in Lieu of MIL-A-8870 (ASG), 31 March 1971.
7. Peloubet, R., Haller, R., Cunningham, A., Cwach, E., Watts, D., "Application of Three Aeroelastic Stability Analysis Techniques", AFFDL-TR-76-89, September, 1976.
8. Roger, K., et al., "B-52 CCV Control System Synthesis", AFFDL-TR-72-92, Vol II, January, 1975.
9. Dusto, A., Brune, G., Dornfeld, G., Mercer, J., Pilet, P., Rubbert, P., Schwanz, R., Smutney, P., Tinoco, E., Weber, J., "A Method for Predicting the Stability Characteristics of Control Configured Vehicles, Vol. I, FLEXSTAB 2.01.00 Theoretical Description", AFFDL-TR-74-91, November, 1974.
10. Kroll, R., Miller, R., "Comparisons of Several Aerodynamic Methods for Application to Dynamic Loads Analyses", NASA CR-137720, July, 1976.
11. Disney, T., Hargrave, W., [Hollenbeck, W.], Eckholdt, D., "Historical Review of C-5A Lift Distribution Control System", "The C-5A Active Lift Distribution Control System", Paper presented at the AFFDL/NASA symposium on advanced control theory, NASA TM X-3409, August, 1976.
12. Schwanz, R., Stockdale, C., "Effect of Structural Idealization on the Aeroelastic Stability and Control Parameters of the C-5A Aircraft", AFFDL-TM-75-172-FGC, December, 1975.
13. Schwanz, R., "Formulations of the Equations of Motion of an Elastic Aircraft for Stability and Control and Flight Control Applications", AFFDL-FGC-TM-72-14, August, 1972.
14. Etkin, B., Dynamics of Flight, 1959.
15. Konar, A., Mahesh, J., Stone, C., Hank, M., "Active Control Synthesis for Flexible Vehicles, Vols. I - III", AFFDL-TR-75-146, July, 1976.
16. Schwanz, R., "Transformations that Relate Flight Control Analysis to Loads and Flutter Analysis for CCV Applications", AFFDL-TM-77-4-FGC, January, 1977.

Table 1. Partial Listing of MILSPEC Statements Relevant to CCV Design

MILSPEC	PRIMARY PARAGRAPHS	OTHER PARAGRAPHS
8785B	6.6 <u>Effects of aeroelasticity, control equipment, and structural dynamics.</u> Since aeroelasticity, control equipment, and structural dynamics may exert an important influence on the airplane flying qualities, such effects should not be overlooked in calculations or analyses directed toward investigation of compliance with the requirements of this specification.	3.1, 3.4, 3.5, 3.7
8860	3.5 <u>Deformations.</u> The cumulative effects of elastic, permanent, or thermal deformations, acting singly or together, which result from application of landing loads, fatigue loads, and limit loads shall not: <ol style="list-style-type: none"> Inhibit or degrade the mechanical operation of the airplane Affect the airplane's aerodynamic characteristics to the extent that performance guarantees or flying qualities requirements cannot be met Require repair or replace of parts. 	3.8, 6.2
8861A	3.14 <u>Stability augmentation devices.</u> The effect of stability augmentation and automatic control devices shall be included, where applicable. The design conditions shall apply for operative, inoperative, and transient modes. In failure cases, any variation or reduction of the device capability shall be included in the structural design condition. <p>3.22.2.1' <u>Airplane turbulence response.</u> Airplane turbulence response shall be characterized by the response parameters A and N_0 which are determined by a dynamic analysis of the airframe. The dynamic analysis shall incorporate rigid body motion, significant flexible degrees of freedom, the flight control system, and the stability augmentation system. Augmentation system requirements shall be consistent with MIL-F-8785. Significant effects shall be represented by equivalent linear representation which shall be demonstrated to be conservative. In conjunction with the dynamic analysis, when specified in the application contract, a flight simulation shall determine the effects of control inputs on structural loads when encountering extreme value turbulence. The turbulence levels shall be of sufficient severity to cause structural limit load occurrences. Adverse coupling shall be corrected. The following definitions shall apply.</p>	3.22
9490D	3.1.11.2 <u>Stiffness.</u> The stiffness of flight control systems shall be sufficient to provide satisfactory operation and to enable the aircraft to meet the stability, control, and flutter requirements as defined in the applicable portions of MIL-F-8785, MIL-A-8870, MIL-F-83300 and MIL-A-8865. Normal structural deflections shall not cause undesirable control system inputs and outputs.	3.1.2, 3.1.3, 3.2.6
8870A	3.2.1 <u>Augmentation systems.</u> For airplanes with augmentation systems, the flutter margins and damping requirements of 3.1 shall be met both with the system inoperative (system off) and with the system operating. In particular, at speeds up to V_L , the operating system shall be stable with: (1) a gain margin of at least ± 6 dB, and (2) separately, a phase margin of at least $\pm 60^\circ$. <p>4.1.1.7 <u>Servo-control analyses.</u> The dynamic characteristics of control surface actuating systems such as servo boost, fully powered servo control, and other types shall be included in the flutter analyses. The effect of high temperatures on the dynamic characteristics of the actuating systems including the hydraulic fluid shall be included. Augmentation systems which may alter the dynamic response of the airplane shall also be included in the flutter analyses; the method and approach used in these analyses shall be subject to review and approval of the procuring activity.</p>	3.2.6, 3.2.7, 4.2.2 4.2.3, 4.2.6
8866A	3.1.1.2 <u>Service loads spectrum.</u> The service-loads spectrum is derived from a collection of load spectra. Each loads spectrum in this collection shall define the expected (average) number of load cycles according to load magnitude for a given source of repeated loads. The loads spectrum for each significant source of repeated loads shall be based on a realistic interpretation of the design usage. The contractor shall include all significant sources of repeated loads. The source of repeated loads may include, but not be limited to, ground handling and taxiing operations, landing operations, flight maneuvers, atmospheric turbulence, in-flight refueling, autopilot, inputs, cabin pressurization, buffeting, terrain-following, and the ground-to-ground cycle.	3.4, 3.5, 3.11

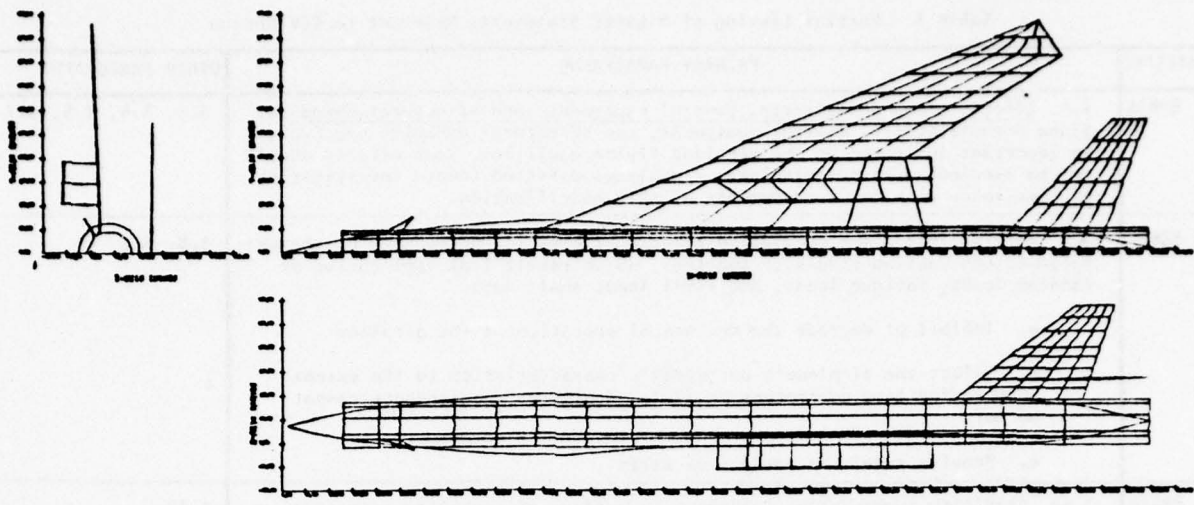


FIGURE 1. Spatial Aerodynamic Finite-Element Representation of a Swept-Wing Aircraft With Double Box Nacelle

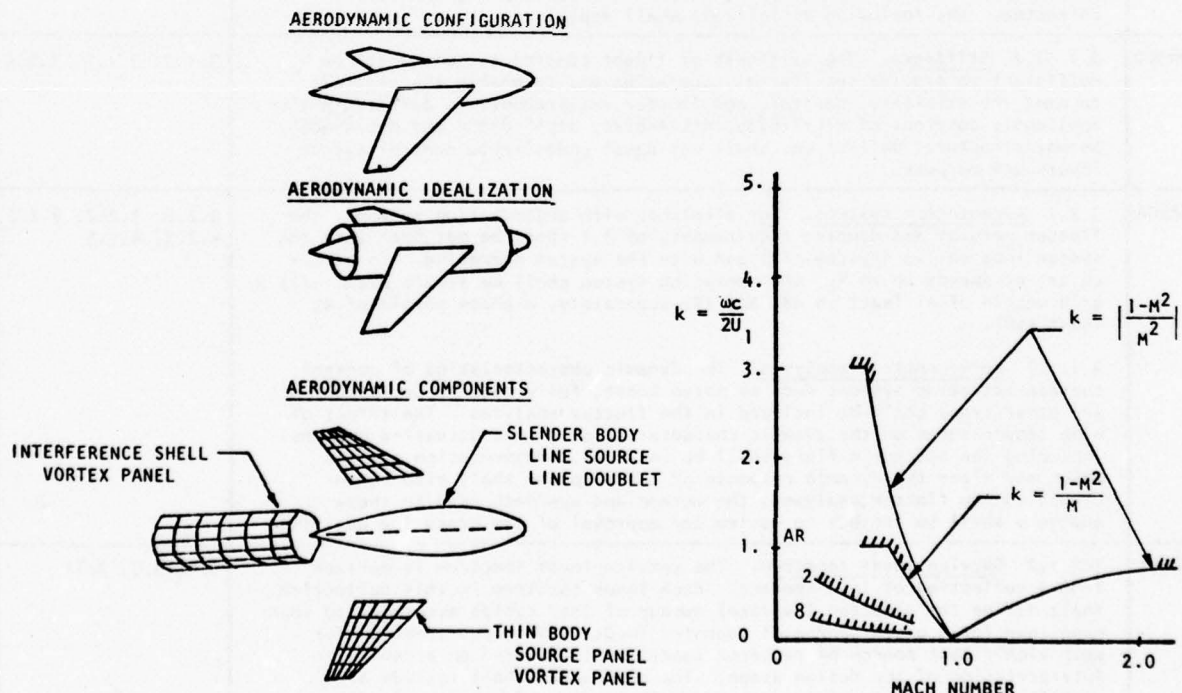


FIGURE 2. Small Perturbation Expansion Parameters and Theoretical Range of Applicability of Low Reduced Frequency Unsteady Aerodynamics Method (Ref. 9)

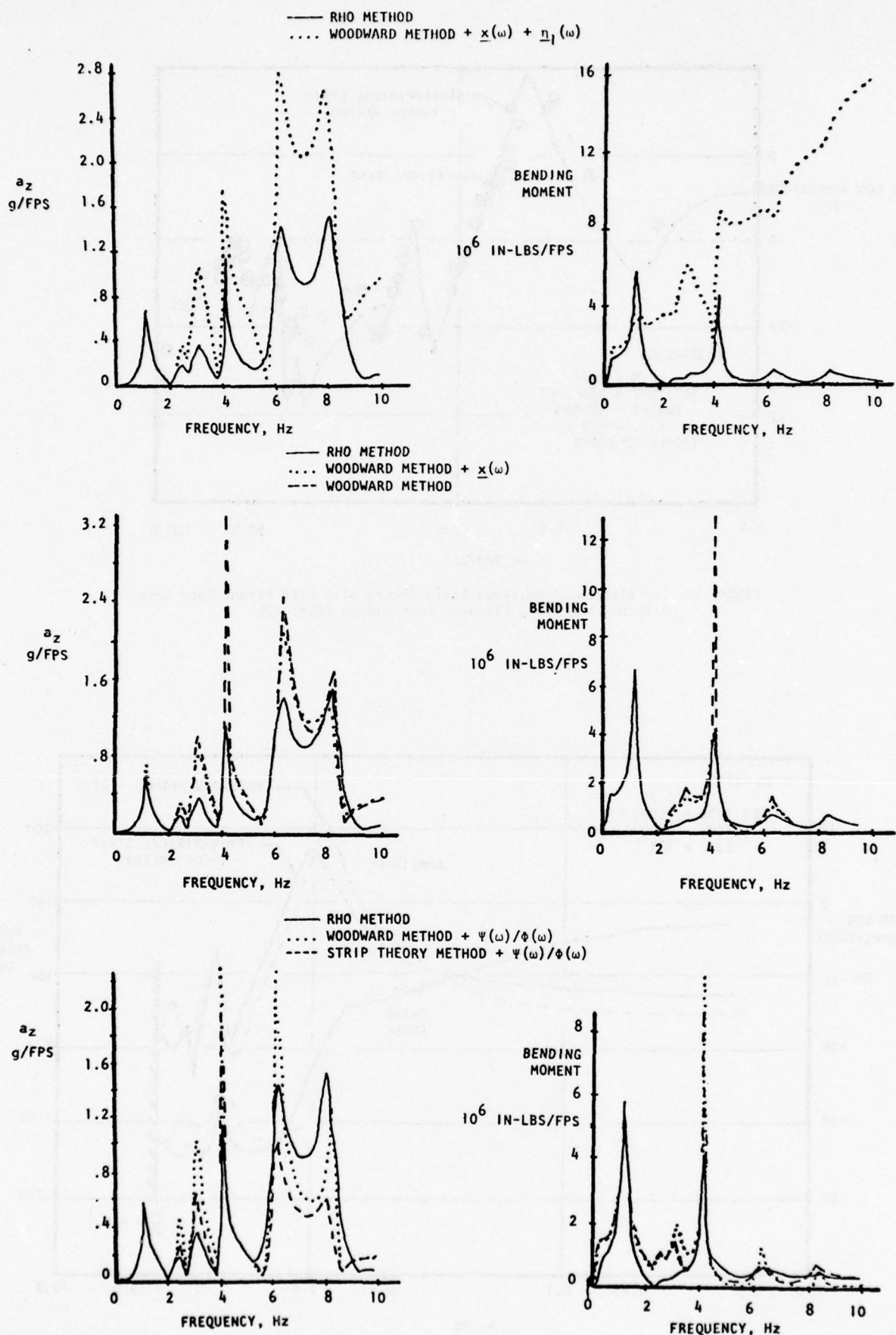


FIGURE 3. Effect of Aerodynamic Formulation on Wing Tip Acceleration and Wing-Root Bending Moment Response Amplitude Due to Vertical Turbulence, $M=0.80$ (Ref. 10)

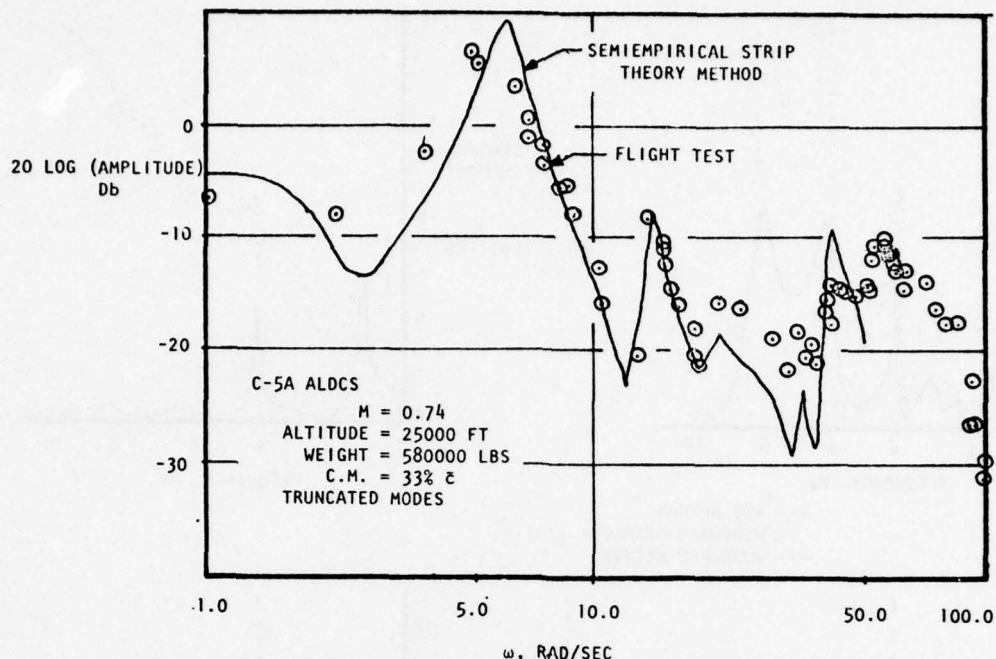


FIGURE 4. Correlation of Unsteady Strip Theory with C-5A Flight Test Data, Aileron Loop Open, Elevator Loop Closed (Ref. 12)

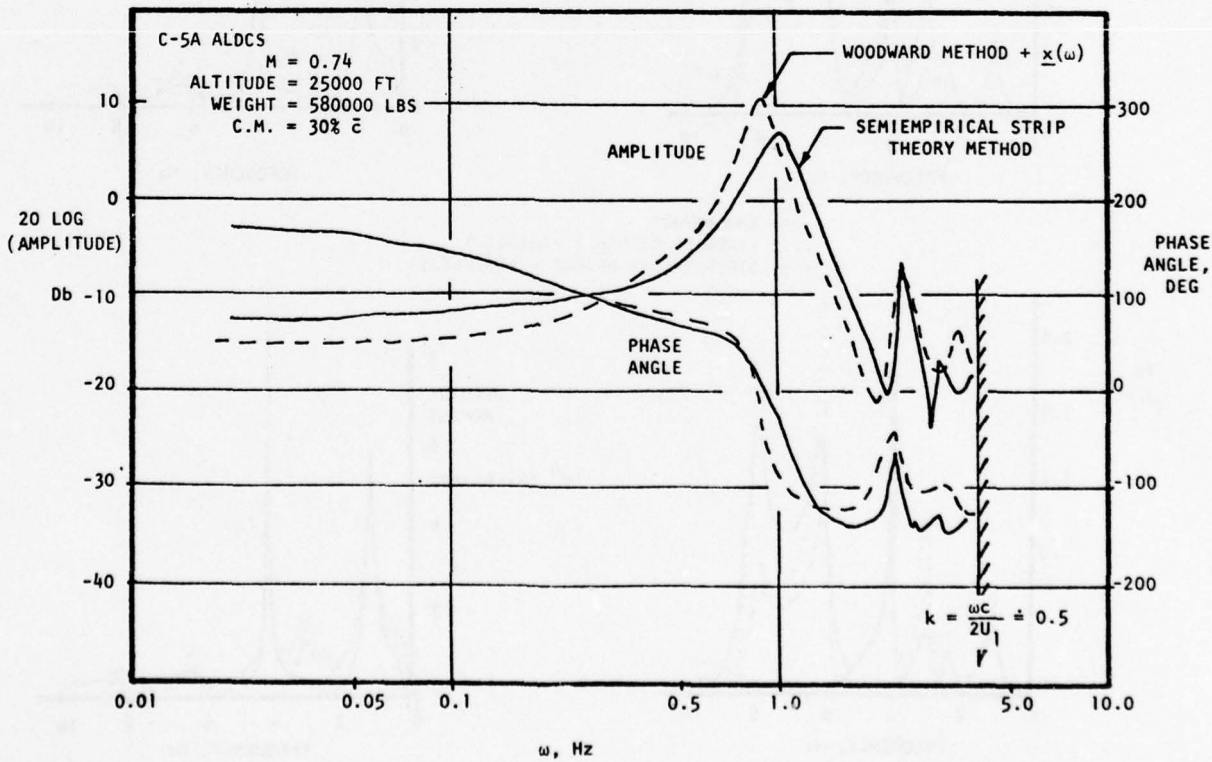


FIGURE 5. Correlation of Unsteady Strip Theory Method with Low Frequency Unsteady Aerodynamic Correction to Woodward Method, Aileron Loop Open, Elevator Loop Closed (Ref. 12)

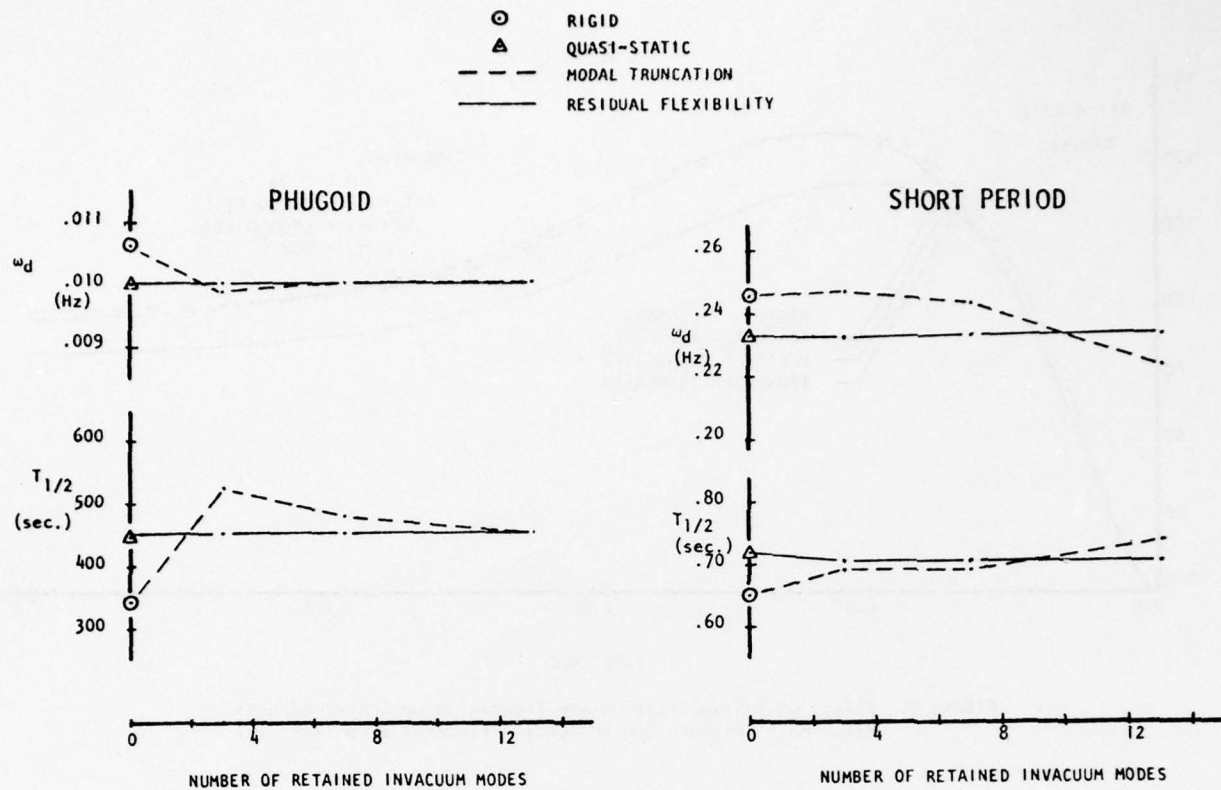


FIGURE 6. Effect of Retained Structural Invacuum Modes on C-5A Mean-Axis System Dynamics (Ref. 12)

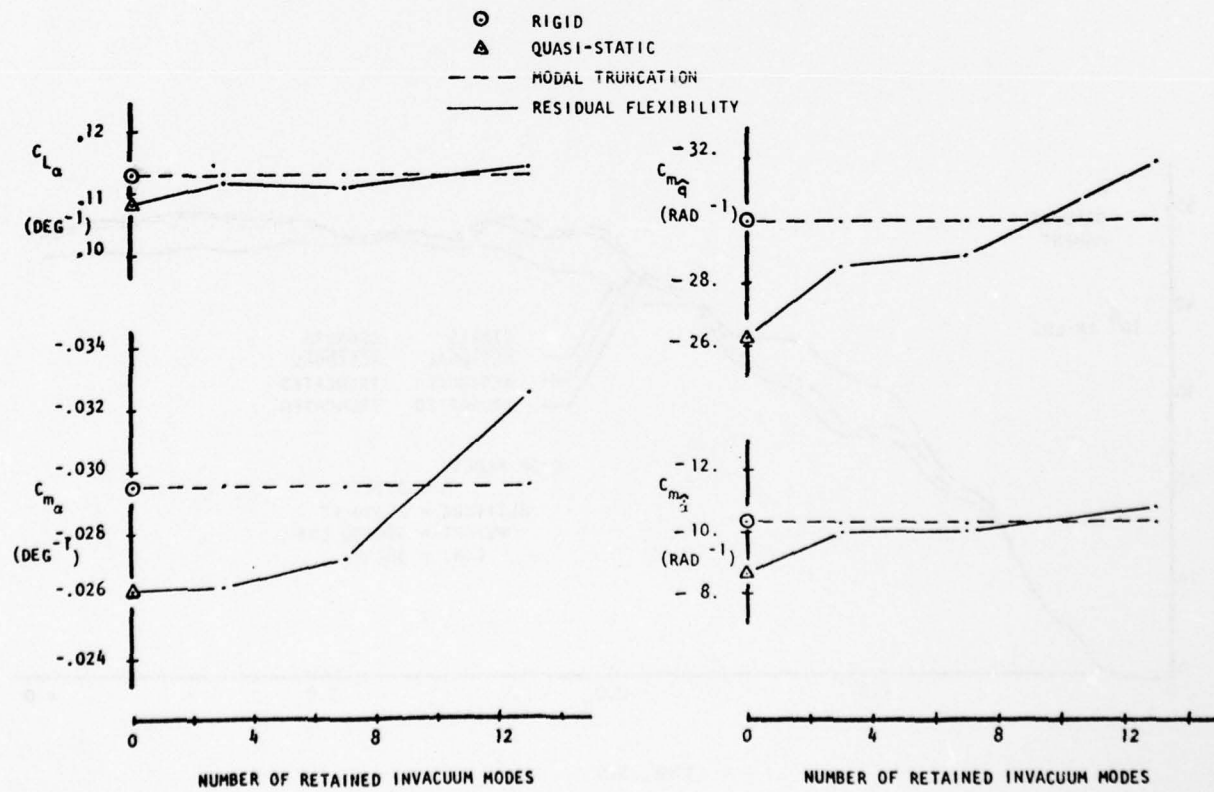


FIGURE 7. Effect of Retained Structural Invacuum Modes on C-5A Mean-Axis Stability Derivatives (Ref. 12)

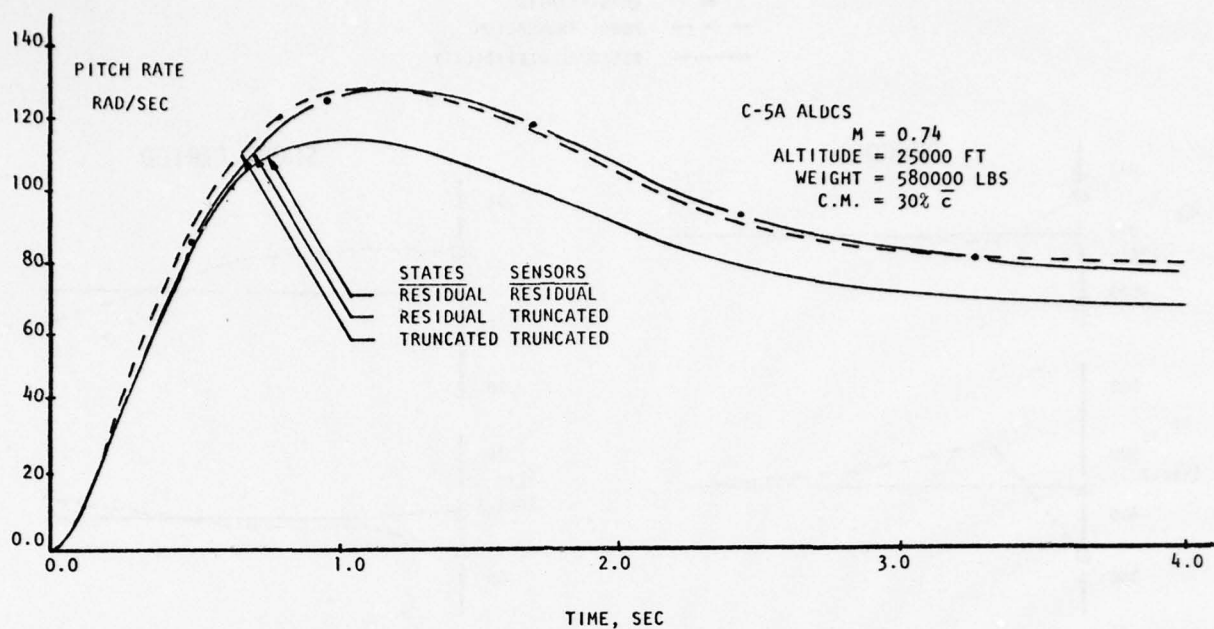


FIGURE 8. Effect of Residualization and Truncation on Center of Mass Pitch-Rate Response Due to Inboard Elevator Step (Ref. 15)

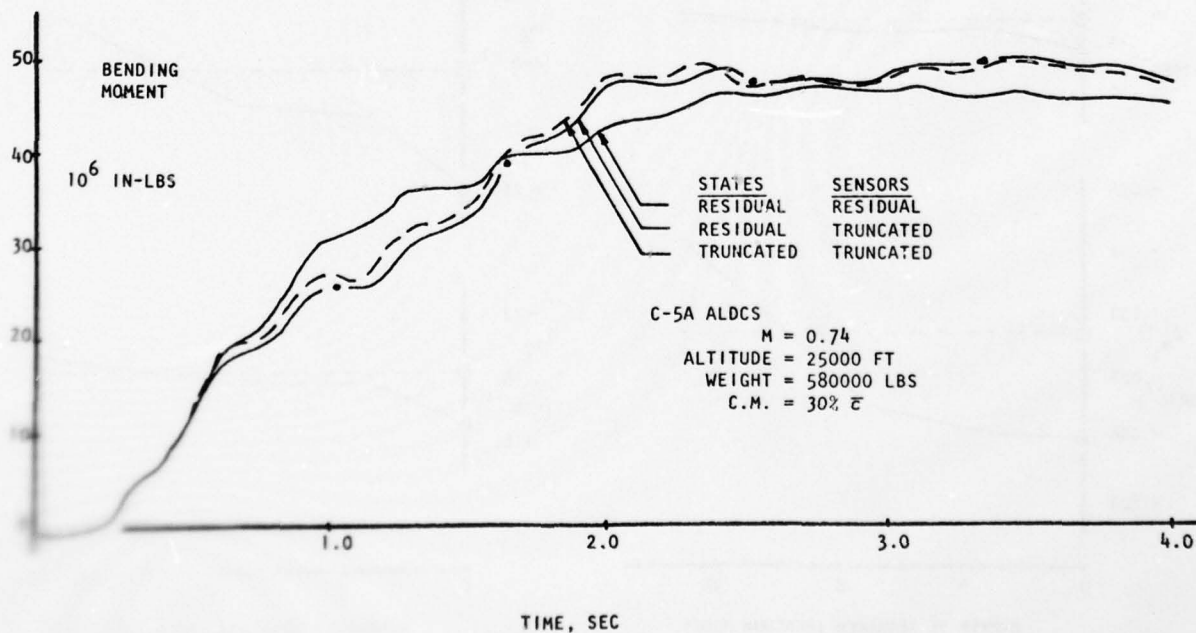


FIGURE 9. Effect of Residualization and Truncation on Wing Root Bending Moment Response Due to Inboard Elevator Step (Ref. 15)

TABLE 2. YF-16 Unaugmented Airplane Sensor Response at Lowest Analysis Frequency (Ref. 7)

Table 2a. Missiles-on, M=0.90, Altitude = 20000 FT.

ANALYSIS METHOD	DEGREES OF FREEDOM	ω (Hz)	a_y/δ_r		$\dot{\psi}/\delta_r$		$\dot{\phi}/\delta_r$		$\dot{\phi}/\delta_a$	
			MAGNITUDE	PHASE (DEG)	MAGNITUDE	PHASE (DEG)	MAGNITUDE	PHASE (DEG)	MAGNITUDE	PHASE (DEG)
TRUNCATED MODES	3	.150	1.3926	177.641	.44280	-104.442	2.6565	158.014	30.664	-18.757
	5	.150	1.3877	177.586	.44121	-104.478	2.8117	156.387	23.988	-19.956
	9	.150	1.2451	177.396	.39706	-104.478	2.8352	156.558	24.024	-20.028
	19	.150	.99952	177.689	.32284	-104.011	2.4617	158.242	15.579	-18.413
RESIDUAL FLEXIBILITY	4	.150	1.0153	177.401	.32537	-104.482	2.2247	157.375	14.431	-19.060
	5	.150	1.0155	177.409	.32537	-104.477	2.1860	157.770	15.485	-18.954
	9	.150	1.0147	177.551	.32509	-104.346	2.1752	157.862	15.440	-18.981

Table 2b. Missiles-off, M=0.90, Altitude = 15000 FT.

TRUNCATED MODES	3	.153	1.6745	177.708	.44257	-106.465	2.6817	165.350	31.714	-11.445
	9	.153	1.4569	177.513	.38580	-106.629	2.3364	165.059	24.341	-11.370
RESIDUAL FLEXIBILITY	4	.153	1.1336	177.444	.29586	-107.011	1.7930	165.835	17.378	-10.909
	9	.153	1.1341	177.643	.30233	-106.359	1.7976	166.193	17.357	-10.620

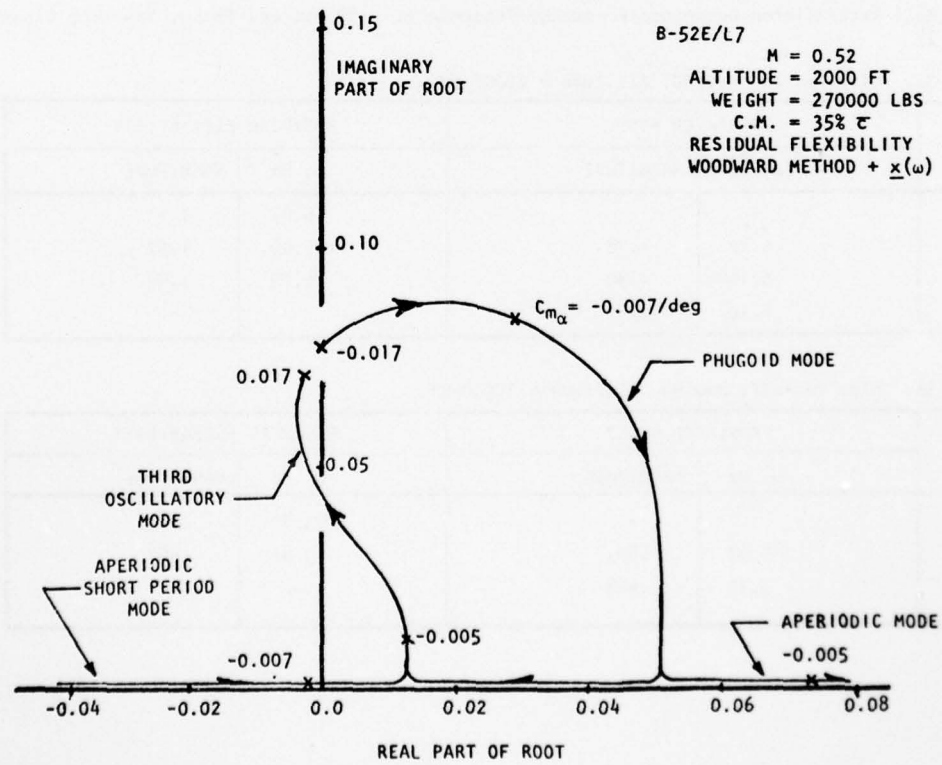
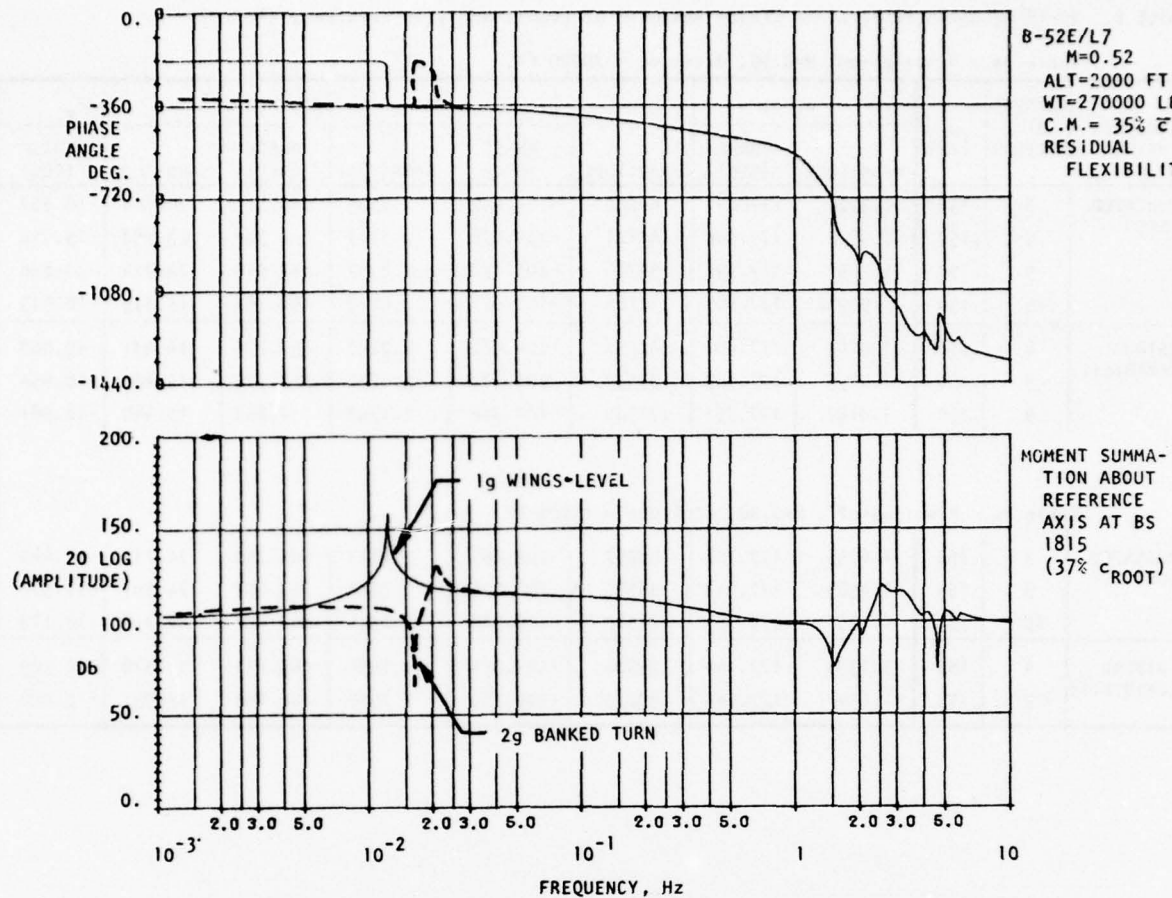
TABLE 3. YF-16 Roll Rate/Aileron Open-Loop Frequency Response at -180 Degrees Phase, Yaw-Loop Closed (Ref. 7)

Table 3a. Missiles-on, M=0.90, Altitude = 20000 FT.

DEGREES OF FREEDOM	TRUNCATED MODES			RESIDUAL FLEXIBILITY	
	ω , Hz	MAGNITUDE		ω , Hz	MAGNITUDE
4	-	-		6.07	1.11
5	6.12	1.78		6.09	1.52
9	6.10	1.80		6.09	1.54
19	6.10	1.55		-	-

Table 3b. Missiles-off, M=0.90, Altitude = 15000 FT.

DEGREES OF FREEDOM	TRUNCATED MODES			RESIDUAL FLEXIBILITY	
	ω , Hz	MAGNITUDE		ω , Hz	MAGNITUDE
4	-	-		3.80	.427
9	3.93	.573		3.81	.467
19	3.77	.418		-	-



YC-14 CONTROL SYSTEM REDUNDANCY

William T. Hamilton
 Vice President - Engineering
 Boeing Aerospace Company
 P.O. Box 3999, M. S. 85-86
 Seattle, Washington 98124

Summary

The YC-14 is the Boeing entry in the USAF Advanced Medium STOL Transport (AMST) program. The task of operating a large jet aircraft into and out of a semi-prepared, 2,000 feet long airstrip with a 27,000 pound payload presents an unusual flight control challenge. The YC-14 answers this challenge using an advanced flight control system that includes digital computers. Excellent STOL flying qualities have been achieved through control wheel steering and speed hold modes. Fail operational, fail safe performance is provided by a triplex flight control system. Aircraft dynamics following an engine failure are docile and do not require immediate pilot attention or unusual skill. The superior capability of digital computers to perform logic functions enables a comprehensive, semi-automated, preflight test. Failures are detected and identified to the Line Replaceable Unit (LRU). The YC-14's use of redundant digital computers in the flight control role is a first for an aircraft designed to demonstrate operational use.

YC-14 Configuration

The YC-14, as shown in Figure 1, incorporates many advanced technology and design-to-cost features. Powered lift is produced by directing the exhaust of two large, modern, high-bypass-ratio turbofan engines over circular cross-section flaps by the Coanda effect. Studies by NASA and Boeing have confirmed the superior performance of Upper Surface Blown (USB) flaps and the Coanda effect in generating powered lift. See References 1 and 2. The engines are located close to the fuselage to insure adequate control following an engine failure. A twin engine configuration was selected because in Boeing's opinion engine procurement and maintenance costs are lower than those for a four engine aircraft, and a modern engine with the desired thrust level was available. USB flap deflections can be modulated at high rates in response to Control and Stability Augmentation (CAS) commands for airspeed control. Cruise speeds in excess of $M = 0.7$ with an unswept wing are achieved through the use of supercritical airfoil sections. Superior rough field operation is attained from a long stroke, high energy absorbing, high flotation, lever action landing gear. Design-to-cost is evidenced by the unswept wing, constant sections in the fuselage and vertical tail, and identical structure in the right and left horizontal stabilizer panels.

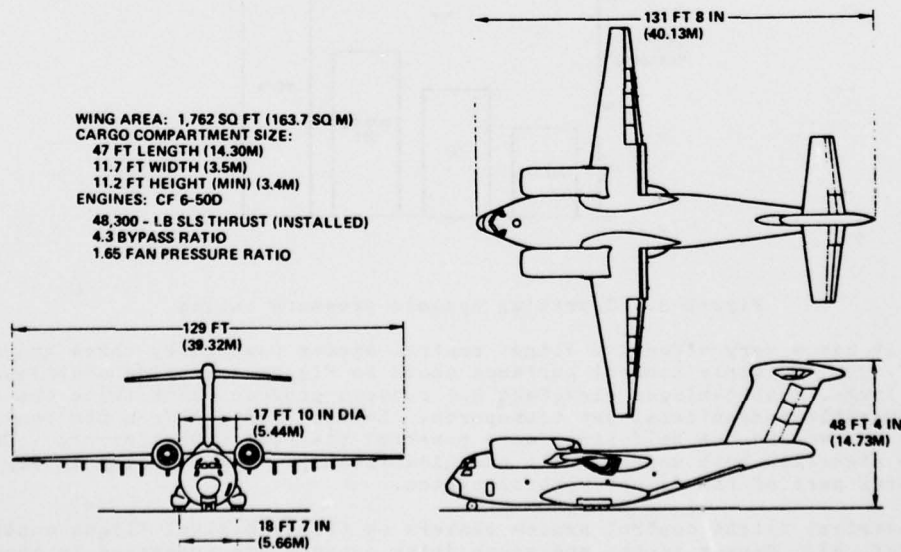


Figure 1 Boeing advanced medium STOL transport prototype - YC-14

Concern is often expressed regarding a twin-engine aircraft's performance with a failed engine. Actually, an aircraft with two engines is designed to have the same residual performance with an engine failed as a four-engine aircraft. As a result, this twin-engine aircraft has 50 percent more installed thrust. This larger thrust installation is economically sound, since engine acquisition and ownership costs are lower for two large engines than for four smaller ones. The normal YC-14 flight control system inherently controls the dynamics following an engine failure so immediate pilot action is not required; nor is unusual piloting skill needed. In addition, advantage was taken of the flight control system's ability to improve STOL performance.

Key design flight conditions are listed in Figure 2. Short takeoff and landing (STOL) is characterized by an 86 Kt approach speed on a 6° glide slope. The operating lift coefficient $\frac{W}{qS} > 3.6$ is over twice that of conventional jet transports. Cruise at

high Mach number and altitude means that all of the transonic aerodynamic phenomena must be considered in the design. Finally, low-altitude, high-speed dash imposes requirements to operate at high dynamic pressures. The ratio of maximum to minimum operating dynamic pressures is about twice that of conventional aircraft and 50 percent more than supersonic transports.

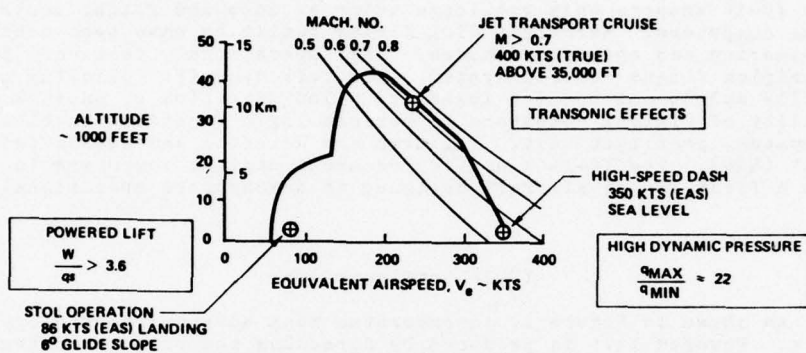


Figure 2. YC-14 key design flight conditions

With the powerful elevators required for STOL operation, control sensitivity is high at cruise speeds. As shown in Figure 3, the ratio of maximum operational dynamic pressure to that at STOL landing is much higher for the YC-14 than for the efficient 727-200 or for an advanced SST. Satisfactory control sensitivity was provided with an elevator ratio changer.

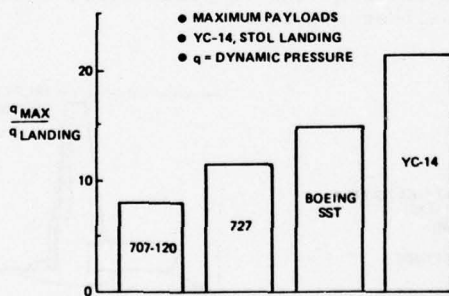


Figure 3. Operating dynamic pressure ratios

The YC-14 has a very effective flight control system powered by three hydraulic systems (Ref. 3). Multiple control surfaces shown in Figure 4 provide additional redundancy. The large, double-hinged elevators and rudders produce about twice the control power of comparable conventional jet transports. Lateral control from ten spoilers and two ailerons is two-and-one half times more powerful than for CTOL aircraft. Control surfaces are signalled both mechanically and electrically. The USB flap is fly-by-wire and an integral part of the flight control system.

The electrical flight control system centers on triple digital flight control computers (Ref. 4). Sensor inputs and servo drive outputs are processed in three interface units. All cross-channel data used for redundant operation is transmitted via fiber optics. Fault detection and channel isolation is automatic. Marconi Elliott Avionics Systems Ltd. of Rochester, Kent, England designed and built the digital control system.

The aircraft also has triple digital air data computers, an inertial navigation system, and an electronic attitude director indicator (EADI). The EADI displays attitude, flight path, altitude and airspeed information supplemented by background real-world television display. Electronic systems are used extensively to enhance YC-14 performance (Ref. 5).

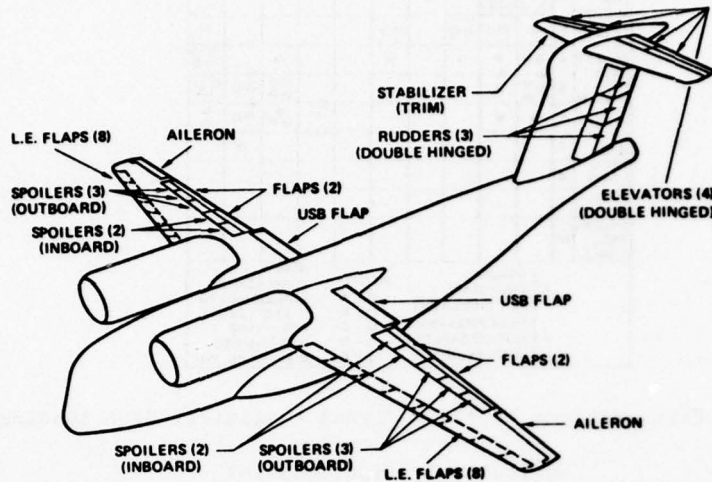


Figure 4. Flight control surfaces

From its inception, Boeing has required superior flying qualities for the YC-14. Powerful controls are provided to enable quick aircraft response to control commands during low airspeed, STOL operation. Since most aircraft accidents occur during takeoffs and landings, and are generally related to flying qualities characteristics, not engine failure, the YC-14 was required to be easy to fly in these critical flight regimes. The pilot is able to direct his attention principally to outside situations inherent in tactical airlift.

STOL aircraft typically experience powerful propulsive lift interaction with their basic stability and control characteristics, and fly on the "backside" of the speed-thrust curve. This is, increased thrust is required to fly at a lower airspeed, a condition opposite to that of most Conventional Takeoff and Landing (CTOL) aircraft. If a pilot attempts to control the flight path angle of a "backside" aircraft using the control column, flight path instability results. Ordinarily, a pilot flying a STOL aircraft has to control attitude with control column and sink rate with engine throttles. While the backside control technique is feasible, the control task is demanding, and as concluded at Boeing, not consistent with effective military operation. As a result, the YC-14 is designed to be controlled with normal pilot techniques. In fact, with the USB flap's high rate performance, the YC-14 is easier to control than contemporary aircraft because of its superior airspeed hold mode. The pilot's control task during landing approach is simply to point the aircraft to the desired touchdown point using one-hand control column and control wheel commands. Airspeed is maintained automatically and accurately.

Fail-operational/fail-safe performance was required to provide desired mission reliability. In the simulators the YC-14's STOL flying qualities with CAS inoperative are rated Level 2, Figure 5, "Flying qualities adequate to accomplish the mission Flight Phase, but some increases in pilot workload or degradation in mission effectiveness, or both exists." However, without CAS, the pilot must use the "backside" control technique in the critical STOL landing flight regime. It was not considered prudent to require this increased pilot workload for tactical airlift. With fail-operational systems, CAS-off operation becomes so infrequent that diversion to an airfield with a longer runway, where a normal CTOL landing can be made, is reasonable. Aircraft and crew safety benefit without unacceptable degradation of mission effectiveness.

Fail-operational/fail-safe performance was achieved through redundant control surfaces and systems. At least three aerodynamic control surfaces actuated by three independent Hydraulic Systems are available for each control axis. Three CAS channels, each powered by a different Electrical System, are also provided for each control axis. Mechanical elements in the Flight Control System (FCS) enable safe controllability with a total Electrical System failure.

PILOT RATING	SYSTEM FAILURES									
	NORMAL OPERATION		SINGLE HYD. OR EFCS SYSTEM		SINGLE-AXIS EFCS HARD-OVER		TOTAL EFCS OFF		ENGINE FAILURE	
	B	F	B	F	B	F	B	F	B	F
SATIS-FAC-TORY FOR MISSION	1		D							
LEVEL 1	2	○○○○○○○○○○	○○○○○○○○○○	○○○○○○○○○○	○○○○○○○○○○	○○○○○○○○○○	○○○○○○○○○○	○○○○○○○○○○	○○○○○○○○○○	○○○○○○○○○○
ACCEPTABLE FOR MISSION	3	○○○○○○○○○○	○○○○○○○○○○	○○○○○○○○○○	○○○○○○○○○○	○○○○○○○○○○	○○○○○○○○○○	○○○○○○○○○○	○○○○○○○○○○	○○○○○○○○○○
LEVEL 2	4	○○○○○○○○○○	○○○○○○○○○○	○○○○○○○○○○	○○○○○○○○○○	○○○○○○○○○○	○○○○○○○○○○	○○○○○○○○○○	○○○○○○○○○○	○○○○○○○○○○
CONTROL-LABLE	5	○○○○○○○○○○	○○○○○○○○○○	○○○○○○○○○○	○○○○○○○○○○	○○○○○○○○○○	○○○○○○○○○○	○○○○○○○○○○	○○○○○○○○○○	○○○○○○○○○○
LEVEL 3	6	●●●●●●●●●●								
UNCONTROL-LABLE	7									
10										

B { BOEING
FIXED-BASE
FLT. SIMULATOR
NASA AMES FSAA
F { MOTION-BASE FLT.
SIMULATOR

PILOTS: TURBULENCE:
 O - A PROBABILITY OF
 □ - B EXCEDENCE
 D - C ○ — 1/10
 △ - D ○ — 1/1000
 E - E ● — 1/100,000

Figure 5. Pilot ratings of YC-14 flying qualities, STOL landings

Longitudinal Flight Control

Pilot control commands are transmitted electrically and mechanically to the elevators, as shown in Figure 6. During flaps-down operation, sensor feedback and pilot's electrical commands are transmitted through the FCE to duplex Series Electrical Command Servos (SECS) plus a SECS model. Since no off-the-shelf SECS with satisfactory features for mechanically

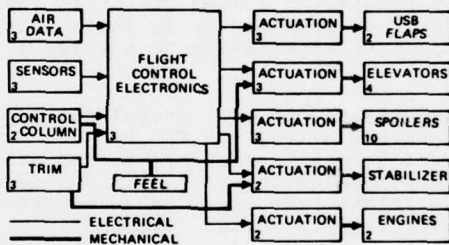


Figure 6. Longitudinal flight control system integration

limiting its output existed, a 747 Parallel Electrical Command Servos (PECS) and its associated longitudinal feel system were used for flaps-up operation. They limit any failure transients caused by the FCE or the PECS within ± 1.0 g's. The YC-14's aerodynamic characteristics enable easy recovery from transients. Cost savings were derived by using only a single-channel PECS during flaps-up operation, although all three FCE channels compute and monitor commands. The C-14 will use the same series servos for flaps-up and flaps-down flight. Elevator actuators are modified 747 components.

Pilot's commands are transmitted electrically to wing spoilers for direct lift control. USB flaps, used to control airspeed during landing approach in addition to providing powered lift, are commanded electrically by the FCE with inputs from selected flap position and aircraft dynamics sensors. Electrical commands are also sent to engine throttles for airspeed control.

An elevator ratio changer is used to reduce control sensitivity during highspeed flight.

The all-movable stabilizer provides longitudinal trim. 747 trim control modules and a 707 jackscrew are used. Automatic trim is commanded by the FCE. When the FCE is disengaged, the pilot can command trim electrically by a thumbswitch on the control wheel, or mechanically by a lever located on the aisle stand.

Lateral Flight Control

Pilot control commands are transmitted electrically and mechanically to ailerons and spoilers, as shown in Figure 7. Sensor feedbacks are transmitted through the FCE to aileron and spoiler SECS during all flight conditions. Aileron actuators are components used on the E-2A airplane. Inboard spoilers and their actuators are 747 units; outboard

spoilers and their actuators are from the 727. An electric actuator, controlled by switches on the aisle stand, recenters the feel mechanism for trim.

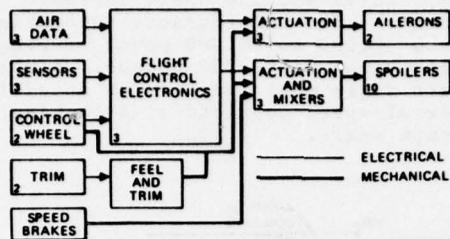


Figure 7. Lateral flight control system integration

Directional Flight Control

Pilot control commands are transmitted mechanically from rudder pedals to the power control actuators, as shown in Figure 8. CAS inputs are series summed at the actuators. Rudder actuators are modifications of those used on the DC-10. Trim is accomplished by mechanically recentering the feel system.

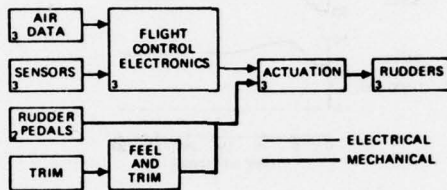


Figure 8. Directional flight control system integration

Aircraft Control Response

Longitudinal Control

The YC-14's response to control inputs during STOL landing approach with the CAS inoperative was described earlier. Longitudinal control response dynamics with the CAS operating are presented in Figure 9. Pitch attitude and flight respond quickly and smoothly to control command. Airspeed drops momentarily from 86 to 84 knots during a positive flight path increase of four degrees in 10 seconds. USB flap deflection decreases automatically from 52 degrees to 38 degrees while gross thrust increases automatically and smoothly from 32,000 pounds to 46,000 pounds. Following control column centering, the new aircraft state is maintained. The smooth, precise performance of pitch CWS and the Speed Hold modes allows the pilot to control the aircraft easily with one hand.

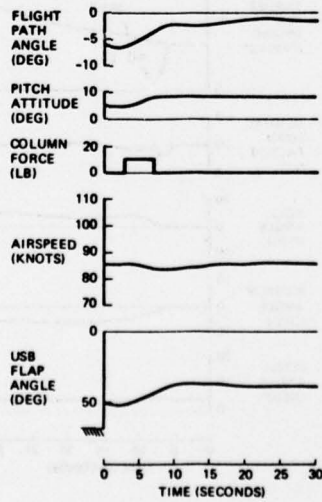


Figure 9. Response to Pitch Command, STOL landing configuration

Speed Hold

The aircraft's response to a speed command increase of 10 knots without other pilot action is presented in Figure 10. As shown, the speed increase is smooth, attaining 95% of the commanded value in 12 seconds. The USB retracts automatically from 52 degrees to 40 degrees. Thrust increases from 32,000 to 48,000 pounds during initial acceleration and then reduces to a steady state value of 40,000 pounds. Since pitch attitude is held constant, steady-state flight path angle must increase as speed is increased. Consequently, the pilot's task to acquire a new airspeed consists of selecting the desired airspeed on the CDP and controlling flight path angle.

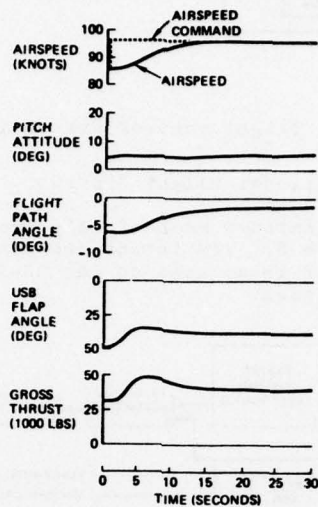


Figure 10. Normal response to speed command, STOL landing configuration

Engine Out

The YC-14's response to an engine failure is docile. The effect of an engine failure during STOL landing approach with the pilot's hands off the controls is presented in Figure 11. First, note the loss of lift from one of the two engines caused only a momentary reduction in normal load factor from 1.0 to 0.92 g's. Within eight seconds, the normal load factor returns to 1.0 g, hands off. The maximum bank angle following the engine hands off, is 9 degrees. The maximum sideslip is 5.5 degrees. Pitch angle is maintained within one-half degree. All of this is accomplished by the FCS as it normally operates during every landing. Obviously, immediate pilot action is not required. The pilot's task, following an engine failure, is simply to command the aircraft to the desired landing point. Thrust is increased on the operating engine automatically to hold airspeed.

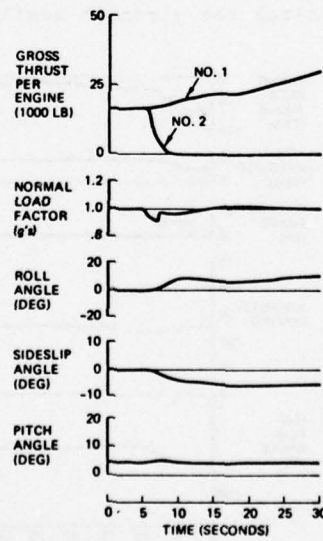


Figure 11. Response to engine failure with pilot "hands off" of controls

Systems used normally during every landing are satisfactory for controlling the YC-14 to a STOL landing with an engine failed. However, the aircraft is in a fairly high drag configuration with spoilers used for lateral trim and, as a result, the glideslope could be flattened only from -6 to -4 degrees. Although -4 degrees performance is adequate to complete a STOL landing under good conditions, flight simulator tests showed it was not forgiving if maneuvering was required to correct for an off-nominal approach. To improve engine-out performance, pressure sensors in each engine transmit signals to the FCE for failure detection. The FCE then commands flap retrim to reduce lateral control spoiler deflection. With the resultant reduced drag, the YC-14 can be pulled up to level flight at STOL landing speed with a failed engine. A landing can be readily completed even when maneuvers are required, or with go-around configuration selected, a positive climb gradient can be attained without air-speed increase. The improved performance with automatic flap retrim thus increases the options available to the pilot.

Conclusions

The YC-14 establishes a new level for tactical transport flight control. Its flying qualities are excellent for either STOL or CTOL operation, and its FCS is a step advancement with its inclusion of triplex, digital flight control electronics. Digital electronics, which are making rapid technical and cost advances, will likely become standard in future flight control systems. The ability of digital computers to perform logic functions enables comprehensive system tests, failure monitoring and identification. These advantages will be reflected in favorable maintenance costs. Finally, the flexibility of digital computers, if used with discipline, enables development of superb flying qualities with fine tuning as required during flight test, and permits aircraft FCS growth as needed for new missions.

List of References

1. Wimpress, J. K., "Upper Surface Blowing Technology as Applied to the YC-14 Airplane," SAE paper 730916, October 1973.
2. Heald, E. R., "External Blowing Flap Technology on the USAF/McDonnell Douglas YC-15 (AMST) Program," SAE paper 730915, October 1973.
3. Lee, A. H., The Boeing Company, "YC-14 Flight Control," AIAA Paper 75-1027, August 1975.
4. Kestek, R. E., The Boeing Company, "YC-14 Digital Flight Control Data Management," AIAA Paper 75-1087, August 1975.
5. Curnutt, R. A. and Tomich, E. J., The Boeing Company, "Electronic Systems Contribution to YC-14 STOL Performance," IEEE EASCON '75 Conference, September 1975.

ÉTUDE EN SOUFFLERIE D'UN SUPPRESSEUR DE FLOTTEMENT

par
Roger DESTUYNDER (*)

RÉSUMÉ

Le contrôle actif du flottement a été expérimenté en soufflerie sur une maquette d'aile munie d'un réservoir extérieur. Les forces aérodynamiques du contrôle étaient engendrées par un aileron classique, piloté par une servo-commande miniaturisée, à partir d'un signal provenant du mouvement de l'aile. Une loi de contrôle unique a été utilisée dans tout le domaine de vitesse. Un gain de plus de 15 % a été obtenu sur la vitesse critique de flottement.

Descripteurs (thèses CEDOCAR) : Vibration structure — Flottement aéroélastique — Oscillation aile — Amortissement vibration — Stabilisation — Servocommandes.

WIND TUNNEL STUDY OF AN ACTIVE FLUTTER SUPPRESSION SYSTEM

SUMMARY

Active flutter control has been experimented in a wind tunnel on a model of wing carrying an external tank. The aerodynamic forces of the control system were generated by a classical aileron, piloted by a miniaturized servo-control from a signal issued by an accelerometer detecting the wing movement. A single control law was used in the whole velocity range. A gain of more than 15 % has been obtained on the flutter critical velocity.

Descriptors (NASA thesaurus): Structural vibration — Flutter — Wing oscillations — Damping — Suppressors — Stabilizers (fluid dynamics) — Automatic control — Dynamic control — Servo-control.

I. — INTRODUCTION

Il y a déjà longtemps que l'on a imaginé de stabiliser un avion qui aurait naturellement tendance au flottement en utilisant une gouverne aérodynamique asservie au mouvement de l'aile. Mais la mise au point de ce système de contrôle actif exige une technologie très développée dans les domaines de l'électronique et des servo-commandes électrohydrauliques et une connaissance précise des forces aérodynamiques qui sont à l'origine des flottements éventuels et des forces aérodynamiques stabilisatrices engendrées par la gouverne de contrôle.

Dans l'état actuel de la technologie et des connaissances en aérodynamique instationnaire, le contrôle actif ne peut pas être considéré comme une solution applicable à tous les cas de flottement. Il constitue, par contre, un moyen valable pour éliminer des flottements apparaissant, sur une structure initialement saine, à la suite de changements de configurations défavorables; les conditions consécutives à ces changements de configuration sont souvent marginales pour le flottement, et celui-ci peut être assez facilement maîtrisé.

La présence de charges sous la voilure des avions militaires provoque des flottements qui entrent dans cette catégorie. En fixant une charge militaire ou un réservoir extérieur de grande inertie avec un support dont la rigidité est forcément limitée, on introduit de nouveaux degrés de liberté qui modifient les modes propres de vibration de la voilure. Certains modes se dédoublent sans que la déformée de l'aile change fondamentalement de nature. Par exemple, le mode de torsion se dédouble en général en une torsion à fréquence relativement élevée, dans laquelle la charge vibre en opposition avec l'aile, et en un mode à basse fréquence où la déformée de l'aile présente toujours le caractère d'une torsion, mais où le mouvement prédominant est l'oscillation de la charge en phase avec l'aile. Ce mode se couple avec la flexion, comme une torsion classique, mais le fait que sa fréquence propre soit plus faible que la fréquence de torsion de l'aile lisse contribue à élargir le domaine de flottement. Toutefois, l'oscillation de la charge, qui est prédominante dans ce mode, lui donne une grande inertie (ou masse généralisée) : on dit que le mode est lourd. Cette particularité contribue à diminuer « l'explosivité » du flottement.

Bien sûr ce flottement, dont le mécanisme reste celui du flottement de flexion-torsion classique, n'est qu'un exemple montrant comment la présence de charges peut aggraver les couplages aéroélastiques.

Mais la difficulté du problème posé par la présence des charges résulte surtout de la multiplicité des configurations de charge qu'un avion peut emporter. Le flottement dépend de la masse et des inerties de ces charges, de leur répartition sous l'aile et de la rigidité des supports. Il est fortement influencé aussi par l'interaction aérodynamique voilure-chARGE, c'est-à-dire qu'il dépend de la forme extérieure des charges. Or, les configurations de charges emportées par un avion donné sont successivement variées : la répartition de masse est souvent asymétrique et elle évolue au cours d'une même mission par suite de la consommation du carburant et des largages successifs.

Comme il est pratiquement impossible de réaliser une structure qui assure l'absence de flottement quelle que soit la répartition des charges avec un devis de masse raisonnable, il faut admettre que l'avion peut se trouver à un moment donné dans une configuration de charge amenant le flottement, et il faut disposer de méthodes et de moyens souples permettant de le faire disparaître sans pénaliser la structure du point de vue massique.

Le contrôle actif apparaît comme un moyen relativement simple et particulièrement bien adapté à cette application. C'est la raison pour laquelle l'ONERA en a entrepris l'étude

en se donnant comme support expérimental une maquette d'aile dans laquelle le flottement est provoqué par la présence d'une charge représentant un réservoir extérieur.

Les forces aérodynamiques de contrôle sont engendrées par une gouverne de bord de fuite classique actionnée par une servo-commande miniature pilotée par un signal électrique élaboré suivant une certaine loi de contrôle, à partir du signal d'un accéléromètre convenablement disposé dans l'aile. La difficulté principale du contrôle actif réside dans la détermination d'une loi de contrôle efficace. Celle-ci a été ajustée en soufflerie. Une loi de contrôle unique a permis d'assurer la stabilité dans tout le domaine de vitesse exploré.

II. — DESCRIPTION DE LA MAQUETTE

L'aile rectangulaire, d'allongement 5,3, est fixée à la paroi (fig. 1). L'épaisseur du profil est de 12 %. Un réservoir de grande dimension est fixé sous la voilure, à 45 % de l'envergure, par une liaison élastique.

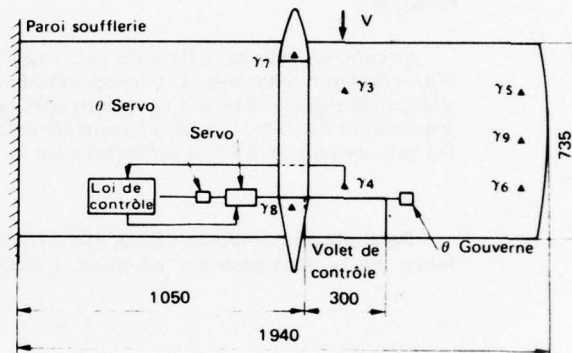


Fig. 1. — Contrôle de flottement sur demi-aile rectangulaire ($\lambda = 5,3$).
Soufflerie S₂ Chalais.

La gouverne, équilibrée autour de son axe d'oscillation, peut être actionnée par une servo-commande électro-hydraulique miniature donnant un couple pur et pilotée par le capteur d'accélération γ_4 . En l'absence de signal de contrôle, la gouverne est verrouillée par la servo-commande qui lui assure une fréquence propre supérieure à 50 Hz.

Après ajustement des caractéristiques structurales, le calcul prévoyait un flottement aux environs de 75 m/s en l'absence de contrôle. Les trois modes retenus dans l'étude du flottement étaient la flexion fondamentale à une fréquence de 9,30 Hz, le tangage du bidon à 13,55 Hz et la torsion de la voilure à 18,67 Hz. Le calcul montre que les autres modes de la structure sont suffisamment éloignés en fréquence pour pouvoir être négligés.

Les caractéristiques de ces trois modes ont été déterminées par un essai de vibration effectué sans loi de contrôle (gouverne verrouillée sur la servo-commande). Les déformées et les masses généralisées sont précisées sur la figure 2. On remarque que les déformées des modes 2 et 3 sont très semblables sur l'aile : seule la participation du bidon diffère en phase et en amplitude.

Toutes les déformées ayant été normées au même point de l'aile, on constate que la masse généralisée du mode de tangage est nettement plus grande que celle des autres modes. L'aile était équipée d'un grand nombre de capteurs accélérométriques, tous réglés pour avoir la même sensibilité.

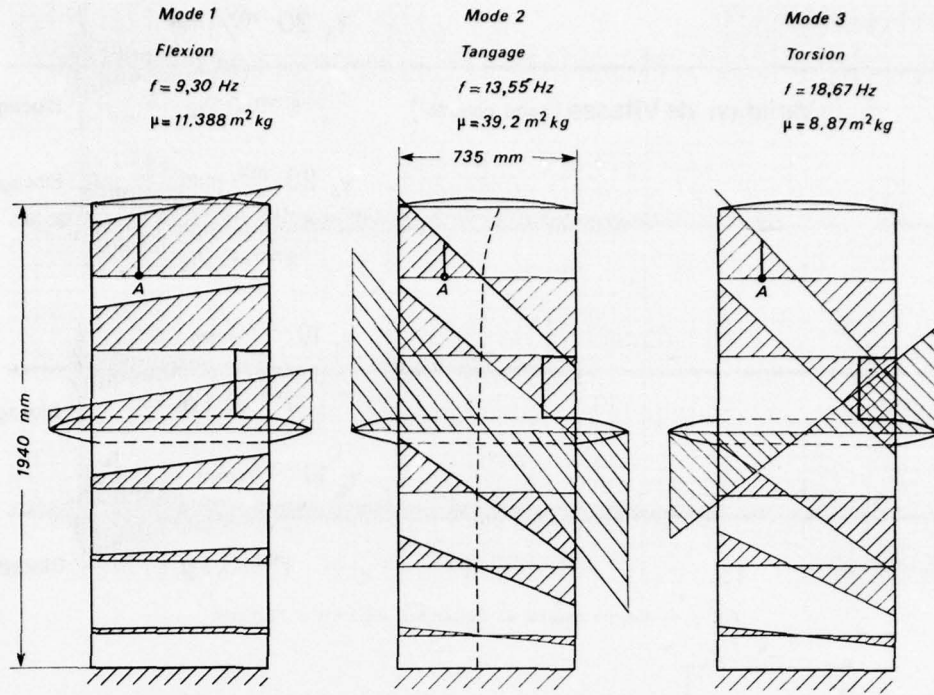


Fig. 2. — Modes propres de l'aile. Déformées normalisées à 1 mètre au point A, fréquence f , masse généralisée μ .

III. — ESSAIS EN SOUFFLERIE SANS LOI DE CONTRÔLE

Dans une première phase la vitesse critique de flottement a été déterminée expérimentalement sans loi de contrôle, et comparée aux résultats des calculs effectués par la méthode de doublets et par une méthode de tranches (coefficients bidimensionnels corrigés d'un effet d'allongement). Les deux méthodes de calcul fournissent des résul-

tats sensiblement identiques et en assez bon accord avec les essais. Les conditions subcritiques ont été déterminées en soufflerie à partir de l'analyse des densités spectrales de la réponse de la maquette à la turbulence naturelle de la soufflerie.

Dans ces essais la gouverne est verrouillée sur l'aile par la servo-commande. La comparaison des fréquences et des amortissements théoriques et expérimentaux est donnée dans la figure 3. On remarque que la cassure de la courbe

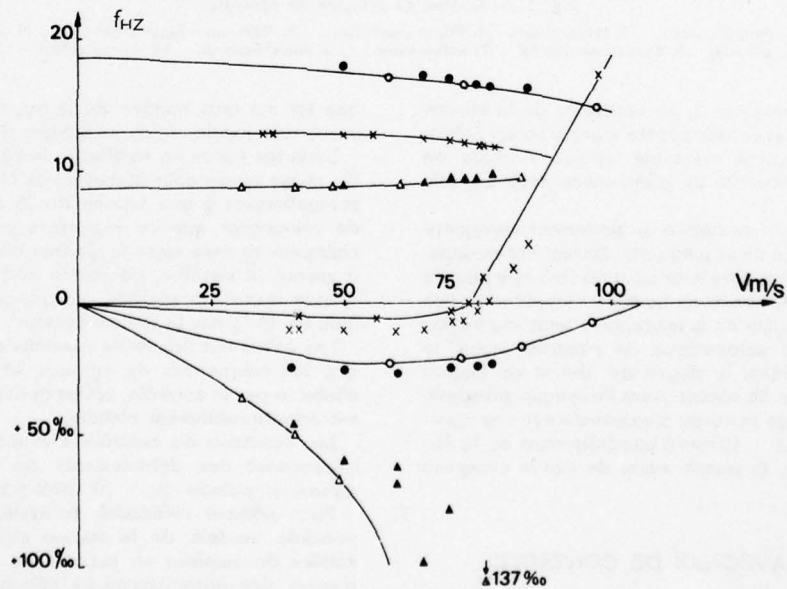


Fig. 3. — Comparaison théorie-expérience sans loi de contrôle.

Calcul sans loi		Essais sans loi	
flexion	$\alpha_0 = 0$	flexion	$\alpha_0 = 3^\circ/\text{oo}$
x tangage bidon	$\alpha_0 = 0$	x tangage bidon	$\alpha_0 = 3^\circ/\text{oo}$
o torsion	$\alpha_0 = 0$	● tension	$\alpha_0 = 5^\circ/\text{oo}$

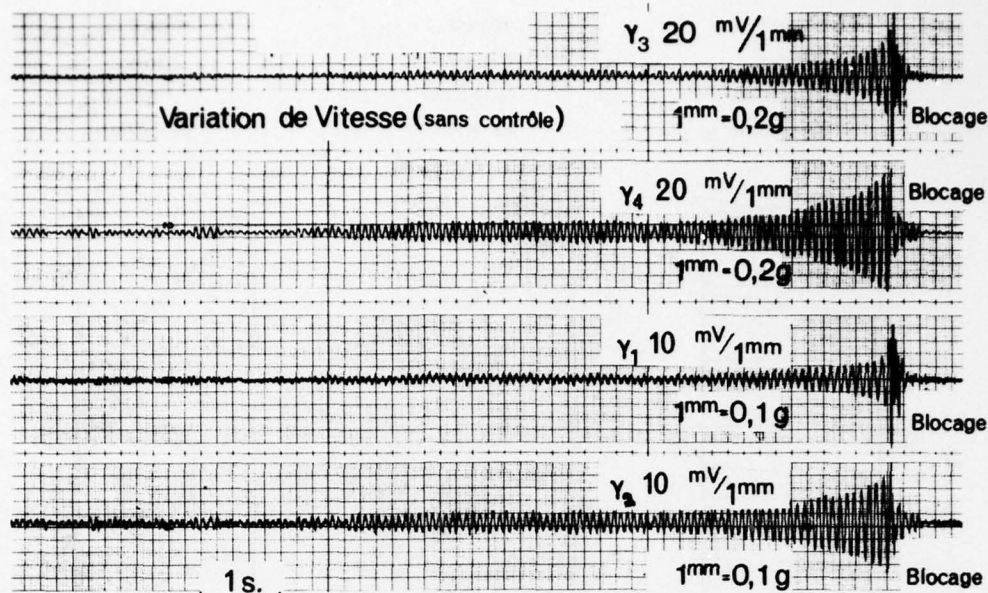
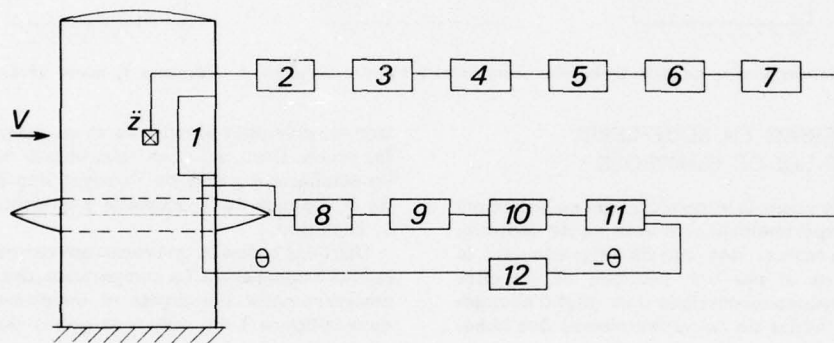
Fig. 4. — Départ naturel en flottement. $76,5 \leq V \leq 77,1 \text{ m/s.}$ 

Fig. 5. — Schéma de principe du contrôle.

1. Aileron. 2. Amplificateur. 3. Intégrateur. 4. Filtre passe haut. 5. Rejecteur basse fréquence. 6. Rejecteur servo. 7. Phase globale. 8. Servo-commande. 9. Servo-valve. 10. Amplificateur. 11. Sommeur. 12. Filtre.

d'amortissement du mode n° 2, au voisinage de la vitesse critique, se retrouve avec des pentes comparables. L'évolution de l'amortissement est lente jusqu'à l'entrée en flottement, mais l'explosivité du phénomène croît au delà de la vitesse critique.

Sur la figure 4 on voit un départ en flottement enregistré par différents capteurs de la maquette. Durant cet enregistrement la vitesse évolue très lentement de 76,5 m/s jusqu'à 77,1 m/s en 15 secondes environ. Lorsque l'amplitude prise par un point de référence de la maquette atteint une valeur donnée, un dispositif automatique de sécurité arrête le flottement en verrouillant le degré de liberté de flexion de la maquette à l'aide de câbles. Dans l'exemple présenté, le point au 1/4 avant de la corde d'extrémité avait au maximum une amplitude de $\pm 10 \text{ mm}$ à une fréquence de 12 Hz; dans le même temps, la pointe avant du bidon atteignait $\pm 80 \text{ mm}$.

IV. — ESSAIS AVEC LOI DE CONTROLE

Le capteur à partir duquel la loi de contrôle est élaborée est placé dans l'aile près de la ligne des noeuds des modes de tangage et de torsion, et détecte donc la réponse du mode de flexion. La réinjection de ce terme se fait à travers

une loi qui tient compte de la fonction de transfert de la servo-commande, selon le schéma de la figure 5.

Dans les essais en soufflerie, le réglage des paramètres de phase et de gain global de la chaîne a été recherché manuellement à une vitesse de 75 m/s. Il est intéressant de remarquer que ce réglage a pu être maintenu sans changement dans toute la gamme des vitesses explorées : il assure la stabilité, du moins jusqu'à 88 m/s qui est la vitesse maximum réalisée, ce qui représente un gain de plus de 15 % sur la vitesse critique.

Les essais ont donné les résultats de la figure 6. On voit que les fréquences de tangage et de torsion sont peu affectées par le contrôle, tandis que la fréquence de flexion est considérablement réduite.

Les réactions du contrôle à la turbulence en soufflerie provoquent des débattements de gouverne $\pm 2^\circ$ alors qu'une amplitude de $\pm 10^\circ$ était possible sans saturation.

Pour montrer l'efficacité du système de contrôle, on a procédé au-delà de la vitesse critique à des coupures suivies de remises en marche du contrôle. La figure 7 montre des enregistrements effectués à une vitesse de 78,5 m/s. Après coupure du contrôle et départ en flottement, la loi est rétablie alors que l'accélération à la pointe avant du bidon atteint $\pm 10 \text{ g}$; le braquage maximum de la gouverne de contrôle passe par une valeur de $+ 8^\circ$. Les

AD-A045 242

ADVISORY GROUP FOR AEROSPACE RESEARCH AND DEVELOPMENT--ETC F/G 1/1
STRUCTURAL ASPECTS OF ACTIVE CONTROLS. (U)

AUG 77

UNCLASSIFIED

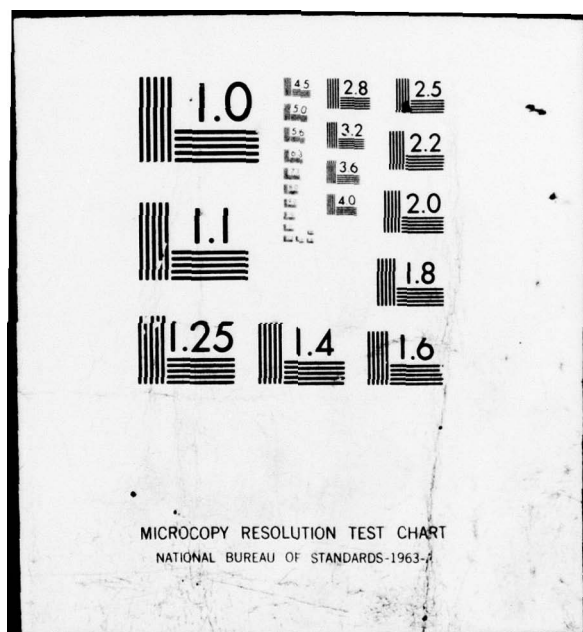
AGARD-CP-228

2 OF 2
AD
A045 242



NL

END
DATE
FILMED
11-77
DDC



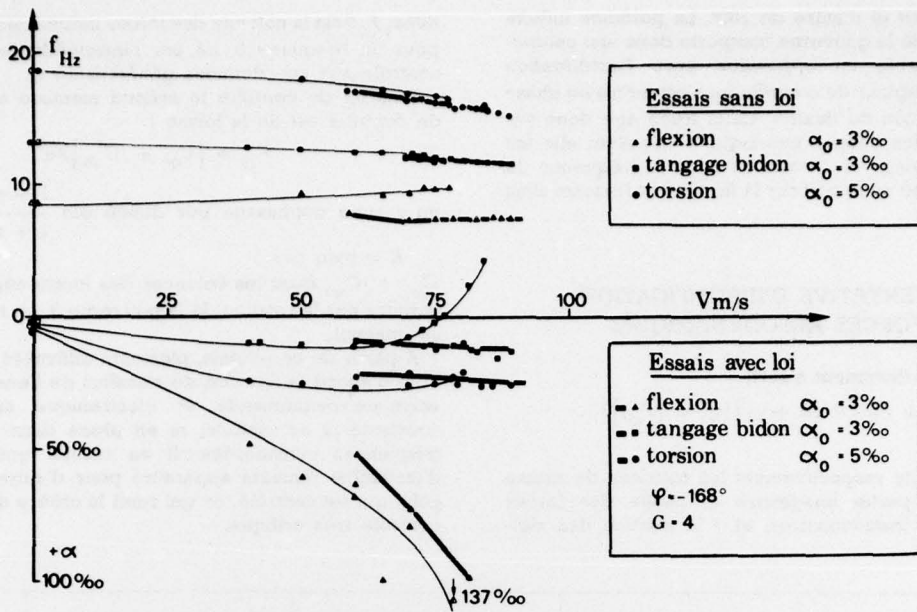


Fig. 6. — Comparaison des essais avec et sans loi de contrôle.

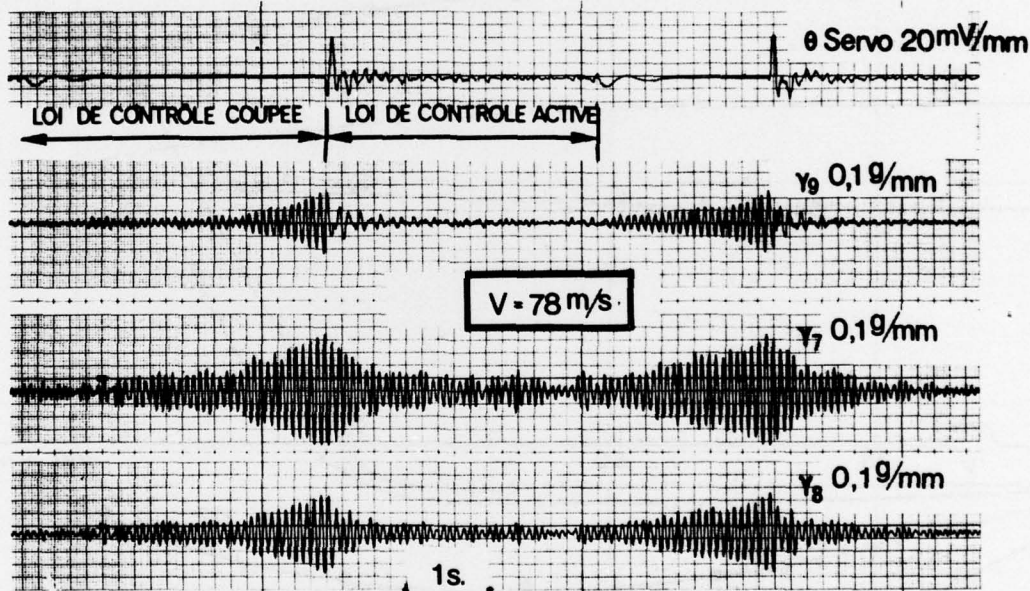


Fig. 7. — Coupure et ramise en marche de la loi de contrôle.

départs en flottement permettent de déterminer la valeur de l'amortissement négatif pour des vitesses au-delà du flottement. Sur le même enregistrement on voit un deuxième départ en flottement à la coupure du contrôle et un arrêt par le système de blocage automatique.

A la même vitesse de 78,5 m/s, une remise en marche du contrôle a été effectuée pendant le flottement alors que l'amplitude de la gouverne avait dépassé la limite de saturation. Même dans ces conditions, le contrôle a amorcé le retour à la stabilité, mais il l'a fait avec un temps de réponse plus long.

Il faut noter que le choix de la phase de contrôle est très critique. Dans le réglage optimum trouvé à 75 m/s, le déphasage de l'ensemble de la chaîne est de 168° à 12 Hz. La tolérance par rapport à ce réglage est faible, puisqu'un

écart de $\pm 7^\circ$ amène des flottements différents du flottement initial. Cette difficulté provient beaucoup du fait que le déphasage de la chaîne de contrôle n'est pas constant dans la bande de fréquence utile, mais varie de 140° à 198° entre 7,5 et 17 Hz. Avec de telles variations de phase, le contrôle peut avoir un effet stabilisateur sur le mode donnant le flottement initial, au voisinage de 12 Hz, et introduire de l'énergie dans un mode de fréquence supérieure ou inférieure. Cette difficulté s'explique par la complexité des fonctions de transferts des servo-commandes électro-hydrauliques; elle n'est pas particulière aux maquettes en soufflerie et doit se retrouver à l'échelle avion. Elle empêche de mettre au point un système fondé sur une loi de contrôle simple. Dans le cas présent, on remarquera que le déphasage de la chaîne de contrôle évolue avec la

fréquence de part et d'autre de 180° . La portance induite par l'oscillation de la gouverne comporte donc une composante prédominante en opposition avec l'accélération détectée par le capteur de contrôle γ_θ , c'est-à-dire en phase avec la déformation de flexion. Cette force agit donc sur le mode de flexion comme une rigidité négative; elle fait baisser sa fréquence et l'écarte ainsi de la fréquence du mode n° 2, comme on le voit sur la figure 6 et favorise ainsi la stabilité.

V. — TENTATIVE D'IDENTIFICATION DES FORCES AÉRODYNAMIQUES

L'équation du flottement s'écrit :

$$[P^2[\mu] + P[\beta] + [A + \gamma]] [q] = [F_{q\theta}]_0$$

où $P = j\omega$.

μ , β , A et γ sont respectivement les matrices de masse généralisée, de partie imaginaire et réelle des forces aérodynamiques instationnaires, et γ la matrice des rigi-

dités; $F_{q\theta}$ est la colonne des forces induites par la gouverne pour un braquage θ , lié par l'intermédiaire de la loi de contrôle aux coordonnées généralisées q .

Sans loi de contrôle le second membre est nul. La loi de contrôle est de la forme :

$$F_{q\theta} = [C'_{q\theta} + jC''_{q\theta}] K e^{i\varphi}$$

$$\text{où } \varphi = \text{un déphasage pur donné par } \frac{1 - \tau P}{1 + \tau P}$$

K = gain pur.

$C'_{q\theta} + jC''_{q\theta}$ étant les colonnes des forces aérodynamiques induites par la rotation de la gouverne θ . Le réglage K et φ est manuel.

A partir de ce schéma, plusieurs difficultés apparaissent. Tout d'abord la fonction de transfert de l'ensemble servo-valve-servo-commande et électronique associée n'est constante ni en module, ni en phase dans la bande des fréquences considérées. Il en résulte que des risques d'instabilité peuvent apparaître pour d'autres modes que celui qui est contrôlé, ce qui rend le critère de la phase de contrôle très critique.

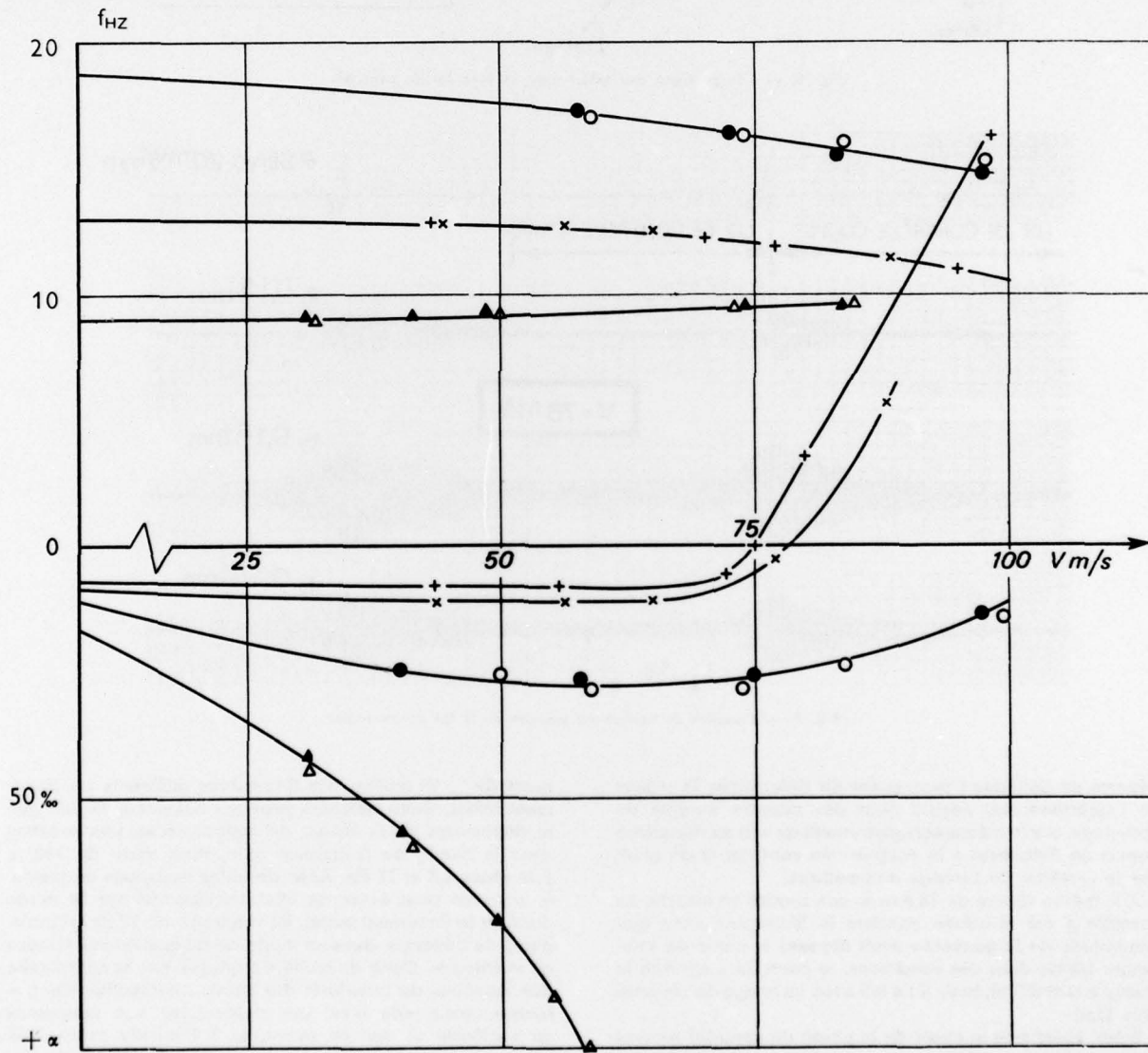


Fig. 8. — Influence de l'identification sur le plan fixe.

Torsion { ● calcul sans correction Tangage { + calcul sans correction Flexion { ▲ calcul sans correction
 ○ calcul avec correction × calcul avec correction △ calcul avec correction.

Pour pallier l'insuffisance des théories qui sont à la base des calculs des forces aérodynamiques instationnaires, insuffisances qui affectent surtout les effets de gouverne, il a paru nécessaire de procéder à une identification des forces aérodynamiques en soufflerie. Cette identification a pour but de déterminer les matrices A , B , C' et C'' .

Le problème a été scindé en deux parties.

a) Détermination des matrices A et B relatives au plan fixe. — Une méthode de tranches, dans laquelle on néglige les forces aérodynamiques agissant sur le réservoir et les effets de couplage aérodynamique entre réservoir et aile, a été utilisée pour calculer les forces aérodynamiques génératrices du système à trois modes (matrices A et B).

La résolution des équations montre que les coefficients de couplage entre modes (coefficients non diagonaux des matrices A et B) ont un effet négligeable jusqu'à une vitesse de 40 m/s, c'est-à-dire que pour des vitesses inférieures à 40 m/s on peut considérer que la fréquence et l'amortissement de chacun des modes est déterminé par les coefficients diagonaux correspondants des matrices A et B . Dans ce cas, les coefficients aérodynamiques de tranche sont liés par des relations linéaires aux variations de fréquence et d'amortissement et peuvent donc être déterminés expérimentalement si l'on sait mesurer les fréquences propres et les amortissements dans le vent avec une précision suffisante.

Les valeurs expérimentales ainsi déterminées diffèrent sensiblement des valeurs théoriques, comme le montre le tableau I dans lequel :

$k_a = k'_a + j\omega_R k'''_a$ est le coefficient de portance dû à la déflexion verticale,

$k_b = k'_b + j\omega_R k'''_b$ est le coefficient de portance dû à la déflexion de torsion,

$m_a = m'_a + j\omega_R m'''_a$ est le coefficient de moment dû à la déflexion verticale,

$m_b = m'_b + j\omega_R m'''_b$ est le coefficient de moment dû à la déflexion de torsion,

ω_R est la pulsation réduite du moment,

$k_d = k'_d + j\omega_R k'''_d$ est le coefficient de portance induit par la rotation de la gouverne,

$m_d = m'_d + j\omega_R m'''_d$ est le coefficient de moment induit par la rotation de la gouverne,

$n_d = n'_d + j\omega_R n'''_d$ est le coefficient de moment de la gouverne.

TABLEAU I
Coefficients relatifs à l'aile

	k'_a $\omega_R = 1$	$k'_b +$ $m'_a = 1$	m'_b $\omega_R = 1$	k'_a	$k'_b +$ m'_a	m'_b
Théorie [réf. 1]	0,054	0,943	-0,139	0,88	1,58	1,08
Expérience	0,050	0,880	-0,126	0,96	1,33	0,79

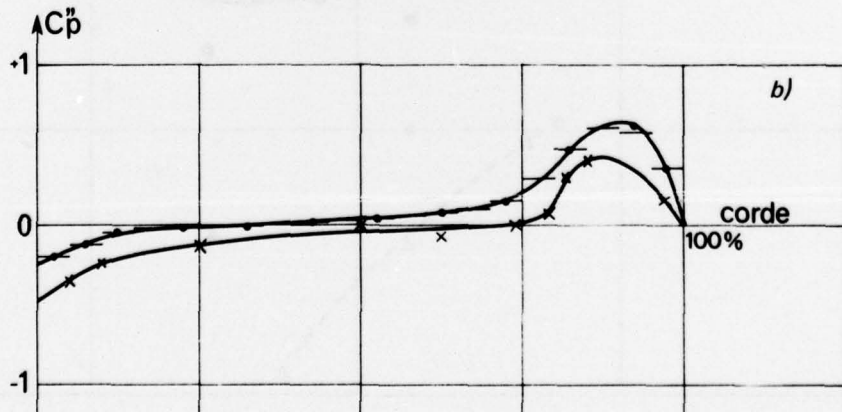
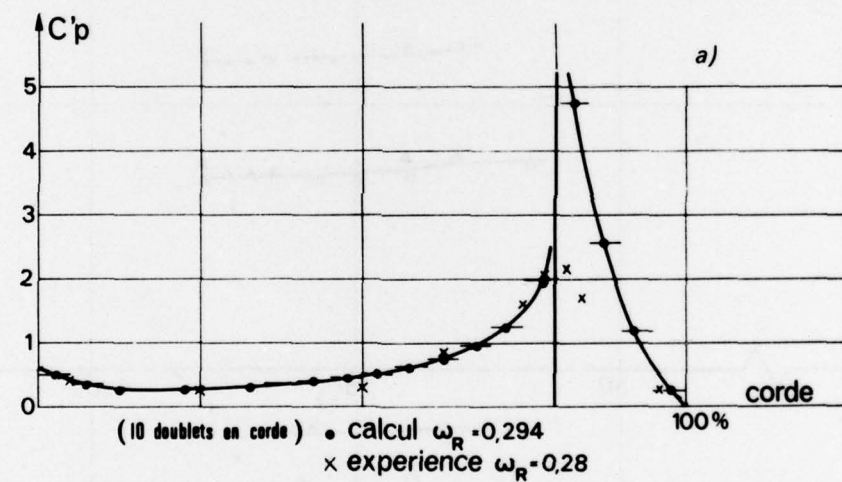


Fig. 9. — Distribution de coefficient de pression.

a) Partie réelle.
b) Partie imaginaire.

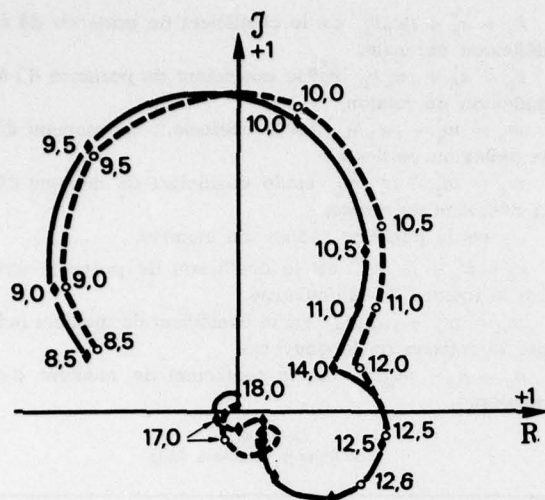


Fig. 10. — Comparaison fonction de transfert.
 Calcul-Essai (diagramme de Nyquist).
 $V = 65 \text{ m/s}$ sans loi de contrôle.

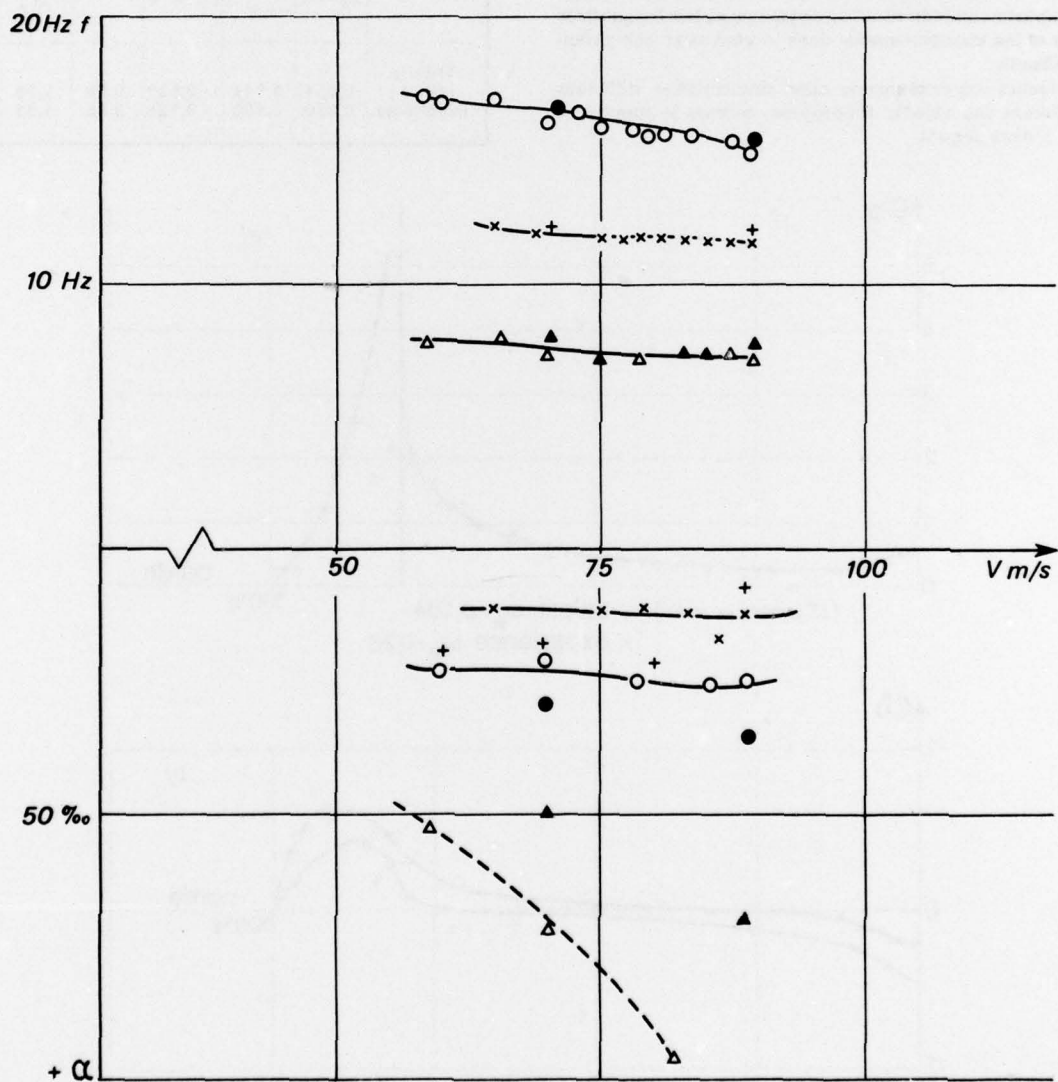


Fig. 11. — Comparaison calcul-essais avec loi de contrôle.

torsion Calcu

avec loi
change

lexion

Essais avec loi flexion + tangage

Essais avec loi
▲ flexion + tangage ● torsion

Dans le calcul des valeurs expérimentales on a supposé que les coefficients ('') et ('') étaient indépendants de la fréquence réduite. L'influence des coefficients corrigés sur le flottement est montrée figure 8.

b) La seconde identification porte sur les termes c' et c'' de la colonne de contrôle. Elle a été réalisée par la mesure des champs de pressions instationnaires induits par une rotation de la gouverne à différentes fréquences et différentes vitesses. La comparaison avec la distribution de C_p instationnaire calculée par une méthode de doublets est donnée sur la figure 9. La corde choisie est la corde médiane de la gouverne. Les pressions étaient mesurées à l'extrados en 10 points.

Les différences entre théorie et expérience sont importantes, sur le module aussi bien que sur la phase.

L'intégrale des pressions expérimentales donne des coefficients de force et de moment qui peuvent être comparés avec les valeurs théoriques.

TABLEAU II
Coefficients relatifs à la gouverne

	k_a	m_a	n_a	k_{ad}	m_{ad}	n_{ad}
Théorie [réf. 1]	0,51	0,45	0,022	- 0,020	0,20	0,025
Essais	0,36	0,32	0,015	+ 0,058	0,17	0,14

Le recouplement entre théorie et expérience porte également sur les fonctions de transfert de la maquette à différentes vitesses. Ces fonctions de transfert expriment le rapport entre la réponse de l'aile et le braquage de la gouverne. Elles ont été déterminées expérimentalement avec une excitation par bruit blanc sur la gouverne.

Le calcul a été effectué avec les coefficients expérimentaux. La figure 10 montre, à une vitesse de 65 m/s, la bonne concordance entre calcul et essai pour le point de l'aile où est placé le capteur qui fournit les informations à la loi de contrôle (fonction de transfert en boucle ouverte). On peut observer qu'en ce point la réponse du mode de flexion $f = 9,8$ Hz est prédominante devant les autres modes.

L'introduction de la loi de contrôle expérimentale dans le calcul corrigé donne finalement, en fonction de la vitesse, une évolution satisfaisante des paramètres de fréquence et d'amortissement. En particulier l'effet de rigidité aérodynamique négative qui écarte le mode 1 du mode 2 est bien représenté figure 11. Le calcul prévoit que la maquette reste stable jusqu'à la vitesse maximum expérimentée, ce qui est conforme à l'expérience. Afin de vérifier la sensibilité de la loi de contrôle à une variation de phase, le calcul a été effectué en introduisant un déphasage supplémentaire de + 5° dans la loi.

L'amortissement du mode de tangage à 88 m/s varie dans ces conditions de + 8% (valeur avec la loi nominale) à 2%. De même un décalage de phase de - 5° conduit à un amortissement de 11%. Cette très grande sensibilité aux paramètres de contrôle, qui est conforme à l'expérience est aggravée par la similitude des déformées d'aile dans les modes de tangage et de torsion qui rend la matrice modale presque singulière.

VI. — CONCLUSION

On a montré qu'il était possible de contrôler un flottement provoqué par la présence d'un réservoir de grande dimension en utilisant une gouverne de bord de fuite classique pour engendrer des forces aérodynamiques stabilisatrices. La stabilité a été obtenue avec une loi de contrôle unique dans toute la gamme de vitesse explorée (de 0 à 88 m/s) alors que le flottement se produisait à partir de 75 m/s en l'absence de contrôle.

DU fait de la complexité des fonctions de transfert de la servo-valve et de la servo-commande, il est difficile de réaliser un système de contrôle dont le fonctionnement se prête à une interprétation simple. Il est également difficile de pré-déterminer la loi de contrôle à cause des incertitudes qui existent dans le calcul des forces aérodynamiques instationnaires et, surtout, des forces aérodynamiques induites par le braquage des gouvernes. Dans le cas présent, la meilleure loi de contrôle a été obtenue par un réglage manuel effectué en soufflerie; mais cette solution n'a été possible que parce qu'il n'existe qu'un réglage de phase et un réglage de niveau.

Par contre, il est assez encourageant de constater que l'identification des forces aérodynamiques effectuée en soufflerie a permis de corriger les forces aérodynamiques théoriques et de retrouver, par un calcul a posteriori, des évolutions de fréquence et d'amortissement et des fonctions de transfert en assez bon accord avec l'expérience.

Manuscrit remis le 17 juin 1976.

RÉFÉRENCES

- [1] CHOPIN S. et SALAÜN P. — Coefficients aérodynamiques instationnaires théoriques en régime subsonique pour une voilure de faible allongement. — Document ONERA non publié (1959).
- [2] HAIDL G. — Active flutter suppression on wings with external stores, dans « Active control systems for loads alleviation, flutter suppression and ride control ». AGARDograph n° 175 (1974), p. 57-76.
- [3] SENSBURG O. and HÖNLINGER H. — Dynamic testing in wind tunnels, dans « Flight ground testing facilities correlation ». AGARD Conf. Proc. n° 187 (1976), mémoire n° 5, part. I.
- [4] NISSIM E. — Active flutter suppression using trailing edge and tab control surfaces. — AIAA paper n° 75-822.

REPORT DOCUMENTATION PAGE			
1. Recipient's Reference	2. Originator's Reference	3. Further Reference	4. Security Classification of Document
	AGARD-CP-228	ISBN 92-835-0200-0	UNCLASSIFIED
5. Originator	Advisory Group for Aerospace Research and Development North Atlantic Treaty Organization 7 rue Ancelle, 92200 Neuilly sur Seine, France		
6. Title	STRUCTURAL ASPECTS OF ACTIVE CONTROLS		
7. Presented at 44th Meeting of the AGARD Structures and Materials Panel held in Lisbon, Portugal on 21 April 1977.			
8. Author(s)	Various		9. Date
			August 1977
10. Author's Address	Various		11. Pages
			106
12. Distribution Statement	This document is distributed in accordance with AGARD policies and regulations, which are outlined on the Outside Back Covers of all AGARD publications.		
13. Keywords/Descriptors	Structures Servomechanisms Adaptive systems	Design criteria Transfer functions Tests	Feedback control
14. Abstract	<p>The Meeting dealt with the philosophy and approach on the use of active controls to realize structural improvements. The question of what constitutes a good balance of effort to achieve a successful active control system was posed. Specifics dealt with the techniques for evaluating the system transfer function, with the relative roles of ground vibration testing, bench testing of component parts and the merits of open and closed loop testing. The question of what is an appropriate index of performance is of central significance.</p> <p style="text-align: center;">↑</p>		

<p>AGARD Conference Proceedings No. 228 Advisory Group for Aerospace Research and Development, NATO STRUCTURAL ASPECTS OF ACTIVE CONTROLS Published August 1977 106 pages</p>	<p>AGARD-CP-228</p> <p>Structures Servomechanisms Adaptive systems Design criteria Transfer functions Tests Feedback control</p>	<p>AGARD Conference Proceedings No. 228 Advisory Group for Aerospace Research and Development, NATO STRUCTURAL ASPECTS OF ACTIVE CONTROLS Published August 1977 106 pages</p>	<p>AGARD-CP-228</p> <p>Structures Servomechanisms Adaptive systems Design criteria Transfer functions Tests Feedback control</p>
	<p>The Meeting dealt with the philosophy and approach on the use of active controls to realize structural improvements. The question of what constitutes a good balance of effort to achieve a successful active control system was posed. Specifics dealt with the techniques for evaluating the system transfer function, with the relative roles of ground vibration testing, bench testing of component parts and the merits of open and closed loop testing. The question of what is an appropriate index of performance is of central significance.</p>	<p>P.T.O.</p>	<p>P.T.O.</p>
<p>AGARD Conference Proceedings No. 228 Advisory Group for Aerospace Research and Development, NATO STRUCTURAL ASPECTS OF ACTIVE CONTROLS Published August 1977 106 pages</p>	<p>AGARD-CP-228</p> <p>Structures Servomechanisms Adaptive systems Design criteria Transfer functions Tests Feedback control</p>	<p>AGARD Conference Proceedings No. 228 Advisory Group for Aerospace Research and Development, NATO STRUCTURAL ASPECTS OF ACTIVE CONTROLS Published August 1977 106 pages</p>	<p>AGARD-CP-228</p> <p>Structures Servomechanisms Adaptive systems Design criteria Transfer functions Tests Feedback control</p>
	<p>The Meeting dealt with the philosophy and approach on the use of active controls to realize structural improvements. The question of what constitutes a good balance of effort to achieve a successful active control system was posed. Specifics dealt with the techniques for evaluating the system transfer function, with the relative roles of ground vibration testing, bench testing of component parts and the merits of open and closed loop testing. The question of what is an appropriate index of performance is of central significance.</p>	<p>P.T.O.</p>	<p>P.T.O.</p>

Papers presented at the 44th Meeting of the AGARD Structures and Materials Panel held in Lisbon, Portugal on 21 April 1977.

Papers presented at the 44th Meeting of the AGARD Structures and Materials Panel held in Lisbon, Portugal on 21 April 1977.

ISBN 92-835-0200-0

Papers presented at the 44th Meeting of the AGARD Structures and Materials Panel held in Lisbon, Portugal on 21 April 1977.

ISBN 92-835-0200-0

Papers presented at the 44th Meeting of the AGARD Structures and Materials Panel held in Lisbon, Portugal on 21 April 1977.

ISBN 92-835-0200-0

4

AGARD
NATO OTAN
7 RUE ANCELLE · 92200 NEUILLY-SUR-SEINE
FRANCE
Telephone 745.08.10 · Telex 610176

**DISTRIBUTION OF UNCLASSIFIED
AGARD PUBLICATIONS**

AGARD does NOT hold stocks of AGARD publications at the above address for general distribution. Initial distribution of AGARD publications is made to AGARD Member Nations through the following National Distribution Centres. Further copies are sometimes available from these Centres, but if not may be purchased in Microfiche or Photocopy form from the Purchase Agencies listed below.

NATIONAL DISTRIBUTION CENTRES

BELGIUM

Coordonnateur AGARD — VSL
Etat-Major de la Force Aérienne
Caserne Prince Baudouin
Place Dailly, 1030 Bruxelles

CANADA

Defence Scientific Information Service
Department of National Defence
Ottawa, Ontario K1A 0Z2

DENMARK

Danish Defence Research Board
Østerbrogades Kaserne
Copenhagen Ø

FRANCE

O.N.E.R.A. (Direction)
29 Avenue de la Division Leclerc
92 Châtillon sous Bagneux

GERMANY

Zentralstelle für Luft- und Raumfahrt-
dokumentation und -information
Postfach 860880
D-8 München 86

GREECE

Hellenic Armed Forces Command
D Branch, Athens

ICELAND

Director of Aviation
c/o Flugrad
Reykjavik

UNITED STATES

National Aeronautics and Space Administration (NASA),
Langley Field, Virginia 23365
Attn: Report Distribution and Storage Unit

ITALY

Aeronautica Militare
Ufficio del Delegato Nazionale all'AGARD
3, Piazzale Adenauer
Roma/EUR

LUXEMBOURG

See Belgium

NETHERLANDS

Netherlands Delegation to AGARD
National Aerospace Laboratory, NLR
P.O. Box 126
Delft

NORWAY

Norwegian Defence Research Establishment
Main Library
P.O. Box 25
N-2007 Kjeller

PORTUGAL

Direccao do Servico de Material
da Forca Aerea
Rua de Escola Politecnica 42
Lisboa
Attn: AGARD National Delegate

TURKEY

Department of Research and Development (ARGE)
Ministry of National Defence, Ankara

UNITED KINGDOM

Defence Research Information Centre
Station Square House
St. Mary Cray
Orpington, Kent BR5 3RE

**THE UNITED STATES NATIONAL DISTRIBUTION CENTRE (NASA) DOES NOT HOLD
STOCKS OF AGARD PUBLICATIONS, AND APPLICATIONS FOR COPIES SHOULD BE MADE
DIRECT TO THE NATIONAL TECHNICAL INFORMATION SERVICE (NTIS) AT THE ADDRESS BELOW.**

PURCHASE AGENCIES

Microfiche or Photocopy

National Technical
Information Service (NTIS)
5285 Port Royal Road
Springfield
Virginia 22151, USA

Microfiche

Space Documentation Service
European Space Agency
10, rue Mario Nikis
75015 Paris, France

Microfiche

Technology Reports
Centre (DTI)
Station Square House
St. Mary Cray
Orpington, Kent BR5 3RF
England

Requests for microfiche or photocopies of AGARD documents should include the AGARD serial number, title, author or editor, and publication date. Requests to NTIS should include the NASA accession report number. Full bibliographical references and abstracts of AGARD publications are given in the following journals:

Scientific and Technical Aerospace Reports (STAR),
published by NASA Scientific and Technical
Information Facility
Post Office Box 8757
Baltimore/Washington International Airport
Maryland 21240, USA

Government Reports Announcements (GRA),
published by the National Technical
Information Services, Springfield
Virginia 22151, USA



Printed by Technical Editing and Reproduction Ltd
Harford House, 7-9 Charlotte St, London W1P 1HD

ISBN 92-835-0200-0